Response to Anonymous Reviewer #1

The author's responses to anonymous reviewer #1's comments are found after each comment. Each comment is in italics and our response is in a normal font. Yellow highlighting is used to identify changes made to the manuscript. We have removed the reviewer's synopsis and recommendation found at the top of the review.

Anonymous Referee #1
Received and published: 22 September 2017

-As a general comment, could the authors use their model (and/or the chemical understanding they have gained while constructing it) to qualitatively explain to a nonexpert reader the reason for the "parabolic" behaviour exhibited by the sensitivity of so many analyte/ion combinations with respect to humidity? (E.g. figures 5,6,7 in their manuscript, and many cases of such behaviour reported elsewhere). I have always assumed the initial increase is due to energy (non)accommodation effects, i.e. water stabilizing the ion-molecule clusters - I guess this is included in the model by reactions of the type R2 being termolecular, while R3 is bimolecular. Is this the explanation for the initial increase, or is the explanation more subtle? And is the subsequent decrease then related mainly to competition by polyhydrates, or what is going on? Also, why does I-(HFo) go up with H2O while I-(HAc) goes down? The model should presumably provide some insight into this. A separate section explaning the reasons for the observed trends (in the SI if the authors feel the manuscript is too long) would be very useful to readers trying to understand the chemistry behind the CIMS measurements.

The reviewer has hit upon the very reason the model was developed. The variability in sensitivity observed with changing water vapor mixing ratio and sample pressure depended upon the reagent ion-analyte pair. To bring this to the fore we have added the following text to the introduction (approximately new line 59).

As will be shown below within the discussion section, depending upon the reagent ion-analyte pair, the effect of water vapor can lead to:

1) a relative constant sensitivity as water vapor mixing ratios increase until near maximum water vapor mixing ratios are encountered after which the sensitivity decreases with increasing water vapor,
2) sensitivity increases as water vapor mixing ratio increases,
3) sensitivity decreases as water vapor mixing ratio increases, and
4) "parabolic" response in which the sensitivity to an ion-analyte cluster is low at low water vapor mixing ratio passes through a maximum sensitivity at an intermediate water vapor mixing ratio and is low again at high water vapor mixing ratio

and ambient pressure changes can lead to decreasing or increasing sensitivity with an increase in sample pressure (flow).

Further the discussion of the schematic mechanism outlined by R1-R4 was intended to explain this behavior. To improve on our explanation there, we have included sets of conditions or assumptions which lead to the observed sensitivity behavior (approx. line 220).

This simple system with a variety of reaction rate coefficients can yield a suite of sensitivity responses to water vapor.
Case 1: Sensitivity independent of water.
Assumptions, water vapor does not deplete the reagent ion concentration and the product $k_{R2f}[M][X^-]$ is much larger than $k_{R3f}K_{R1}[H_2O]$ over the range of [H_2O] encountered.
Case 2: Sensitivity increases with water vapor mixing ratio.
Assumptions, water vapor does not deplete the reagent ion concentration and the product $k_{R2f}[M][X^-]$ is smaller than $k_{R3f}K_{R1}[X^-][H_2O]$ over the range of [H_2O] encountered.
Case 3: Sensitivity decreases with water vapor mixing ratio.
Assumption set A: water vapor depletes the reagent ion concentration via R1 and successive hydration reactions represented by:

$$X^-(H_2O)_{m-1} + H_2O + M \leftrightarrow X^-(H_2O)_m + M \quad \text{(R1')}$$

and reactions like R3f are slow.
Assumption set B: product $k_{R3r}[X\text{-}(A)][H_2O]$ becomes progressively larger than the sum of $k_{R2f}[M][X\text{-}]$ and $k_{R3f}K_{R1}[X^-][H_2O]$ as [H_2O] increases.

-Line 79: the word "expected" is a bit confusing: why did the authors "expect" to see these signals if the reactions forming the hydrates in question have too positive enthalpies/free energies? Am I missing something here? (The whole sentence is actually a bit hard to parse, I would suggest reformulating it.)

Agree with the reviewer. The intent was to indicate the effective "declustering energy" of the CDC (collision dissociation chamber, entrance plate and octopole). This section has been rewritten for clarity (approximately new line 76).

The physical PCIMS instrument is described in O'Sullivan et al. (2017), Treadaway (2015) and Treadaway et al. (2017). A physical description of the instrument and calibration schemes are presented in the Appendix. The instrument flow and electronic configuration described in the Appendix was used throughout the field and laboratory work reported here. The PCIMS m/z range was 1-500 m/z and the mass resolution was 1.0 m/z. The main component effecting ion-cluster transmission through the system was the collision dissociation chamber (CDC) consisting of an entrance plate and octopole ion guide. The CDC plate DC voltage and the octopole DC and RF voltages were adjusted to maximize the transmission of the hydroperoxide analyte cluster ions $O_2^-(CO_2)(H_2O_2)$ and $O_2^-(CH_3OOH)$ and to reduce the signal from other ions near their respective masses. To estimate the "declustering" energy employed, an analysis of the thermodynamics of the following hydration reactions:

$$O_2^-(H_2O)_{n-1} + H_2O \rightleftarrows O_2^-(H_2O)_n; \quad n = 1 - 5,$$

$$CO_3^-(H_2O)_{n-1} + H_2O \rightleftarrows CO_3^-(H_2O)_n; \quad n = 1-3,$$
$$NO_3^-(H_2O)_{n-1} + H_2O \rightleftarrows NO_3^-(H_2O)_n; \quad n = 1-2,$$

and

$$I^-(H_2O)_{n-1} + H_2O \rightleftarrows I^-(H_2O)_n; \quad n = 1-4,$$

and the PCIMS signals of the respective hydrates was done. There was an absence of signals for $O_2^-(H_2O)_{n>3}$, $CO_3^-(H_2O)_{n>2}$ and $I^-(H_2O)_{n>1}$ clusters. The absence of these clusters suggested a CDC "declustering" enthalpy cut off at -50 kJ mol^{-1} or a CDC "declustering" Gibbs energy of -20 kJ mol^{-1}. The thermodynamic data used in this analysis were from NIST Chemistry WebBook SRD69 (Bartmess, 2016).

-The resolution of the figures are quite poor, making the figures hard to read - could you please make higher-quality figures? (Perhaps the poor resolution is due to some format conversion issue?) Also some of the figures could be made larger (e.g. Fig 1 & 2).

Agree with the reviewer. Figures have been redrafted to improve quality and readability for publication in AMT.

-I found the concept that the acidity of XH (or alternatively basicity of X-) can be used to quantitatively predict the (relative) binding of X- to different analytes quite interesting (R5 and surrounding discussion). Could this correlation be used more generally?

The short answer is yes and besides the reference to Böhringer et al. [1984] a few examples are given here. The first use of gas phase acidity we have found as it relates to our work comes from Dzidic et al. [1974] in which he discusses oxygen superoxide ions, the transfer of a proton from several organic compounds, specific to our interests, from acetic acid with the production of an acetate ion. Gas phase acidity was more recently used by Veres et al. [2008] and Roberts et al. [2010] in an analysis of negative ion proton transfer chemical ionization as it relates to the use of acetate ion as a reagent to ionize organic acids with lower acidities. Bertram et al. [2011] used gas phase acidity in a discussion of two possible outcomes of acetate chemistry proton transfer resulting in both negative analyte ion formation by proton transfer or in acetate-analyte cluster formation. Bertram [Pers. Comm., Department of Chemistry, University of Wisconsin, Madison, WI) further explored the use of oxygen superoxide ion (O2-) as a reagent ion for formic acid (HFo) and observed both O2-(HFo) clusters and Fo- as products (approximately at a 3:1 proportion).

Oxygen superoxide ion reactions with organic compounds were specifically raised by Anonymous Reviewer 2 and its chemistry is commented on in our response to Anonymous Reviewer 2.

-Line 220-221, please specify that the pictures are plotted for the case A=H2O2 (this is sort of implicit from the discussion above, but specifying it would help the reader).

We have added the following sentence to the text at line 259

Fig 2 is plotted with $A = H_2O_2$ as introduced in R2-R4.
and the following sentence to the figure caption for Fig. 2.
R1-R4 refer to reactions introduced in the text with $A = H_2O_2$.

-Line 375, "too peaked" is a bit ambiguous, please reformulate

This section now near line 417-421 was revised and now reads:
The simulated O_2^- hydroperoxide cluster sensitivity showed too steep of an increase to the maximum value and then too steep of a decrease after the maximum as water vapor mixing ratio varied from 10 to 20,000 ppm. The maximum sensitivity was at water vapor mixing ratios near a few 100 ppm. The addition of reactions leading to higher order ion hydrates, $(H_2O)_{n>1}$, carbonates, $(CO_2)_{n>1}$, mixed hydrate-carbonates, $(H_2O)_m(CO_2)_n$, were included to reduce the steepness on each side of the maximum (see supplemental information for details).

-Line 394: "preoxide" => "peroxide"

This was corrected and is at new line 436.

-Line 98 of the Supplemental Information: the number 10ˆ-2 J / mol K seems too small (comparing e.g. to entropies given in the tables), pehaps the authors meant kJ / mol K, or alternatively 10ˆ+2?

The reviewer is correct, the intended value was of order 10^2 J mol^{-1} K^{-1} and the text in line 98 has been revised.

Response to Anonymous Reviewer #2

The author's responses to anonymous reviewer #1's comments are found after each comment. Each comment is in *italics* and our response is in a normal font. Cyan highlighting is used to identify changes made to the manuscript. We have removed the reviewer's synopsis and recommendation found at the top of the review.

Anonymous Referee #2
Received and published: 22 December 2017

1) *The authors have done a commendable job trying to develop a mechanistic understanding of the ion chemistry occurring in their chemical ionization region. The ion chemistry chosen seems rather complicated, but it seems the broad trends can be rationalized. One aspect I didn't see directly addressed was proton abstraction from weak acids by O2-. Could this be more explicitly stated as to whether e.g. acetate ions or other carboxylate ions are produced, and if so what would be the resulting secondary ion chemistry in the flow reactor. Would that produce other possible interfering ions?*

The reviewer is correct and we did not include or discuss reactions involving proton abstraction by oxygen superoxide ions, O_2^-. We did consider this at a cursory level because of the work of Dzidic et al. [J. Amer. Chem. Soc., 96, 5258-5259, 1974] and the summary of reaction rate constants between $O_2^-$and organic compounds by Ikezoe et al. [1987]. We believed the paucity of reaction rate coefficients and the lack of organic compound measurements in our laboratory experiments would make model predictions extremely speculative. At least with our sensitivity work, we could constrain the model with observations.

The reviewers comment did encourage us to reevaluate this process in the context of our modeling activity. We note the use of gas phase acidity to evaluate acetate ion as a reagent ion in negative-ion proton-transfer by Veres et al. [Int'l J. Mass Spect. 274, 48–55, 2008], Roberts et al. [Atmos. Meas. Tech., 3, 981-990, 2010] and Bertram et al. [Atmos. Meas. Tech., 4, 1471–1479, 2011]. In Bertram et al., they point out that acetate ion chemistry proceeds through two channels, proton transfer as the reviewer noted and by cluster ion formation:
$CH_3C(O)O^- + HAnalyte \rightarrow CH_3C(O)OH + Analyte^-$
$CH_3C(O)O^- + HAnalyte \rightarrow CH_3C(O)O^-(HAnalyte)$
Further, Bertram [Timothy Bertram, Pers. Comm., Department of Chemistry, University of Wisconsin, Madison, WI, 2018] shared observations from his laboratory in which they worked with O_2^- as a potential CIMS reagent ion for formic acid. He observed both formate ion (proton abstraction channel) and the $O_2^-(HC(O)OH)$ cluster ion as products at approximately a 1:3 proportion, respectively. In our own laboratory work, Treadaway et al. [Atmos. Meas. Tech. Disc., 2017, doi:10.5194/amt-2017-344] included results showing O_2^- cluster ion formation with acetic acid and hydroxyacetaldehyde. She reviewed the limited data in hand and within the precision of the CIMS quadrupole instrument did not detect acetate ion or the $CH(O)CH_2O^-$ (hydroxy acetaldehyde anion) at m/z 59. As a significant caveat, 59 is adjacent to CO_3^- at m/z 60 which is a major ion in our system.

We have added the following in the discussion section to address the reviewers general concern regarding potential interferences and their specific comment regarding acetate. (near line 586).

In review, it was pointed out the model did not include the ion-neutral chemistry of organic compounds, specifically the potential for oxygen superoxide ion to abstract a proton from acetic acid and subsequently acetate ion to abstract a proton from weaker acids. Currently, the paucity of reaction rate coefficients for $O_2^- + organic$ reactions precludes their inclusion in our model. We must note, the potential exists for such chemistry to impact the simulations and we are unable to quantitatively assess their importance.

2) It is not clear how O3- and CO3- ions are generated.

The reaction pathways leading to O3- and CO3- ions are explicitly presented in Table A4 as they relate to potential interferences. This was implicit in the discussion of interferences now at lines 549 and 550, which we have modified to be more explicit and now reads:

The interference ion production pathways involving NO_2^-, NO_3^-, CO_3^-, O_3^-, and $O_2^-(O_2)$ are outlined in the Appendix, Table A4.

3) The role of O3 was not well developed in that I couldn't follow why it was tested aside from possibly causing an interfering ion in the O2- chemistry. What about I- chemistry?

Gas phase chemistry of I- with O3 proved difficult to find. I-O3 cluster formation and loss is included (Table A2). The bimolecular reaction rate coefficient of cluster formation is about a factor of 100 smaller than the collision limit. The rate data are from Williams et al. [2002]. This same reference states: *"The I- ion was observed to cluster with O3 to form IO3- with a rate constant of approximately 1x10^{-11} cm^3 s^{-1}, which is a factor of 2 above our detection limit, and no other product channels were observed."* This reference further goes on to state the rates of reaction of I- with O2 is less than 1x10^{-13} *cm^3 s^{-1}.* Consequently, we did not explore this path further with respect to ozone or oxygen.

4) There are some rate constants given without units.
Reaction rate coefficient units are specified in Table A2 and in the text (new lines 172-173)

An ion-neutral model to investigate chemical ionization mass spectrometry analysis of atmospheric molecules - application to a mixed reagent ion system for hydroperoxides and organic acids

Brian G. Heikes[1], Victoria Treadaway[1], Ashley S. McNeill[1,2], Indira K. C. Silwal[3,4] and Daniel W. O'Sullivan[3]

[1]Graduate School of Oceanography, University of Rhode Island, Narragansett, RI, 02882, USA
[2]Department of Chemistry, The University of Alabama, Tuscaloosa, AL, 35401, USA
[3]Chemistry Department, United States Naval Academy, Annapolis, MD, 21402, USA
[4]Department of Chemistry, University of Maine, Orono, 04469, USA

Correspondence to: Brian Heikes (bheikes@uri.edu)

Abstract. An ion-neutral chemical kinetic model is described and used to simulate the negative-ion chemistry occurring within a mixed-reagent ion chemical ionization mass spectrometer (CIMS). The model objective was the establishment of a theoretical basis to understand ambient pressure (variable sample flow and reagent ion carrier gas flow rates), water vapor, ozone and oxides of nitrogen effects on ion-cluster sensitivities for hydrogen peroxide (H_2O_2), methyl peroxide (CH_3OOH), formic acid (HFo) and acetic acid (HAc). The model development started with established atmospheric ion chemistry mechanisms, thermodynamic data and reaction rate coefficients. The chemical mechanism was augmented with additional reactions and their reaction rate coefficients specific to the analytes. Some existing reaction rate coefficients were modified to enable the model to match laboratory and field campaign determinations of ion-cluster sensitivities as functions of CIMS sample flow rate and ambient humidity. Relative trends in predicted and observed sensitivities are compared as instrument specific factors preclude a direct calculation of instrument sensitivity as a function of sample pressure and humidity. Predicted sensitivity trends and experimental sensitivity trends suggested the model captured the reagent ion and cluster chemistry and reproduced trends in ion-cluster sensitivity with sample flow and humidity observed with a CIMS instrument developed for atmospheric peroxide measurements (PCIMS). The model was further used to investigate the potential for isobaric compounds as interferences in the measurement of the above species. For ambient O_3 mixing ratios more than 50 times those of H_2O_2, $O_3^-(H_2O)$ was predicted to be a significant isobaric interference to the measurement of H_2O_2 using $O_2^-(H_2O_2)$ at m/z 66. O_3 and NO give rise to species and cluster ions, $CO_3^-(H_2O)$ and $NO_3^-(H_2O)$, respectively, which interfere in the measurement of CH_3OOH using $O_2^-(CH_3OOH)$ at m/z 80. The $CO_3^-(H_2O)$ interference assumed one of its O atoms was ^{18}O and present in the cluster in proportion to its natural abundance. The model results indicated monitoring water vapor mixing ratio, m/z 78 for $CO_3^-(H_2O)$ and m/z 98 for isotopic $CO_3^-(H_2O)_2$ can be used to determine when $CO_3^-(H_2O)$ interference is significant.

Similarly, monitoring water vapor mixing ratio, m/z 62 for NO_3^- and m/z 98 for $NO_3^-(H_2O)_2$ can be used to determine when $NO_3^-(H_2O)$ interference is significant.

Keywords: Chemical ionization mass spectrometry, multi-reagent ion, hydrogen peroxide, methyl peroxide, formic acid, acetic acid, cluster-ion chemistry, negative ion kinetics, model.

1 Introduction

Atmospheric measurements of hydrogen peroxide (H_2O_2), methyl peroxide (CH_3OOH), formic acid (hereafter referred to as HFo), and acetic acid (hereafter referred to as HAc) have evolved over the past half century. Current state-of-the-art measurements use chemical ionization mass spectrometry (e.g., Crounse et al., 2006; de Gouw and Warneke, 2007; Veres et al., 2008; St. Clair et al., 2010; Le Breton et al., 2012; Lee et al., 2014; Baasandorj et al., 2015; O'Sullivan et al., 2017; Treadaway et al., 2017) with a variety of reagent ions (e.g., H_3O^+, O_2^-, CF_3O^-, I^-, $CH_3C\langle O\rangle O^-$, $O_2^-\langle CO_2\rangle$). O'Sullivan et al. (2017) and Treadaway et al. (2017) have presented a hybrid reagent ion instrument for the simultaneous measurement of the peroxides and organic acids. Here an ion-neutral chemical kinetic model is described and used to simulate the negative-ion chemistry occurring within their mixed-reagent gas chemical ionization mass spectrometer (PCIMS). The "P" is derived from the instrument's original configuration to measure H_2O_2 and CH_3OOH (O'Sullivan et al., 2017), and which was later modified to quantify HFo and HAc (Treadaway, 2015; Treadaway et al., 2017).

The PCIMS instrument and basic ion cluster schemes are described in O'Sullivan et al. (2017), Treadaway (2015), and Treadaway et al. (2017). Serendipity led to the use of a mixed reagent gas stream composed of nitrogen (N_2), oxygen (O_2), carbon dioxide (CO_2) and iodomethane (CH_3I). O_2 and CO_2 reagent gases provided O_2^-, $O_2^-(O_2)$and $O_2^-(CO_2)$ as reagent ions. CH_3I reagent gas yielded iodide ions (I^-). The PCIMS instrument was specifically designed as an aircraft flyable instrument and was flown on the NCAR-HIAPER (UCAR/NCAR-EOL, 2005) aircraft in the Deep Convective Clouds and Chemistry experiment (DC3; Barth et al., 2016) and on the NCAR C-130 (UCAR/NCAR-EOL, 1994) aircraft in the Front Range Air Pollution and Photochemistry Experiment (FRAPPE; https://www2.acom.ucar.edu/frappe). In these programs, a fixed area critical orifice was used on the sample inlet to PCIMS. Consequently, the air sample flow rate into the instrument varied with ambient sample pressure and analyte sensitivity (defined as the cluster ion counts per second per analyte reaction cell mixing ratio, e.g., cps/ppb), varied with ambient pressure. As documented for many atmospheric CIMS instruments (e.g., Slusher et al., 2004; Crounse et al., 2006; St. Clair et al., 2010; Le Breton et al., 2012; Lee et al., 2014; Baasandorj et al., 2015), analyte sensitivity was dependent upon the reaction cell water vapor mixing ratio. The humidity and pressure sensitivity dependencies were complex and explored in the laboratory to improve calibration. As will be shown below within the discussion section, depending upon the reagent ion-analyte pair, the effect of water vapor can lead to:

1) a relative constant sensitivity as water vapor mixing ratios increase until near maximum water vapor mixing ratios are encountered after which the sensitivity decreases with increasing water vapor,
2) sensitivity increases as water vapor mixing ratio increases,
3) sensitivity decreases as water vapor mixing ratio increases, and
4) "parabolic" response in which the sensitivity to an ion-analyte cluster is low at low water vapor mixing ratio passes through a maximum sensitivity at an intermediate water vapor mixing ratio and is low again at high water vapor mixing ratio

and ambient pressure changes can lead to decreasing or increasing sensitivity with an increase in sample pressure (flow). The objective of this paper is to present a model chemical mechanism which provides a theoretical basis to investigate the influences of ambient pressure (variable sample flow and reagent ion carrier gas flow rates), water vapor and other trace gases: ozone (O_3), nitric oxide (NO), nitrogen dioxide (NO_2) and nitric acid (HNO_3) on ion-cluster sensitivities for H_2O_2, CH_3OOH, HFo, and HAc. The model is extensible to simulating the negative ion chemistry of other reagent gas, ion source and reaction cell or drift-tube systems.

2 Methods

2.1 PCIMS Instrument

The physical PCIMS instrument is described in O'Sullivan et al. (2017), Treadaway (2015) and Treadaway et al. (2017). A physical description of the instrument and calibration schemes are presented in the Appendix. The instrument flow and electronic configuration described in the Appendix was used throughout the field and laboratory work reported here. The PCIMS m/z range was 1-500 m/z and the mass resolution was 1.0 m/z. The main component effecting ion-cluster transmission through the system was the collision dissociation chamber (CDC) consisting of an entrance plate and octopole ion guide. The CDC plate DC voltage and the octopole DC and RF voltages were adjusted to maximize the transmission of the hydroperoxide analyte cluster ions $O_2^-(CO_2)(H_2O_2)$ and $O_2^-(CH_3OOH)$ and to reduce the signal from other ions near their respective masses. To estimate the "declustering" energy employed, an analysis of the thermodynamics of the following hydration reactions:

$$O_2^-(H_2O)_{n-1} + H_2O \rightleftarrows O_2^-(H_2O)_n; \quad n = 1-5,$$

$$CO_3^-(H_2O)_{n-1} + H_2O \rightleftarrows CO_3^-(H_2O)_n; \quad n = 1-3,$$

$$NO_3^-(H_2O)_{n-1} + H_2O \rightleftarrows NO_3^-(H_2O)_n; \quad n = 1-2,$$

and

$$I^-(H_2O)_{n-1} + H_2O \rightleftarrows I^-(H_2O)_n; \quad n = 1-4,$$

and the PCIMS signals of the respective hydrates was done. There was an absence of signals for $O_2^-(H_2O)_{n>3}$, $CO_3^-(H_2O)_{n>2}$ and $I^-(H_2O)_{n>1}$ clusters. The absence of these clusters suggested a CDC "declustering" enthalpy cut off at -50 kJ mol^{-1} or a CDC "declustering" Gibbs energy of -20 kJ mol^{-1}. The thermodynamic data used in this analysis were from NIST Chemistry WebBook SRD69 (Bartmess, 2016).

PCIMS uses a mixed reagent ion chemistry: O_2^-, $O_2^-(CO_2)$ and I^- to produce cluster ions with H_2O_2 [$O_2^-(H_2O_2)$, $O_2^-(CO_2)(H_2O_2)$, $I^-(H_2O_2)$ at masses 66, 110 and 161, respectively], with CH_3OOH [$O_2^-(CH_3OOH)$, mass 80], with HFo [$I^-(HFo)$, mass 173] and HAc [$I^-(HAc)$, mass 187]. There is a weaker signal for $I^-(CH_3OOH)$ at mass 175 but it is not considered in the model. For completeness, its sensitivity as a function of reaction cell water mixing ratio is shown in Fig. S1 and its sensitivity relative to $I^-(H_2O_2)$, $I^-(HFo)$ and $I^-(HAc)$ is shown in Fig. S2 of the Supplemental Information.

In flight, ambient air was sampled through a heated probe held at 30°C in DC3 and 70°C in FRAPPE. The higher temperature in FRAPPE was used to partially alleviate an inlet contamination issue. Sample air is passed from the inlet to the instrument using heated PFA ® Teflon tubing. All "wetted" surfaces from the probe to the physical instrument are PFA ® Teflon. The inlet system is pumped by the instrument's vacuum system and by a second scroll pump (Varian model IDP-3) to increase sample airflow though the inlet tubing improving response time and ameliorating potential wall artifacts in H_2O_2, CH_3OOH, HFo, and HAc. Standard additions of hydroperoxides were performed in DC3 and hydroperoxide and organic acid standard additions were performed in FRAPPE. The gas standards were added before a selectable entrance to two traps in series (Carulite-200 ®, Carus Corp., Peru, IL; NaOH on fiberglass wool). There was a constant flow of standard gas to within 0.3 m of the inlet and a "draw-back" line was used to divert the standard and an equal amount of sample air to waste under normal conditions (Fig. A2b). A 2-way valve on the "draw-back" line of the syringe addition system and a 3-way valve near the instrument inlet (Fig. A2b) were used to select between 1 of 4 modes: 1) the sample air, 2) sample air with gas standard addition, 3) sample air passed through the traps as a field blank, or 4) sample air with gas standards added and passed through the traps to evaluate trap efficiency. In this way instrument calibration and trap efficiency were monitored.

H_2O_2, CH_3OOH and CD_3OOH (trideuterated methyl peroxide) gas standard additions are available for research flights 6-22 in DC3. H_2O_2 and HFo standard additions are reported for all 15 research flights in FRAPPE. However, in FRAPPE, the instrument experienced severe vibration in flight, which caused “chatter” in the MFCs, and there was a significant contaminant in the hanger. Consequently, CH_3OOH calibrations were reported for the last 11 flights after the MFC mounts were reconfigured and “chatter” was greatly reduced. HAc standard additions were only available for a portion of these FRAPPE flights as the contamination problem was minimized only on longer flights or after high altitude runs. The standard additions used here were further screened to ensure each standard addition cycle, (ambient air, ambient air with gas standards added, ambient air), was completed at constant pressure (altitude).

The laboratory calibration set up is described fully in Treadaway (2015) and only briefly here (block schematic shown in Fig. A2a). A pure-air generator (Model 737-10A, Aadco Instruments Inc., Cleves, OH) supplied the carrier air stream at 10 slpm (standard liters per minute, $T_{ref}=0$ °C, $P_{ref}=1013.25$ hPa). This air stream was split between dry (5-10 slpm) and humidified lines (0-5 slpm) and the total flow was maintained at 10 slpm. The water concentration in the humidified line is controlled with two gas washing bottles and a gas-water equilibration coil immersed in a water bath held at either 15 or 25 °C. At the latter bath temperature, it was necessary to reset the room temperature from 22 to 30 °C to prevent condensation in the line. For some experiments, gas standard additions were performed with an external Henry's Law type equilibration coil with concurrent aqueous flow at 0.4 mL min^{-1}, air flow at 0.4 slpm, gas and aqueous flows are separated at the end of the coil using a cyclone separator, and the coil-cyclone are immersed in a water bath held at 15 °C. The Henry's Law system was plumbed to the carrier air stream after the humidification line. A needle valve was used to simulate lower ambient pressures (Fig. A2a) as in flight. The aircraft standard addition system was also used and this remained plumbed downstream of the laboratory air pressure control system. Air pressures between 120 and 1013 hPa were sampled (nominally set at 120, 180, 300, 600 and 1013 hPa). By changing the proportion of air flow through the dry (10, 9, 8, 7, 6 and 5 slpm) and humidified lines (0, 1, 2, 3, 4, and 5 slpm) and the inlet pressure, it was possible to alter the reaction cell water vapor mixing ratio from 30 to 20,000 ppm.

2.2 Ion-Neutral Chemical Mechanism

The chemical mechanism is guided by the ion-neutral reaction suites and kinetic summaries of Albritton (1978), Huertas et al. (1978) Ikezoe et al. (1987), Turunen et al. (1996), Kazil (2002), Popov (2010), Kovács et al. (2016) developed to simulate ion-neutral chemistry of the atmosphere. Necessary modifications and extensions of the chemical mechanisms to fit the PCIMS sensitivities are described here and in more detail within the Supplemental Information.

Some trace components of ambient air can compete for the reagent ions and ion-neutral clusters effecting the yield (sensitivity) of the analyte ion clusters of interest and as well as forming isobaric interfering ion or ion clusters. Analyte ion-clusters and identified potential interfering ion species at specific m/z ratios are listed in Table 1. Also listed are primary ion cluster m/z ratios used to assess potential isobaric interferences. For example, m/z 78 is used to monitor $CO_3^-(H_2O)$, which in turn is used to estimate the potential interference at m/z 80 from $CO_3^-(H_2O)$ should one of its four O atoms be a mass 18 stable isotope of oxygen, ^{18}O, and present at its natural abundance of 0.204%.

Time-dependent concentrations of 73 species (neutrals, ions and ion-clusters), listed in Appendix Table A1, are predicted in time according to the 209 bi- and ter-molecular reactions presented in Appendix Table A2. Analyte cluster ion formation reactions are relisted in Table A3 for clarity. Potential isobaric interference ion cluster formation reaction sequences are listed in Table A4 for clarity, as well. A set of 72 ordinary differential equations was solved using the *ode23t* solver (MatLab version R2016b, The MathWorks, Inc.) with relative tolerance equal to 3x10^{-9} and the absolute tolerance equal to 3x10^{-12}.

2.3 Reaction Rate Coefficients

Reaction rate coefficients are taken from Popov (2010), Kazil (2002), Ikezoe et al (1987), Kawamoto and Ogawa (1986), Fahey et al. (1982), Albritton (1978), Huertas et al. (1978), Fehsenfeld and Fergusson (1974), Adams et al. (1970), Fehsenfeld et al. (1969; 1967), and references therein. Reaction rate coefficient units are s^{-1}, cm^{3} molec^{-1} s^{-1}, and cm^{6} molec^{-2} s^{-1} for uni-, bi- and ter-molecular reactions, respectively. Equilibrium constants determined using reaction Gibbs energy, have been converted appropriately assuming (ideal gas behavior, T$_{ref}$ = 298.15 K, P$_{ref}$ = 1013.25 hPa, and N$_{ref}$ = 2.46x10^{25} molec m^{-3}). Most of the reaction rate coefficients were experimentally determined and a few were theoretically estimated (e.g., Kazil, 2002; Iyer et al., 2016). However, some of the rate constants listed in the above compilations were simply presumed (e.g., Mohnen, 1972; Huertas et al., 1978) and these presumptions have carried forward into later works. Several rate coefficients were estimated from the Gibb's reaction energy, $\Delta\ G^o_{rxn}$, or equilibrium constant, K_{eq}, with either a measured forward or reverse reaction rate coefficient following Albritton (1978), *i.e.*, $K_{eq} = \frac{k_{for}}{k_{rev}}$ and $K_{eq} = e^{\{\Delta G^o_{rxn}/(RT_o)\}}$. The majority of Gibbs reaction energies are taken directly from the NIST Chemistry WebBook (Bartmess, 2016). Generally available neutral, ion and ion-cluster formation enthalpy, entropy and Gibb's formation energy for the $O_2^- - O_2 - CO_2 - H_2O -$ hydroperoxide system are listed in Table A5 in the Appendix. Reaction enthalpy, reaction entropy and Gibb's reaction energies for this system are listed in Table A6 in the Appendix. Notes on the development of the thermodynamic Tables A5 and A6 are given in supplement information section 1.1. As called out below and in the supplemental information, care is required in applying $K_{eq} = \frac{k_{forward}}{k_{reverse}}$ as the implied reaction system may not represent a simple concerted reaction pair in equilibrium but involve a reaction sequence in steady-state. For several of the ion-hydrate cluster reactions:

$$X^-(H_2O)_{n-1} + H_2O + M \leftrightarrow X^-(H_2O)_n + M \qquad K_{eq} = \frac{k_{hydration}}{k_{dehydration}} = e^{\{\Delta G^o_{rxn}/R/T_o\}}$$

neither the forward termolecular hydration rate constant ($k_{hydration}$) nor the bimolecular dehydration rate constant ($k_{dehydration}$) is known. In this case, rate coefficients are estimated from the observation that a strong correlation exists between the log of $k_{dehydration}$ and the Gibbs energy of the hydration reaction ($\Delta\ G^o_{rxn}$). The correlation is shown in Fig. 1a. Known dehydration rate coefficients include those that are experimentally determined by direct measurement of $k_{dehydration}$ and those that are estimated from the hydration equilibrium constant and a measured $k_{hydration}$. For the cases in which neither $k_{hydration}$ or $k_{dehydration}$ is known, $k_{dehydration}$ is first estimated using ΔG^o_{rxn} as its predictor (i.e., the linear regression model "fit" in Fig. 1a) and $k_{hydration}$

is subsequently estimated from the predicted $k_{dehydration}$ value and K_{eq}. Fig. 1b shows known $k_{hydration}$ and estimated $k_{hydration}$ plotted as a function of $\Delta\ G^o_{rxn}$. Note further that, with only a few exceptions, individual $k_{hydration}$ rates fall within a factor of two of the mean value (dashed green line) and are near the collision limit. A factor of two falls within the accepted uncertainty estimated for the reaction rate coefficients. The uncertainties in ion-molecule reaction rate coefficients as reported by their original authors are included in the summary by Ikezoe et al. (1987). Typically, reaction rate coefficient uncertainty is reported to be a factor of two (e.g., Albritton, 1978; Fahey et al., 1982; Ikezoe et al., 1987). Although for a few reactions, "best" reaction rate coefficient uncertainties of ±20% can be found (e.g., Ikezoe et al., 1987). Here a factor of two is taken as the uncertainty in the reaction rate coefficients. Additional notes on the development of reaction rate coefficients are given in sections 1.2-1.4 of the supplemental information.

The following generic equilibrium reaction sequences, after, e.g., Crounse et al. (2006) and Le Breton et al. (2011), are used to describe negative ion, X^-, cluster formation with an analyte, A, representing H_2O_2, CH_3OOH, HFo, and HAc:

$$X^- + H_2O + M \leftrightarrow X^-(H_2O) + M \qquad \text{(R1)}$$

$$X^- + A + M \leftrightarrow X^-(A) + M \qquad \text{(R2)}$$

$$X^-(H_2O) + A \leftrightarrow X^-(A) + H_2O \qquad \text{(R3)}$$

Reactions R1-R3 correspond to our reactions (22) - (45). As discussed below, we have added poly-hydrate "switching" type reactions:

$$X^-(H_2O)_n + A \leftrightarrow X^-(A)(H_2O)_{n-1} + H_2O \qquad \text{(R4)}$$

to account for observed higher order humidity effects on O_2^-, $O_2^-(CO_2^-)$ and I^- hydroperoxide and organic acid sensitivity. This simple system with a variety of reaction rate coefficients can yield a suite of sensitivity responses to water vapor.

Case 1: Sensitivity independent of water.

Assumptions, water vapor does not deplete the reagent ion concentration and the product $k_{R2f}[M][X^-]$ is much larger than $k_{R3f}K_{R1}[H_2O]$ over the range of $[H_2O]$ encountered.

Case 2: Sensitivity increases with water vapor mixing ratio.

Assumptions, water vapor does not deplete the reagent ion concentration and the product $k_{R2f}[M][X^-]$ is smaller than $k_{R3f}K_{R1}[X^-][H_2O]$ over the range of $[H_2O]$ encountered.

Case 3: Sensitivity decreases with water vapor mixing ratio.

Assumption set A: water vapor depletes the reagent ion concentration via R1 and successive hydration reactions represented by:

$$X^-(H_2O)_{m-1} + H_2O + M \leftrightarrow X^-(H_2O)_m + M \qquad \text{(R1')}$$

and reactions like R3f are slow.

Assumption set B: product $k_{R3r}[X-(A)][H_2O]$ becomes progressively larger than the sum of $k_{R2f}[M][X-]$ and $k_{R3f}K_{R1}[X][H_2O]$ as [H_2O] increases.

For the most part, our ion-analyte cluster reaction kinetics are unstudied. The ion hydration kinetics of R1 are discussed above. Measured reaction rate coefficients were available for H_2O_2 clustering with NO_2^-, NO_3^-, Cl^-, and HSO_4^- (Böhringer et al., 1984). Iyer et al. (2016) using *ab initio* methods estimated reaction rate coefficients and binding energies for I^- with HFo and HAc. They also calculated binding energies for I^- reactions with H_2O_2 and CH_3OOH (Iyer, Pers. Comm., 2017). The calculated binding energies for $I^-(HFo)$, $I^-(HAc)$, $I^-(H_2O_2)$, and $I^-(CH_3OOH)$ were 100, 73, 70, and 60 kJ mol^{-1}, respectively. Iyer et al. predicted sensitivities for the Lee et al. (2014) instrument using the calculated binding energies and measured sensitivities. We have normalized these to $I^-(HFo)$ and the predicted relative sensitivities were 1.000, 0.034, 0.007, and 0.001 for $I^-(HFo)$, $I^-(HAc)$, $I^-(H_2O_2)$ and $I^-(CH_3OOH)$, respectively. These were consistent with the observations of O'Sullivan et al. (2017) in which they noted observing $I^-(H_2O_2)$ and sometimes $I^-(CH_3OOH)$ clusters with the PCIMS instrument and with Treadaway et al. (2017) in which they observed a weak standard addition calibration signal for $I^-(CH_3OOH)$ during FRAPPE and in the laboratory in preparation for FRAPPE (unpublished; in the supplemental information Fig. S1), and relative to those for $I^-(HFo)$, $I^-(HAc)$, and $I^-(H_2O_2)$ (supplemental information Fig. S2). In contrast to the prediction of Iyer, Treadaway et al. observed comparable sensitivities for $I^-(HAc)$ and $I^-(H_2O_2)$.

At the constant reaction cell instrument pressure of 22 hPa, the forward rate coefficient for R2 was taken to be constant and the reaction and its rate coefficient were given as a pseudo-bimolecular reaction with an initial reaction rate coefficient of 3×10^{-9}, which is near the bi-molecular collision limits calculated by Kazil (2002) and Iyer et al., (2016). This reaction rate coefficient was presumed for R3, as well, although in the literature switching reaction rate coefficients on the order of 10^{-10} are also used as estimates.

The reverse reaction coefficient of R2 is estimated using the assumed forward rate constant and the equilibrium constant for R2. As noted above, reaction Gibbs energies and equilibrium constants are available for R1 (Bartmess, 2016). A more limited set of Gibbs energies and equilibrium constants are available for R2 with H_2O_2 as the analyte (Böhringer et al., 1984; Cappa et al., 2001; Messer et al., 2000; O'Sullivan et al., 2017). Following Böhringer, we have used known reaction enthalpies, ΔH°_{R5}, or reaction Gibbs energies, ΔG°_{R5}, of the ion protonation reaction, R5,

$$X^- + H^+ \leftrightarrow XH \qquad \text{(R5)}$$

as linear predictors of the reaction Gibbs energy for R1 and R2, ΔG°_{R1} *and* ΔG°_{R2} and ΔG°_{R2}, (and therefore the equilibrium constant) with $A = H_2O_2$ and $X^- = O_2^-$, $O_2^-(CO_2)$ or I^-. Fig. 2a illustrates the linear relationships between ΔG°_{R5} with ΔG°_{R1} for H_2O, and with ΔG°_{R2} for H_2O_2. Fig. 2b shows the linear relationship between ΔG°_{R5} and ΔG°_{R3}, where $\Delta G^{\circ}_{R3} = \Delta G^{\circ}_{R2} -$

ΔG°_{R1}. Fig 2 is plotted with $A = H_2O_2$ as introduced in R2-R4. The predicted equilibrium constants, K_{R2}, for O_2^-, $O_2^-(CO_2)$ and I^- are 3.2x10^{16}, 3.5x10^{7}, and 1.4x10^{7} (atm^{-1}), respectively. The coefficients of determination were the same regardless of whether ΔH°_{R5} or ΔG°_{R5} was used to predict ΔG°_{R1} or ΔG°_{R2} and subsequently ΔG°_{R3}. As noted in the supplemental information, there is some question as to whether $O_2^-(CO_2)(H_2O)$ follows a simple reaction pair or involves a more complex set of reactions at steady state and a linear prediction of ΔG°_{R3} could be an oversimplification and a source of error for reaction rate constants involving this species.

The kinetics and equilibrium constants for CH_3OOH ion cluster formation are more speculative. Cappa et al. (2001) using *ab initio* methods have estimated ΔH°_{R2} and ΔG°_{R2} for cluster formation with CO_3^-, -69 and -34 kJ/mol, respectively, and ΔH°_{R3} and ΔG°_{R3} for R3, -17 and -9 kJ/mol, respectively. Iyer (Pers. Comm., 2016) estimated the CH_3OOH binding energy with I^- is -60 kJ/mol. Messer et al. (2000) also using *ab initio* methods examined the kinetics and energetics of H_2O_2 and CH_3OOH cluster ion formation with F^-. They reported theoretical collision-limit rate coefficients of 1.42x10^{-9} and 1.47x10^{-9}, respectively, for reactions with $F^-(H_2O)_3$. Their theoretical rate coefficients were bracketed by their experimental determined rates of 0.96 – 1.92x10^{-9}. The $F^-(H_2O)_3$ ion was the predominant reagent ion under their experimental humidity conditions that gave rise to an ion-peroxide signal. Messer et al. further stated the rate of reaction was relatively unchanged for F^- hydration numbers less than 6. Payzant and Kebarle (1972), Fehsenfeld and Ferguson (1974), and Fahey et al. (1982) discussed reaction rates of O_2^- with variable numbers of water molecules attached and indicated they varied only slightly with different extents of hydration. We have therefore assumed the reaction rate coefficients for hydrated O_2^- ions with H_2O_2 and CH_3OOH do not vary significantly with hydration. The forward rate constants for R2, R3 and R4 are set at near the collision rate for H_2O_2 and CH_3OOH. As a caveat, we note some switching reaction rate coefficients for less tightly bound neutral species, e.g., O_2, CO_2, H_2O, are reported to be on the order of 10^{-10}.

Water vapor is commonly added to the CH_3I reagent gas stream in I^- based CIMS instruments because it enhances sensitivity for some analytes (e.g., Slusher et al., 2004; Le Breton et al., 2011). Whether this is because H_2O is a better third body energy carrier, such as in R2, or adds a switching reaction, R3, to the instrument's development of an $I^-(A)$ cluster ion is not clear, though discussions point to the latter. Per Iyer et al. (2016), the R2 forward reaction rate coefficient is initially set at the collision limit for HFo and HAc. The forward reaction rate coefficients for these two compounds in R3 were set initially at the collision limit. Last, the hydration equilibrium constants for I^- are such that under our laboratory and field experimental conditions, I^- and $I^-(H_2O)$ dominate over $I^-(H_2O)_{n>1}$ ions. Even so at the highest humidities studied it was necessary to include R4 for n=2, but inclusion of R4 with n>2 was unnecessary even when the R4 reaction rate coefficient was set at the collision limit.

Last, Iyer et al. (2016) examined the probability of collisional stabilization of HFo (atom number 5) compared to maximum sensitivity molecules (atom number >8) and found the former gave sensitivities dependent on reaction cell pressure, whereas, the latter were independent of pressure. Our analytes have between 4 and 6 atoms and our use of collision limit reaction rate coefficients could have resulted in an over prediction of the rates of I^- cluster formation.

2.4 Model Assumptions

Individual model runs are performed in two stages. The first simulated the chemistry of the ion source region (alpha emitter, and reagent ion gas mixture). The product ion outflow of the source was then instantaneously mixed with the sample air stream and the ion-neutral chemistry of the reaction cell was simulated second. The following assumptions were made:

1) alpha particle emission was uniform along the ion source tube length.

2) the ions directly generated by the alpha particles passing through >99% N_2 gas consisted solely of e^- and N_2^+ ions; the mechanism included several negative ions and N_2^+ is the only positive ion considered.

3) the energy of a ^{210}Po alpha particle is 5.3 MeV; the formation enthalpy of a N_2^+ and e^- ion pair from N_2 gas is 34 eV; thus, as a zeroth order estimate, a 20 mCi ^{210}Po alpha source (the stated activity of the NRD P-2130 Electrostatic Eliminator ®) generated on the order of 10^{14} ion pairs per second.

4) ion and neutral molecule concentrations varied along the flow direction and were radially uniform in the ion source tube and reaction cell.

5) gas fluid flow in the ion source tube and in the reaction cell followed plug-flow.

6) the reagent gas stream and ambient air stream were mixed instantaneously and uniformly at the point of contact.

7) ion clusters containing N_2, O_2, and CO_2 as neutrals were not considered with the exceptions of $O_2^-(CO_2)$ and $O_2^-(O_2)$.

8) wall effects on negative ions, neutral species and heterogeneous chemistry were ignored. The first assumption is supported by the fact the ion source tube and reaction cell walls have a -2V bias applied.

9) the negative ion positive ion recombination was parameterized using a single pseudo positive ion, “N_2^+”, that reacts with each negative ion and whose rate constant followed Kazil (2002) and was tracked through:

$$N_2^+ + X_i^- \xrightarrow{k=6x10^{-8}(300/T)+1.25x10^{-25}[M](300/T)} neutral\ products \qquad (157_i)$$

where, 157_i indicated the reaction was included for each of the negative ion species.

2.5 Initial Concentrations

The initial reagent gas mixture was composed of N_2, O_2, CO_2, and CH_3I in proportions that vary with sample air pressure and sample-air flow rate. The total flow rate through the reaction cell was constant at 4.68 slpm (standard liters per minute; T_{ref} = 0 °C, P_{ref} = 1013.25 hPa). The ambient air sample flow rate varied (range 0.3 to 3 slpm) with ambient pressure (range 120 to 1013.25 hPa) as did the N_2 flow rate through the ion-source tube (range 2.1 to 4.3 slpm). Reagent gas concentrations in the ion-source tube varied accordingly and their initial concentrations for different sample pressures and flow conditions are listed in Table 2. Six representative pressures are shown, which span the range of pressures encountered in the DC3 and FRAPPE airborne field campaigns and in the laboratory work. The ion source tube and reaction cell temperature and pressure were taken to be 25 °C and 22 hPa, respectively. The model chemical system was then integrated in time for the length of the gas transit time through the ion source tube.

Ambient air was then mixed with the reagent ion stream. Ambient air, for the purpose of defining reaction cell ion concentration and analyte ion-molecule cluster concentration, included N_2 (~79 %), O_2 (~21 %), CO_2 (~400 ppm), CH_4 (~2 ppm), H_2 (~0.5 ppm), N_2O (~0.32 ppm), O_3 (~0.05 ppm), NO (~ 1 ppb), NO_2 (~1 ppb), HNO_3 (~1 ppb), H_2O_2 (~1 ppb), CH_3OOH (~1 ppb), HFo (~1 ppb) and HAc (~1 ppb). The noble gases, carbon monoxide, and other oxygenated volatile organic compounds were not considered here. The air-sample water vapor mixing ratio was varied from 10 to 31700 ppm to span the range found in the troposphere. Simulation results are presented as a function of reaction cell water vapor mixing ratio and ambient sample pressure.

3 Model Results

The development of ions along the length of the ion-source tube for representative ambient pressures of 1013 and 307 hPa is illustrated in Fig. 3 for the fully developed model. The total ion density was at or near steady-state approximately 2/3s of the way through the ion source tube, although $O_2^-(CO_2)$ increased throughout the length of the source tube at the expense of O_2^- and $O_2^-(O_2)$ (blue traces). Distance along the length of the source tube is displayed on the x-axis instead of time because the time of transit through the tube varied with air-sample pressure.

In the ion-source tube, electrons (e^-) were captured by O_2 and dissociatively captured by CH_3I:

$$e^- + O_2 \overset{M}{\rightarrow} O_2^- \qquad (1), (2)$$

$$e^- + CH_3I \rightarrow I^- + CH_3 \qquad (3)$$

The M indicates a third molecule participates in the reaction. A portion of the initial O_2^- reacted with O_2, CO_2 and CH_3I in the source tube and in the reaction cell yielding secondary I^- and $O_2^-(CO_2)$ and $O_2^-(O_2)$ cluster ions:

$$O_2^- + CH_3I \rightarrow\rightarrow I^- + O_2 + CH_3 \qquad (4)$$

$$O_2^- + CO_2 \overset{M}{\rightarrow} O_2^-(CO_2) \qquad (5)$$

$$O_2^- + O_2 \overset{M}{\rightarrow} O_2^-(O_2) \qquad (55)$$

Note: reaction numbers follow their order within the model reactions presented in Table S4 in the supplemental information. Reaction (4) was inferred based on O_2^- reactivity with CH_3F, CH_3Cl, CH_3Br, CF_4, CF_3Cl, CF_3Br, and CF_3I (Fehsenfeld et al., 1975; Streit, 1982; McDonald and Chowdhury, 1985; Grimsrud, 1992; Morris, 1992; Kazil, 2002). At high CH_3I mixing ratios such as those used in Slusher et al. (2004) and Le Breton (2012) without O_2 or CO_2, CH_3I initially captured the electrons and I^- was the primary negative reagent ion generated within the ion source tube. For our reagent mixture, the model indicated approximately 20% of the initial electrons lead to I^- formation and 80% to O_2^- and its clusters. The secondary formation of I^- from O_2^- was small. At the end of the ion source tube, the concentrations of the primary reagent ions: $O_2^-, O_2^-(CO_2)$ and I^-, were predicted at comparable concentrations.

In the termolecular reactions above, others below, and in Appendix Table A2, M represented the concentration of all other gases, mostly N_2 followed by O_2, H_2O, Ar and CO_2, whereas in the experiments used to determine reaction rate constants, M usually represented a single predominant gas like O_2, CO_2, Ar or He. N_2 or H_2O were seldom included as the third body. In the case of electron attachment, Pack and Phelps (1966) noted faster rates of e^- attachment with H_2O as the third body compared to O_2 or CO_2 and that rates with these two gases were faster than those when N_2 was the third body. Under humid conditions in the reaction cell section, this was a potential source of error, larger than the factor of two given above. Electron concentrations at the end of the source tube were predicted, under our assumptions, to be a factor three larger than any of the other reagent ions.

Fig. 4 shows the predicted concentrations of I^-, O_2^-, $O_2^-(CO_2)$, O_3^- and CO_3^- ions, ion-hydrates and analyte-ion clusters along the length of the reaction cell after the ion source stream was mixed with the sample air stream for the fully developed model. In Fig. 4, distance along the reaction cell was used for the x-axis for consistency with Fig. 3, although the transit time through this section was constant and time or distance were equivalent. The reaction cell transit time was 17.8 ms. Two representative simulations are shown, one with an atmospheric pressure and subsequent sample flow rate commensurate with 1013 hPa and air sample water vapor mixing ratio of 17800 ppm (16 °C dew point temperature) and the other with a sample pressure of 307 hPa, a commensurate sample flow rate and water vapor mixing ratio of 1000 ppm (−32 °C frost point temperature). The corresponding reaction cell water vapor mixing ratios were ~9700 ppm and ~130 ppm, respectively. The ions and ion-hydrates were at or near steady-state approximately 1/3 of the way down the reaction cell length. The ion-analyte clusters increased steadily down the length of the cell (Fig. 4e), with the exception of $I^-(H_2O_2)$ and $I^-(HAc)$ and possibly $O_2^-(H_2O_2)$, which peaked at 1 to 3 cm and then decline with distance down the remainder of the reaction cell. The was attributed to the time needed to form the clusters of interest and their titration after formation by ion-ion recombination with N_2^+. This suggested a longer flow tube could improve sensitivity for those ions which have not reached their maximum value by the end of the reaction cell but at the expense of those clusters which have already peaked.

The ambient ozone mixing ratio was set to 50 ppb in all cases show here. No appreciable difference in $O_2^-(H_2O_2)$, $O_2^-(CH_3OOH)$, $O_2^-(CO_2)(H_2O_2)$, $O_2^-(H_2O_2)$, $I^-(HFo)$ and $I^-(HAc)$ sensitivity was observed when the assumed sample O_3 mixing ratio was halved, doubled, or set to 500 ppb. The latter was apropos to the UTLS (upper troposphere lower stratosphere). Simulated hydroperoxide and organic acid sensitivities were relatively unchanged even with a 10-fold increase in O_3. However, as will be discussed later, O_3 influenced potential isobaric interferences at m/z 66, $O_3^-(H_2O)$, and 80, ^{18}O of $CO_3^-(H_2O)$ and the changes in O_3 resulted in a nearly proportionate increase in these ions. As an aside to O_3^- and CO_3^- chemistries, O'Sullivan et al. (2017) proposed to use CO_3^- as a hydroperoxide reagent ion following the work of Cappa and Elrod (2001) but were unsuccessful in its implementation. Our simulations indicated O'Sullivan's O_3 reagent concentrations were likely too low.

Fig. 5a-10a show experimentally determined sensitivities as a function of reaction cell water vapor mixing ratio for $O_2^-(H_2O_2)$, $O_2^-(CH_3OOH)$, $O_2^-(CO_2)(H_2O_2)$, $I^-(H_2O_2)$, $I^-(HFo)$ and $I^-(HAc)$, respectively. The field and laboratory calibration data were primarily dependent upon humidity and secondarily on sample ambient pressure. The experimental data were first binned by humidity irrespective of ambient or sample pressure. The horizontal bar of the plus symbol denotes the limits of a reaction cell water vapor mixing ratio bin and is plotted at the mean sensitivity for that bin. The length of the vertical bar of the plus symbol indicates one standard deviation of the bin and the variability was due to variations arising from pressure, ambient concentrations during the standard addition, systematic variations due to water vapor across a bin, calibration gas precision and instrument precision. The yellow shaded portions outlined the experimentally determined sensitivity from laboratory experiments and field calibrations from DC3 and FRAPPE.

Fig. 5b-10b show the model simulated ion-analyte cluster sensitivities at the end of the reaction cell as a function of reaction cell water vapor mixing ratio and ambient sample pressure for the fully developed model. The simulated ion-analyte cluster sensitivities are expressed in arbitrary units as Lee et al. (2014) and Iyer et al. (2016) have argued instrumental factors make it nearly impossible to map simulated instrument sensitivity to that determined experimentally. However, assuming instrumental process effects were proportional for each individual ion-neutral cluster, instrument sensitivity trends with pressure and water vapor for each ion-neutral should be captured by the simulations and scalable on an individual basis. "Sensitivity" as shown is the ion-cluster concentration divided by the analyte's ambient mixing ratio, 1 ppb, and was expected to be proportional to counts per ppb. These were further scaled to a maximum of 1 by dividing the predicted sensitivities by the maximum sensitivity calculated for that cluster regardless of sample pressure or humidity.

4 Discussion

The initial model mechanism including O_2^-, $O_2^-(H_2O)$, $O_2^-(CO_2)$, I^- and $I^-(H_2O)$ alone was unable to simulate the sample pressure and water dependent trends in sensitivity for $O_2^-(H_2O_2)$, $O_2^-(CH_3OOH)$, $O_2^-(CO_2)(H_2O_2)$, $I^-(H_2O_2)$, $I^-(HFo)$ and $I^-(HAc)$, not shown. The simulated O_2^- hydroperoxide cluster sensitivity showed too steep of an increase to the maximum value and then too steep of a decrease after the maximum as water vapor mixing ratio varied from 10 to 20,000 ppm. The maximum sensitivity was at water vapor mixing ratios near a few 100 ppm. The addition of reactions leading to higher order ion hydrates, $(H_2O)_{n>1}$, carbonates, $(CO_2)_{n>1}$, mixed hydrate-carbonates, $(H_2O)_m(CO_2)_n$, were included to reduce the steepness on each side of the maximum (see supplemental information for details).

The mechanism so modified remained insufficient to reproduce the O_2^- and $O_2^-(CO_2)$ peroxide sensitivities as a function of reaction cell H_2O mixing ratio and ambient sample pressure (not shown) observed in the field and laboratory measurements. Multiple avenues were explored including (see Supplemental Information):

1. modification of reaction rate coefficients for reactions (12), (13), (14), (21), (24), (147), and (148), which describe the $O_2^- - (H_2O) - (CO_2)$ switching system,
2. the inclusion of reactions (149) - (152) allowing for higher order hydrates to form the analyte cluster ions for peroxides,
3. the inclusion of O_3 reactions with O_2^- to yield O_3^- and subsequent CO_3^- ions,
4. invoking a new carbonation reaction (199),

$$O_2^-(H_2O_2) + (CO_2) + M \rightarrow O_2^-(CO_2)(H_2O_2) + H_2O + M \qquad (199)$$

5. the addition of reactions (204) - (209) allowing for higher order hydrates of I^- to form the analyte cluster ions for hydrogen peroxide and the organic acids.

The addition of O_3 chemistry had little effect on sensitivity, whereas the first two changes improved the pressure dependent sensitivity and water vapor trends for the O_2^- hydroperoxide clusters but did not significantly improve the pressure and water vapor sensitivity trends in $O_2^-(CO_2)(H_2O_2)$, necessitating a process like reaction (199).

Under low water vapor conditions the model under predicted $O_2^-(H_2O_2)$ and $O_2^-(CH_3OOH)$ at higher sample pressures relative to low sample pressures. This was primarily due to the conversion of most of the O_2^- reagent ion to $O_2^-(CO_2)$ in the absence of water vapor (e.g., Kebarle et al., 1972). The conversion of O_2^- to O_3^- was of minor influence. Significantly, at higher water vapor mixing ratios, the O_2^- hydroperoxide clusters and the $O_2^-(CO_2)(H_2O_2)$ cluster were under predicted because of O_2^- hydrate formation, $O_2^-(H_2O)_{n=1,5}$ and the switching reactions included in the initial mechanism:

$$O_2^-(H_2O) + H_2O_2 \rightarrow O_2^-(H_2O_2) + H_2O \qquad (28)$$

$$O_2^-(H_2O) + CH_3OOH \rightarrow O_2^-(CH_3OOH) + H_2O \tag{36}$$

with rate coefficients set at approximately the collision limit (3x10^{-9}) were unable to simulate enough hydroperoxide cluster formation.

A solution to the low humidity problem was suggested by the work of Fehsenfeld and Ferguson (1974), Fahey et al. (1982) and Böhringer et al. (1984). Böhringer et al. suggested there is a hierarchical shift in cluster ion ligands, $X^- \cdot L$, according to ion-ligand bond energy (E_{bond}), for a specific ion. Their ordering followed: $E_{bond}(X^- \cdot H_2O) < E_{bond}(X^- \cdot SO_2) < E_{bond}(X^- \cdot H_2O_2) < E_{bond}(X^- \cdot HCl) < E_{bond}(X^- \cdot HNO_3)$. Adams et al., (1970), Fehsenfeld and Ferguson (1974) and Fahey et al. (1982) presented and discussed the thermodynamics and kinetics of O_2^-, $O_2^-(O_2)$, $O_2^-(CO_2)$, $O_2^-(H_2O)_{n=1,3}$ and $O_2^-(CO_2)(H_2O)_{n=1,3}$. Their bond energies suggested the series given by Böhringer et al. could be extended to include O_2 and CO_2 as ligands with O_2 more weakly bound than H_2O and with CO_2 and H_2O being comparable bound, such that: $E_{bond}(X^-N_2) < E_{bond}(X^-O_2) < E_{bond}(X^-H_2O) \approx E_{bond}(X^-CO_2) < E_{bond}(X^-SO_2) < E_{bond}(X^-H_2O_2) \approx E_{bond}(X^-CH_3OOH) < E_{bond}(X^-HCl) < E_{bond}(X^- \cdot HNO_3)$. Last, *ab initio* calculations suggested the ligand bond energy of CH_3OOH lies above H_2O and near or just below H_2O_2 (Cappa and Elrod, 2001) or well above that of both H_2O and H_2O_2 (O'Sullivan et al., 2017). Consequently, we have speculated that both peroxides may readily switch with the CO_2 in $O_2^-(CO_2)$ and have included the following two CO_2 – peroxide "switching" reactions in the model mechanism:

$$O_2^-(CO_2) + H_2O_2 \rightarrow O_2^-(H_2O_2) + CO_2 \tag{160}$$

$$O_2^-(CO_2) + CH_3OOH \rightarrow O_2^-(CH_3OOH) + CO_2 \tag{161}$$

From sensitivity studies varying forward rate constants, k_{160} and k_{161}, rate coefficient values of 2x10^{-12} and 1x10^{-12} cm^{-3} molec^{-1} s^{-1}, respectively, or greater were sufficient to remove the pressure dependent discrepancy in O_2^- peroxide sensitivity noted at low water vapor mixing ratios. The magnitude of these rate coefficients was reasonable given the bonding energy progression and the rate coefficients reported by Adams et al. (1970) for CO_2 – H_2O switching reactions:

$$O_2^-(H_2O) + CO_2 \rightarrow O_2^-(CO_2) + H_2O \qquad k_{12}=\sim 6\text{x}10^{-10} \tag{12}$$

$$O_2^-(CO_2) + H_2O \rightarrow O_2^-(H_2O) + CO_2 \qquad k_{13}=\sim 2\text{x}10^{-10} \tag{13}$$

where, $k_{13}=k_{12}/K_{eq}(2.3)$, and those estimated by Fahey et al. (1982) for:

$$O_2^-(H_2O)_2 + CO_2 \rightarrow O_2^-(CO_2)(H_2O) + H_2O \qquad k_{147}=7\text{x}10^{-11} \tag{147}$$

and

$$O_2^-(CO_2)(H_2O) + H_2O \rightarrow O_2^-(H_2O)_2 + CO_2 \qquad k_{148}\sim 1\text{x}10^{-9} \tag{148}$$

Finally, a new hybrid clustering reaction was invoked:

$$O_2^-(H_2O_2) + (CO_2) + M \rightarrow O_2^-(CO_2)(H_2O_2) + M \qquad k_{199}=5.0\text{x}10^{-29} \tag{199}$$

which finally enabled the modified chemical mechanism to resolve the pressure and water vapor trends in O_2^- and $O_2^-(CO_2)$ peroxide sensitivities as shown in Figs 5b-7b. This reaction has a calculated Gibb's reaction energy of 7 kJ mol^{-1} (see supplemental information) and therefore is not spontaneous. However, as discussed within the supplement, the reaction is expected to be exothermic, many of the formation and reaction enthalpy and Gibb's energy terms used to derive this value were from experimental data having factor of two uncertainties in rates and 5 to 10 kJ mol^{-1} uncertainties. A Gibb's reaction energy of 7 kJ mol^{-1} is at the 6th significant figure of the *ab initio* calculations and may be near the limit of the theoretical calculations of O'Sullivan et al. (2017) from which it was derived.

The pressure and humidity trends exhibited in the laboratory CH_3I experiments and in the field calibrations for H_2O_2 (Fig. 8; DC3 and FRAPPE); HFo (Fig. 9; FRAPPE) and HAc (Fig. 10; FRAPPE) could not be reconciled using only monohydrate switching reactions (30-33, 38-41, and 42-45). The decrease in sensitivity with increasing humidity was too steep (not shown), and hypothesized reactions (204-209) were added. These reactions likely summarize multistep sequences such as:

$$I^-(H_2O)_n + A \rightarrow I^-A(H_2O)_{n-1} + H_2O$$

$$\ldots$$

$$I^-A(H_2O) \overset{M}{\rightarrow} I^-A + H_2O$$

where A represents H_2O_2, HFo or HAc. It should be noted that reactions (205), (207) and (209) involving $I^-(H_2O)_3$ were inconsequential in reconciling the observed pressure and humidity trends in sensitivity even when reaction rate coefficients were set equal to those of reactions (204), (206), and (208). Consequently, the reaction rate coefficients for the $I^-(H_2O)_3 + A$ reactions were unconstrained by our analyses.

The families of O_2^- and I^- concentrations from the full-model chemical mechanism are shown in Fig. 11 as a function of reaction cell water vapor mixing ratio for several sample pressures. Sample flow rate (sample pressure) had virtually no effect on I^- and $I^-(H_2O)_n$ concentrations, whereas, the reaction cell water vapor mixing ratio has a very strong effect on $I^-(H_2O)_n$ at all levels and on I^- when the mixing ratio is above 10^3 ppm. Sample flow rate and reaction cell water vapor mixing ratio have a profound effect on $O_2^-(H_2O)_n$ and $O_2^-(CO_2)_n$ speciation and their concentrations. It was the steep drop in $O_2^-(CO_2)$ at water vapor mixing ratios greater than 10^2 ppm, which necessitated the invocation of a reaction like (199) to predict the experimental sensitivity trends observed at m/z 110 for $O_2^-(CO_2)(H_2O_2)$.

The $I^-(H_2O_2)$ sensitivity was a critical test point in adjusting the laboratory and FRAPPE CH_3I concentrations to best match the sensitivity observed in DC3 (Treadaway, 2015; Treadaway et al., 2017). The measurement objective in DC3 was the quantification of H_2O_2 and CH_3OOH and it was conducted without organic acid field standards. During DC3 it was recognized there were quantifiable but uncalibrated signals at spectral locations attributed to $I^-(HFo)$ and $I^-(HAc)$ (Treadaway, 2015;

Treadaway et al. 2017). Post mission calibrations and calibrations during the FRAPPE field campaign with hydroperoxides provided an estimate of the CH_3I reagent concentration as evidence by $I^-(H_2O_2)$ and its trends with pressure and humidity (Fig. 8). The modeled trends in $I^-(H_2O_2)$ reinforce this and provide collaborative data supporting the extrapolation of the laboratory and FRAPPE HFo and HAc sensitivities to DC3 (Treadaway, 2015; Treadaway et al., 2017).

Many of the reaction rate coefficients used to model analyte cluster ion sensitivity trends with water vapor and pressure have been estimated by ourselves and others. This introduces uncertainties to the results but within the constraints of the calibration data. The reaction rate coefficient for reaction (38) is used as an example of the constraints placed on the rate of (38) in the context of reactions (38) - (41), the I^- hydrate reactions (17), (18), (78) - (81) and the inferred higher hydrate switching reactions (206) and (207). The estimated rate was $1.5\text{x}10^{-10}$ cm^3 $molec^{-1}$ s^{-1}. Doubling the rate constant for (38) led to a flattening of the linear trend in $I^-(HFo)$ sensitivity with water vapor at low water vapor mixing ratios and too sharp a peak at the maximum sensitivity. Halving the reaction rate coefficient for (38) excessively steepened the trend in $I^-(HFo)$ sensitivity with water vapor. The reaction rate coefficient for reaction (40) would have to exceed the bimolecular rate limit in order to increase the reaction rate coefficient for (39) and maintain the observed sensitivity trend. The same would also apply to reaction (206) needed to broaden the maximum in sensitivity in $I^-(HFo)$ at 10,000 ppm water vapor. The reaction rate coefficient for (38) could be reduced but would require proportionate reductions in the reaction rate coefficients for the linked reactions to maintain the modeled sensitivity trend. A halving or doubling was used for the purpose of illustration as this was within the range of uncertainty quoted for many of the measured reaction rate coefficients in the literature.

The model was further used to examine the potential for isobaric interference at m/z 80, where CH_3OOH is observed, and at m/z 66, a potential m/z for H_2O_2 (Table 1). Fig. 12a shows the predicted concentrations of $O_2^-(H_2O_2)$, ^{18}O of $NO_2^-(H_2O)$, $O_3^-(H_2O)$, and ^{18}O of $O_2^-(O_2)$ all of which would appear at m/z 66. The interference ion production pathways involving NO_2^-, NO_3^-, CO_3^-, O_3^-, and $O_2^-(O_2)$ are outlined in the Appendix, Table A4. Fig. 12b shows the predicted concentrations of $O_2^-(CH_3OOH)$, ^{18}O of $CO_3^-(H_2O)$, and $NO_3^-(H_2O)$, which would all be observed at m/z 80. The simulations assumed the ambient air contained NO, NO_2, HNO_3, H_2O_2, CH_3OOH, HFo and HAc at mixing ratios of 1 ppb for each. O_3 and CO_2 were assumed to be 50 ppb and 400 ppm, respectively. The ambient water vapor mixing ratio and sample pressure were varied from 10 to $3\text{x}10^5$ ppm and from 120 to 1013 hPa, respectively. Note that while reaction cell water vapor pressures from 1 to 10^5 ppm can be prescribed, the higher mixing ratios at the lower sample pressures simulated were unrealistic owing to the decrease in air temperature, maximum dew point temperature and consequent decrease in maximum air saturation vapor pressure with decreasing air pressure (increasing altitude). The dotted lines (left panel) indicate the contribution to m/z 66 from $O_3^-(H_2O)$ which was proportional to the O_3 mixing ratio but which passed through a maximum with respect to water vapor, increasing at lower humidities due to (19) and then decreasing at higher humidities due to (72). At the highest sample pressure, O_3=200 ppb yields a maximum predicated interference of ~1.6x10^6 A.U. at 2x10^3 ppm of water and was comparable to the predicted signal from 1 ppb H_2O_2. Increasing NO_2 to 100 ppb lead to a ^{18}O of $NO_2^-(H_2O)$ predicted interference comparable to the signal for 1 ppb H_2O_2. Note reductions in H_2O_2 mixing ratios increase the potential for interference by these other gases. ^{18}O of $O_2^-(O_2)$ is not predicted to be a significant interference at any of the pressures or humidities examined. The above discussion assumes PCIMS does not inherently discriminate between clusters due to instrumental factors.

The measurement of CH_3OOH at m/z 80 is predicted to suffer from interference by both ^{18}O of $CO_3^-(H_2O)$, and $NO_3^-(H_2O)$. O_3 through reaction sequence (8), (9), and (15) leads to the formation of $CO_3^-(H_2O)$ and a predicted inference was proportional to the O_3. The predicted interference as a function of H_2O mixing ratio passed through a maximum, increasing at first due to (15) and then decreasing due to (53). NO primarily through reactions with O_3^- or $O_2^-(H_2O)_{n\geq 1}$ produced NO_3^-, which went on to form a hydrate. The predicted $NO_3^-(H_2O)$ interference also passed through a maximum as a function of water vapor due to reactions (115) and (116). At reaction-cell water-vapor mixing ratios greater than a few hundred ppm, O_3 = 50 ppb and NO = 1 ppb gave predicted interference signals comparable to the signal from 1 ppb of CH_3OOH. In the DC3 project after research flight 12 and throughout FRAPPE, m/z 78 was monitored for $CO_3^-(H_2O)$ to ensure an ^{18}O isotope of this compound did not appreciably interfere in the measurement of CH_3OOH. Similarly, m/z 62, 78 and 98, corresponding to NO_3^-, $CO_3^-(H_2O)$ and $NO_3^-(H_2O)_2$ or ^{18}O of $CO_3^-(H_2O)_2$ were monitored to ensure $NO_3^-(H_2O)$ did not appreciably interfere in the CH_3OOH measurement. As above this assumes PCIMS does not inherently discriminate between clusters due to instrumental factors nor does it discriminate between the oxygen isotopic clusters of $CO_3^-(H_2O)$.

Currently, experimental kinetic data to examine the isobaric interferences for $I^-(HFo)$ and $I^-(HAc)$ by ethanol and propanol, methyl formate, or glycolaldehyde, respectively are unavailable. Treadaway (2015) and Treadaway et al. (2017) tested ethanol and 1-propanol and 2-propanol at very low and high water vapor conditions and found the sensitivity for $I^-(HFo)$ was 100 times that for $I^-(ethanol)$ and the sensitivity for $I^-(HAc)$ was 100 times that for I^- clustering with either 1- or 2-propanol. These relative sensitivities agreed with those predicted by Iyer (Pers. Comm., 2017) for HFo, HAc, ethanol and 2-propanol based upon their calculated binding energies with I^-.

In review, it was pointed out the model did not include the ion-neutral chemistry of organic compounds, specifically the potential for oxygen superoxide ion to abstract a proton from acetic acid and subsequently acetate ion to abstract a proton from weaker acids. Currently, the paucity of reaction rate coefficients for $O_2^- + organic$ reactions precludes their inclusion in our model. We must note, the potential exists for such chemistry to impact the simulations and we are unable to quantitatively assess their importance.

5 Conclusions

An ion-neutral chemical kinetic model is described and used to simulate the negative-ion chemistry occurring within a mixed-reagent ion chemical ionization mass spectrometer (CIMS). The model established a theoretical basis for investigation of ambient pressure (variable sample flow and reagent ion carrier gas flow rates), water vapor, ozone and oxides of nitrogen effects on ion-cluster sensitivities for hydrogen peroxide (H_2O_2), methyl peroxide (CH_3OOH), formic acid ($HCOOH$) and acetic acid (CH_3COOH). The model was builts with established mechanisms, thermodynamic data and reaction rate coefficients and these were augmented with additional reactions with estimated reaction rate coefficients. Some existing reaction rate coefficients were modified to enable the model to match laboratory and field campaign determinations of ion-cluster sensitivities as functions of CIMS sample flow rate and ambient humidity. Relative trends in sensitivity were compared as instrument specific factors preclude a direct calculation of instrument sensitivity. Predicted sensitivity trends and experimental sensitivity trends suggest the model captured the PCIMS reagent ion and cluster chemistry and reproduced observed trends in ion-cluster sensitivity with sample flow and humidity. The model was further used to investigate the potential for isobaric compounds as interferences in the measurement of the above species. For ambient O_3 mixing ratios more than 50 times those of H_2O_2, $O_3^-(H_2O)$ is predicted to be a significant isobaric interference to the measurement of H_2O_2 using $O_2^-(H_2O_2)$ at m/z 66. O_3 and NO give rise to species and cluster ions, $CO_3^-(H_2O)$ and $NO_3^-(H_2O)$, respectively, which interfere in the measurement of CH_3OOH using $O_2^-(CH_3OOH)$ at m/z 80. The $CO_3^-(H_2O)$ interference requires one of the O atoms to be the stable isotope ^{18}O. The model results indicate monitoring water vapor mixing ratio, m/z 78 for $CO_3^-(H_2O)$ and m/z 98 for isotopic $CO_3^-(H_2O)_2$ can be used to determine when ^{18}O of $CO_3^-(H_2O)$ interference is significant. Similarly, monitoring water vapor mixing ratio, m/z 62 for NO_3^- and m/z 98 for $NO_3^-(H_2O)_2$ can be used to determine when $NO_3^-(H_2O)$ interference is significant.

Acknowledgements: This research was supported through grants from the United States National Science Foundation: ATM-09222886 and ATM-1063467 (DWO) and ATM-1063463 (BGH) and a contract from the Colorado Department of Public Health and the Environment (BGH). We are indebted to S. Iyer (Dept. of Chemistry, University of Helsinki, Helsinki, Finland) for graciously sharing additional ab initio calculations cited in this manuscript. The authors thank D. Tanner, G. Huey, and R. Stickle (THS Instruments, LLC) for advice and patience. We thank the members of the DC3/SEACRS and FRAPPE/DISCOVER-AQ science teams and thank the NCAR-EOL Research Aviation Facility fight crew and staff for the quality of their data and for making the flight programs successful. Disclaimer: The manuscript has not been reviewed by the Colorado Department of Public Health and Environment. The scientific results and conclusions, as well as any views or

opinions expressed herein, are those of the author(s) and do not necessarily reflect the views of the Department or the State of Colorado.

References

Adams, N. G., Bohme, D. K., Dunkin, D. B., Fehsenfeld, F. C., and Ferguson, E. E.: Flowing afterglow studies of formation and reactions of cluster ions of O_2^+, O_2^- , and O^-, J. Chem. Phys., 52, 3133-3140, doi: 10.1063/1.1673449, 1970.

Albritton, D. L., Ion-neutral reaction-rate constants measured in flow reactors through 1977, Atom. Data Nucl. Data Tables, 22, 1-101, 1978.

Arshadi, M. and Kebarle, P.: Hydration of OH^- and O^- in the gas phase. comparative solvation of OH^- by water and the hydrogen halides: effects of acidity, J. Phys. Chem., 74, 1483-1485, 1970.

Baasandorj, M., Millet, D. B., Hu, L., Mitroo, D., and Williams, B. J.: Measuring acetic and formic acid by proton-transfer-reaction mass spectrometry: sensitivity, humidity dependence, and quantifying interferences, Atmos. Meas. Tech, 8, 1303-1321, doi:10.5194/amt-8-1303-2015, 2015.

Bartmess, J.E.: "Negative Ion Energetics Data" in NIST Chemistry WebBook, NIST Standard Reference Database Number 69, Eds. P. J. Linstrom and W. G. Mallard, National Institute of Standards and Technology, Gaithersburg MD, 20899, http://webbook.nist.gov, retrieved August 19, 2016.

Barth, M. C., and 47 others: The Deep Convective Clouds and Chemistry (DC3) field campaign, Bull. Amer. Meteor. Soc., 96, 1281-1309, 2015.

Böhringer, H., Fahey, D. W., Fehsenfeld, F. C., and Ferguson, E. E.: Bond energies of the molecules H_2O, SO_2, H_2O_2, and HCl to various atmospheric negative ions, J. Chem. Phys., 81, 2805-2810, doi: 10.1063/1.447953, 1984.

Cappa, C. D. and Elrod, M. J.: A computational investigation of the electron affinity of CO_3 and thethermodynamic feasibility of $CO_3^-(H_2O) + ROOH$ reactions, Phys. Chem. Chem. Phys., 3, 2986-2994, doi: 10.1039/b102981a, 2001.

Crounse, J. D., McKinney, K. A., Kwan, A. J., and Wennberg, P. O.: Measurement of gas-phase hydroperoxides by chemical ionization mass spectrometry, Anal. Chem. 78, 6726–6732, 2006.

de Gouw, J. and Warneke, C.: Measurements of volatile organic compounds in the Earth's atmosphere using proton-transfer reaction mass spectrometry, Mass Spectrom. Rev., *26*, 223–257, 2007.

Dotan, I., Davidson, J. A., Streit, G. E., Albritton, D. L., and Fehsenfeld, F. C., A study of the reaction $O_3^- + CO_2 \rightarrow CO_3^- + O_2$ and its implication on the thermochemistry of CO_3 and O_3 and their negative ions, J. Chem. Phys., 67, 2874-2879, doi: 10.1063/1.435155, 1977.

Fahey, D.W., Böhringer, H., Fehsenfeld, F.C., and Ferguson, E. E.: Reaction rate constants for $O_2^-(H_2O)_n$ ions n = 0 to 4, with O_3, NO, SO_2, and CO_2, J. Phys. Chem., 76, 1799-1805, doi: 10.1063/1.443220, 1982.

Fehsenfeld, F. C., Schmeltekopf, A. L., Schiff, H. I., and Ferguson, E. E.: Laboratory measurements of negative ion reaction of atmospheric interest, Planet. Space Sci., 15, 373-379, 1967.

Fehsenfeld, F. C., Ferguson, E. E., and Bohme, D. K.: Additional flowing afterglow measurements of negative ion reactions of D-region interest, Planet. Space Sci., 17, 1759-1762, 1969.

Fehsenfeld, F. C. and Ferguson, E. E.: Laboratory studies of negative ion reactions with atmospheric trace constituents, 3181-3193, doi: 10.1063/1.1682474, 1974.

Fehsenfeld, F.C., Howard, C.J., and Schmeltekopf, A.L.: Gas phase ion chemistry of HNO3, J. Chem. Phys., 63, 2835 - 2841, doi: 10.1063/1.431722, 1975.

Goldsmith, C.F., Magoon, G. R., and Green, W. H.: Database of small molecule thermochemistry for combustion, J. Phys. Chem. A, 116, 9033-9057, 2012.

Grimsrud, E.P.: Gas-phase ion chemistry within the electron capture detector, Mass Spectrom. Rev., 10, 457-489, doi:10.1002/mas.1280100602, 1991.

Hiraoka, K. and Yamabe, S.: Formation of the chelate bonds in the cluster $O_2^-(CO_2)_n$, $CO_3^-(CO_2)_n$, and $NO_2^-(CO_2)_n$, J. Chem. Phys., 97, 643-650, doi:10.1063/1.463560, 1992.

Huertas, M. L., Fontan, J., Gonzalez, J.: Evolution times of tropospheric negative ions, Atmos. Environ., 12, 2351-2362, 1978.

Ikezoe, Y., Matsuoka, S., Takebe, M., and Viggiano, A.A.: Gas phase ion-molecule reaction rate constants through 1986, Ion Reaction Research Group of The Mass Spectroscopy Society of Japan, Tokyo, 1987.

Iyer, S., Lopez-Hilfiker, F., Lee, B. H., Thornton, J. A., and Kurtén, T.: Modeling the detection of organic and inorganic compounds using iodide-based chemical ionization, J. Phys. Chem. A, 120, 576−587, doi: 10.1021/acs.jpca.5b09837, 2016.

Kawamoto, H. and Ogawa, T.: First model of negative ion composition in the troposphere, Planet Space Sci., 34, 1229 – 1239, 1986.

Kazil, J.: The University of Bern atmospheric ion model: time-dependent ion modeling in the stratosphere, mesosphere and lower thermosphere, Ph.D. Thesis, University of Bern, Bern, Switzerland, 2002.

Kebarle, P., French, M., and Payzant, J. D.: Reaction mechanisms and bonding energies for ion-hydrates (ion-water clusters) of ionospheric interest, in: Aeronomy Report No. 48, COSPAR Symposium on D- and E-Region Ion Chemistry - An Informal Record, Eds. C. F. Sechrist, Jr., and M.A. Geller, University of Illinois at Urbana-Champaign, Urbana, IL, 1972.

Kovács, T., Plane, J. M. C., Feng, W., Nagy, T., Chipperfield, M. P., Verronen, P. T., Andersson, M. E., Newnham, D. A., Cliverd, M. A., and Marsh, D. R.: D-region ion–neutral coupled chemistry (Sodankylä Ion Chemistry, SIC) within the Whole Atmosphere Community Climate Model (WACCM 4) –WACCM-SIC and WACCM-rSIC, Geosci. Model Dev., 9, 3123-3136, doi: 10.5194/gmd-9-3123-2016, 2016.

Le Breton, M., McGillen, M. R., Muller, J. B. A., Bacak, A., Shallcross, D.E., Xiao, P., Huey, L. G., Tanner, D., Coe, H., and Percival, C. J.: Airborne observations of formic acid using a chemical ionization mass spectrometer, Atmos. Meas. Tech., 5, 3029-3039, 2012.

Lee, B. H., Lopez-Hilfiker, F. D., Mohr, C., Kurtén, T., Worsnop, D. R., and Thornton, J. A.: An iodide-adduct high-resolution time-of-flight chemical-ionization mass spectrometer: application to atmospheric inorganic and organic compounds, Environ. Sci. Tech., 48, 6309-6317, doi: 10.1021/es500362a, 2014.

McDonald, R.N. and Chowdhury, A.K.: Gas-phase ion-molecule reactions of dioxygen anion radical (O2-), J. Am. Chem. Soc., 107, 4123 -4128, 1985.

Messer, B. M., Stielstra, D. E., Cappa, C. D., Scholtens, K. W., and Elrod, M. J.: Computational and experimental studies of chemical ionization mass spectrometric detection techniques for atmospherically relevant peroxides, Intl. J. Mass Spect., 197, 219-235, 2000.

Mohnen, V. A.: Negative ions in air-like gas mixtures, P. Appl. Geophys., 100, 123-132, 1972.

Mohnen, V. A.: Formation, nature, and mobility of ions of atmospheric importance, 5th Intl. Conf. on Atmos. Elect., Garmisch Partenkirchen, Germany, 2-7 September, 1974.

Morris, R.A.: Gas-phase reactions of oxide and superoxide anions with CF4, CF3Cl, CF3Br, CF3I, and C2F4 at 298 and 500 K, J. Chem. Phys., 97, 2372 – 2381, doi: 10.1063/1.463941, 1992.

O'Sullivan, D. W., Silwal, I. K. C., McNeill, A. S., Treadaway, V., and Heikes, B. G.: Quantification of gas phase hydrogen peroxide and methyl hydroperoxide in ambient air: Using atmospheric pressure chemical ionization mass spectrometry with O_2^-, $O_2^-(CO_2)$ reagent ions, submitted to: Int'l. J. Mass Spectrom., 2017.

Pack, J. L. and Phelps, A. V.: Electron attachment and detachment II. Mixtures of O_2 and CO_2 and O_2 and H_2O, J. Chem. Phys., 45, 4316-4329, 1966.

Payzant, J. D. and Kebarle, P.: Kinetics of reactions leading to $O_2^-(H_2O)_n$ in moist oxygen, J. Chem. Phys., 56, 3482, doi: 10.1063/1.1677723, 1972.

Popov, N. A.: Evolution of the negative ion composition in the afterglow of a streamer discharge in air, Plasma Physics Reports, 36, 812–818, 2010, translated from Fizika Plazmy, 36, 867–873, 2010.

Slusher, D. L., Huey, L. G. Tanner, D. J., Flocke, F. M., and Roberts, J. M.: A thermal dissociation-chemical ionization mass spectrometry (TD-CIMS) technique for the simultaneous measurement of peroxyacyl nitrates and dinitrogen pentoxide, J. Geophys. Res., 109, D19315, doi:10.1029/2004JD004670, 2004.

St. Clair, J. M., McCabe, D. C., Crounse, J. D., Steiner, U., and Wennberg, P. O.: Chemical ionization tandem mass spectrometry for the in-situ measurement of methyl hydrogen peroxide, Rev of Sci. Instr., 81, doi: 941021-941026, 2010.

Streit, G.E.: Gas-phase reactions of O- and O2- with a variety of halogenated compounds, J. Phys. Chem., 86, 2321-2324, 1982.

Treadaway, V.: Measurement of formic and acetic acid in air by chemical ionization mass spectroscopy: airborne method development, MS Thesis, University of Rhode Island, Kingston, RI, available at: http://digitalcommons.uri.edu/theses/603/, 82 pp, 2015.

Treadaway, V., Heikes, B.G., McNeill, A. S., Silwal, I. K. C., and O'Sullivan, D. W.: Measurement of formic acid, acetic acid, hydrogen peroxide, and methyl peroxide in air by chemical ionization mass spectroscopy: airborne method development, submitted to: Atmos. Meas. Tech., 2017.

Turunen, E., Matveinen, H., Tolvanen, J., and Ranta, H.: D-region ion chemistry model, STEP Handbook of ionospheric models, SCOSTEP Secretariat, Boulder, Colorado, 1996.

UCAR/NCAR - Earth Observing Laboratory. NSF/NCAR Hercules C130 Aircraft. UCAR/NCAR - Earth Observing Laboratory. https://doi.org/10.5065/D6WM1BG0 Retrieved December 20, 2016, 1994.

UCAR/NCAR - Earth Observing Laboratory. NSF/NCAR GV HIAPER Aircraft. UCAR/NCAR - Earth Observing Laboratory. https://doi.org/10.5065/D6DR2SJP Retrieved December 14, 2016, 2005.

Veres, P., Roberts, J.M., Warneke, C., Welsh-Bon, D., Zahniser, M., Herndon, S., Fall, R., de Gouw, and J.: Development of Negative-Ion Proton-Transfer Chemical-Ionization Mass Spectrometry (NI-PT-CIMS) for the Measurement of Gas-Phase Organic Acids in the Atmosphere, Int. J. Mass Spectrom., doi:10.1016/j.ijms.2008.04.032, 2008.

Williams, S., Campos, M. F., Midey, A. J., Arnold, S. T., Morris, R. A. and Viggiano, A. A.: Negative ion chemistry of ozone in the gas phase, J. Phys. Chem. A, 106, 997-1003, 2010.

Table 1: PCIMS m/z for species clusters of interest and potential isobaric interfering ions or ion clusters at the mass resolution of the quadrupole mass selector.

m/z	Ion or ion-neutral cluster$^{\#}$
50	$O_2^-(H_2O)$, ^{18}O of O_3^-
60	CO_3^-
62	NO_3^-, ^{18}O of CO_3^-
66	**$O_2^-(H_2O_2)$**, ^{18}O of $NO_2^-(H_2O)$, $O_3^-(H_2O)$, ^{18}O of $O_2^-(O_2)$
76	$O_2^-(CO_2)$
78	$CO_3^-(H_2O)$, ^{18}O of $O_2^-(CO_2)$
80	**$O_2^-(CH_3OOH)$**, $NO_3^-(H_2O)$, ^{18}O of $CO_3^-(H_2O)$, $NO_2^-(H_2O_2)$, ^{18}O of O_2^-(HFo), $O_2^-(CH_2(OH)_2)$
83	**$O_2^-(CD_3OOH)$**
110	**$O_2^-(CO_2)(H_2O_2)$**
147	$I^-(H_2{}^{18}O)$
161	**$I^-(H_2O_2)$**, $I^-({}^{18}O{}^{16}O)$
173	**I^-(HFo)**, I^-(EtOH), $I^-(C^{18}O^{16}O)$
175	I^-**(CH_3OOH)**, $I^-(CH_2(OH)_2)$, $I^-(O_3)$
187	**I^-(HAc)**, I^-(MeFo), I^-(PrOH), I^-(2-PrOH), I^-(GA),

$^{\#}$**boldface** indicates a primary PCIMS analyte ion cluster mass; ”^{18}O of “ indicates one of the ion cluster’s oxygen atoms is a mass 18 isotope of oxygen; in CD_3OOH the D represents deuterium atoms; EtOH refers to ethanol, PrOH refers to 1-propanol, 2-PrOH refers to 2-propanol; $CH_2(OH)_2$ refers to methane-diol; MeFo refers to methyl formate; GA refers to hydroxy acetaldehyde (aka. glycolaldehyde).

Table 2: Initial reagent gas flow rates and reagent gas mixing ratios at six sample air pressures.

Sample Pressure, hPa[1]	120	180	306	600	800	1013
N_2 flow rate, slpm[2]	4.27	4.23	3.98	2.99	2.58	2.05
CO_2 in air flow rate, slpm	0.08	0.08	0.08	0.08	0.08	0.08
CH_3I in N_2 flow rate, slpm	0.0005	0.0005	0.0005	0.0005	0.0005	0.0005
CH_3I, ppb[3]	0.575	0.580	0.616	0.814	0.939	1.174
CO_2 ppm[4]	7.36	7.42	7.88	10.42	12.02	15.02
O_2 ppm	3678	3712	3941	5212	6015	7512
N_2, ppm	996322	996288	996059	994788	993866	992488

[1] pressure in hPa (hecto-Pascal, equivalent to milli-bars).

[2] slpm, standard liters per minute (T_{ref} = 0 °C; P_{ref} = 1013.25 hPa).

[3] ppb, parts per billion (molecular mixing ratio times 10^9).

[4] ppm, parts per million (molecular mixing ratio times 10^6).

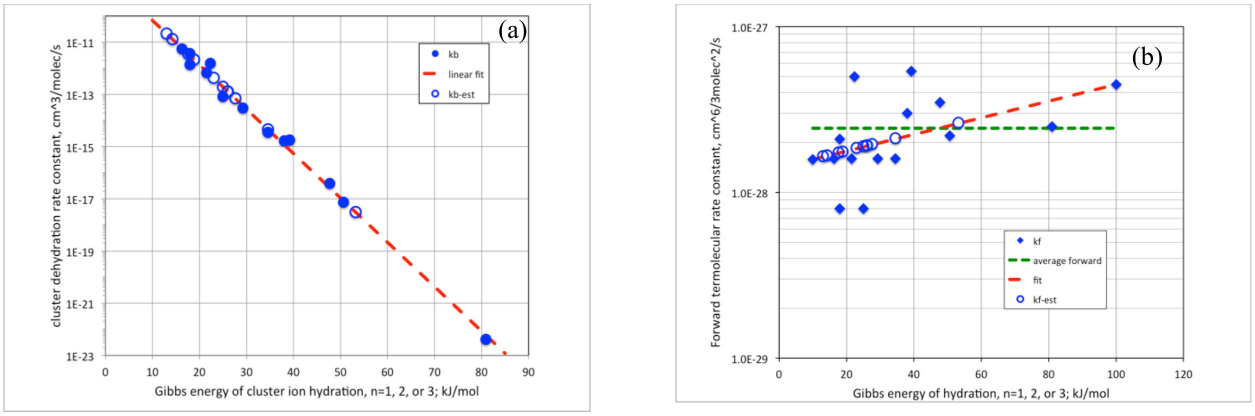

Figure 1: Ion-cluster dehydration (a) and hydration (b) reaction rate coefficients plotted as a function of the Gibbs reaction energy ($\triangle G^{o}_{rxn}$) for I^-, O_2^-, O_3^-, CO_3^-, HO^-, NO^-, NO_2^-, and NO_3^- ions for n=1-3 water molecules. Solid circles are reported rate coefficients from the literature (see text) and open circles are estimates based upon linear regression of $\ln(k_{dehydration})$ versus $\triangle G^{o}_{rxn}$ or $k_{hydration} = k_{dehydration} \times K_{eq}$.

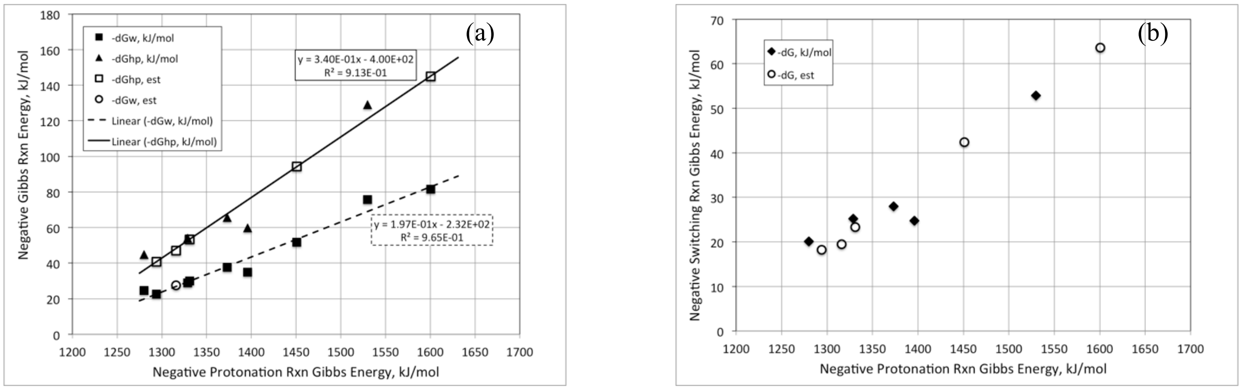

Figure 2: Relationship between the ion-protonation reaction Gibbs energy, $-\Delta G^{\circ}_{R4}$, and (a) ion-hydration reaction Gibbs energy, $-\Delta G^{\circ}_{R1}$, and ion-H_2O_2 cluster reaction Gibbs energy, $-\Delta G^{\circ}_{R2}$, or (b) H_2O and H_2O_2 switching reaction Gibbs energy, $-\Delta G^{\circ}_{R3}$. R1-R4 refer to reactions introduced in the text with $A = H_2O_2$. **Filled symbols denote measured values and open symbols indicate estimated values. The lines indicate least square linear regression fits with the regression constants and coefficient of determination given in the respective boxes. The use of negative values of the Gibbs energy of reaction follows NIST (Bartmess, 2016) nomenclature.**

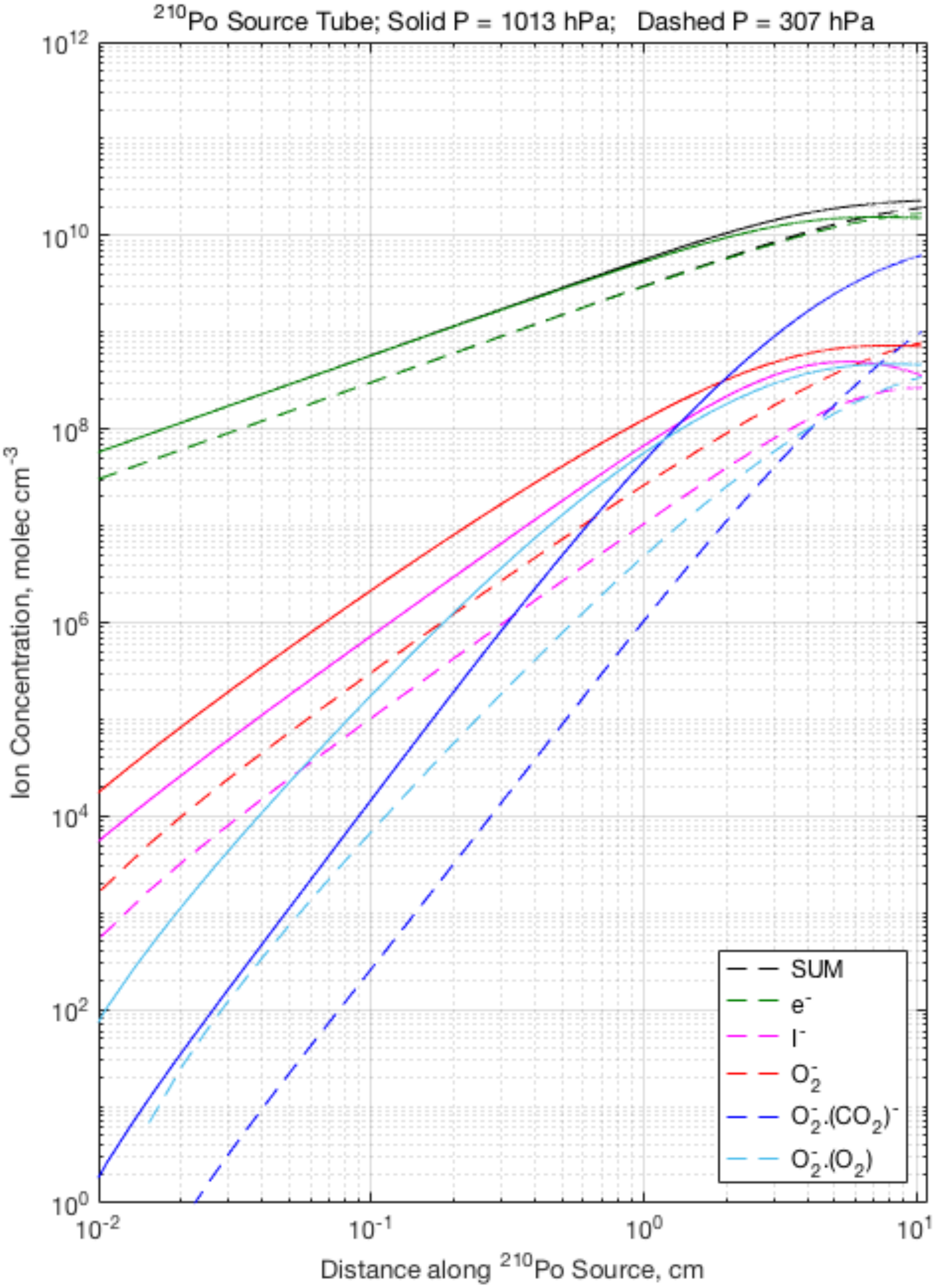

Figure 3: Ion densities – arbitrary units – along the ^{210}Po source tube for flow conditions of 307 hPa ambient pressure (dashed lines) and 1013 hPa (solid lines). The predominant ion after e^- is $O_2^-(CO_2)$ and I^- is the smallest.

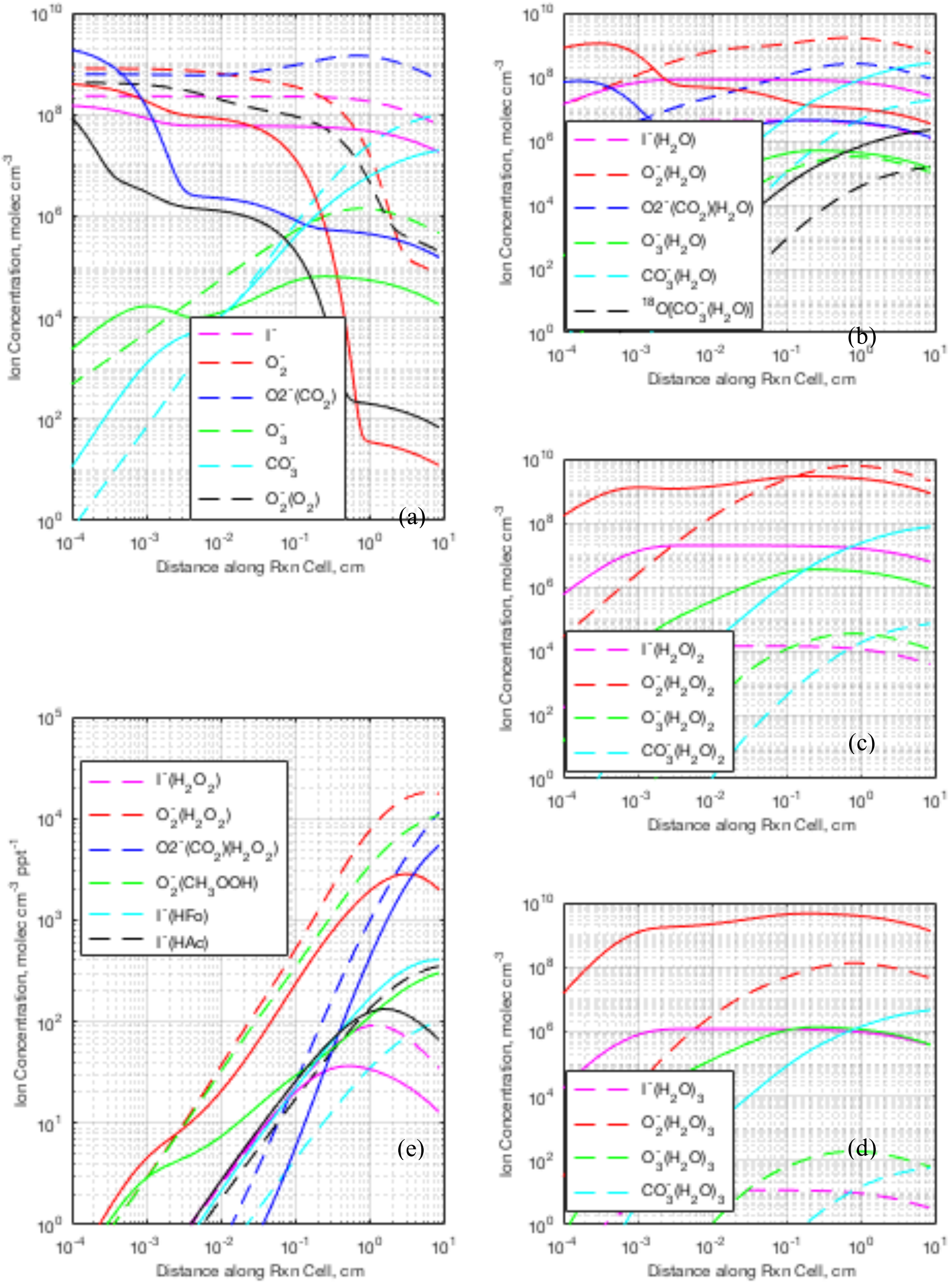

Figure 4: Simulated ion-cluster densities along the reaction cell path for ambient pressure of P_a=307 hPa and reaction cell H_2O=133 ppm (dashed line) or P_a=1013 hPa and reaction cell H_2O=9706 ppm (solid line). Ambient O_3 was set equal to 50 ppb for both pressures. Reaction cell time of transit is t_x=17.8 ms. (a) Unhydrated reagent ion density. (b) First-hydrate reagent ion density. (c) Second-hydrate reagent ion densities. (d) Third-hydrate reagent ion densities. (e) Ion-analyte cluster ion density– arbitrary units.

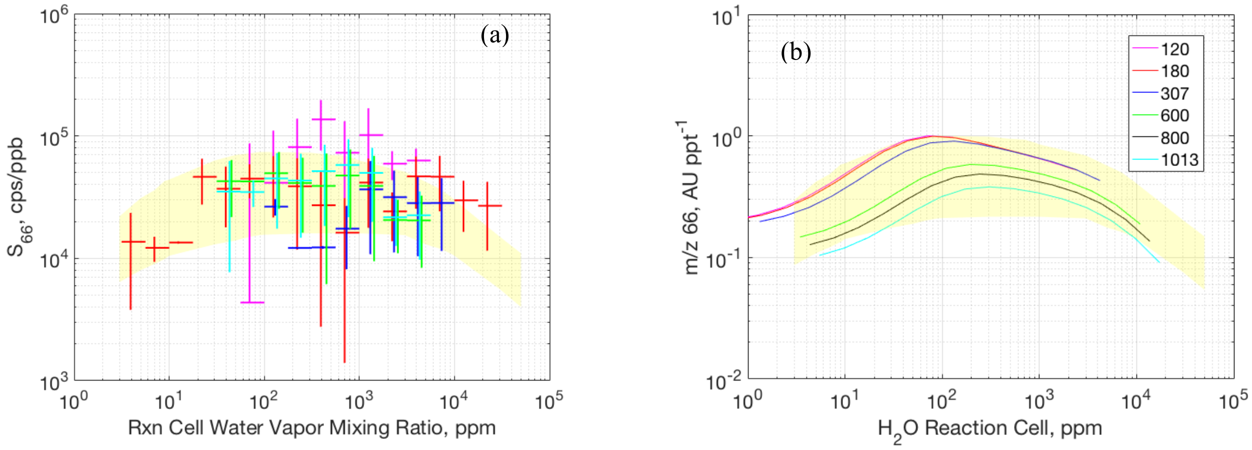

Figure 5: (a) Experimental sensitivity (counts per second per ppb, cps/ppb) trend in $O_2^- \cdot (H_2O_2)$ as a function of reaction cell water vapor mixing ratio (χ_{H_2O}, ppm), from DC3 (red), FRAPPE (blue), and the laboratory [$F_{CH_3I} = 0.0005$ (cyan) and 0.001 (green) slpm]. All calibrations were binned by χ_{H_2O} and bin widths are shown by the horizontal lines. Vertical bars indicate one standard deviation of a bin and includes sample pressure variation effects, water variation within a bin, precision of the standard addition calibration gas concentration, instrument precision and ambient mixing ratio variation across the standard addition period. There were fewer than 4 observations per bin in FRAPPE for water vapor mixing rations less than 10^3 ppm. Magenta crosses in (a) correspond to DC3 post mission calibrations without the addition of CH_3I and after there had been multiple refills of the reagent CO_2 in air bottle. (b) normalized simulated sensitivity as a function of χ_{H_2O} for 6 different sample pressures as shown in the legend. The yellow shading maps the trends in experimental sensitivity (a) to the calculated trends in sensitivity (b) using the same normalization process.

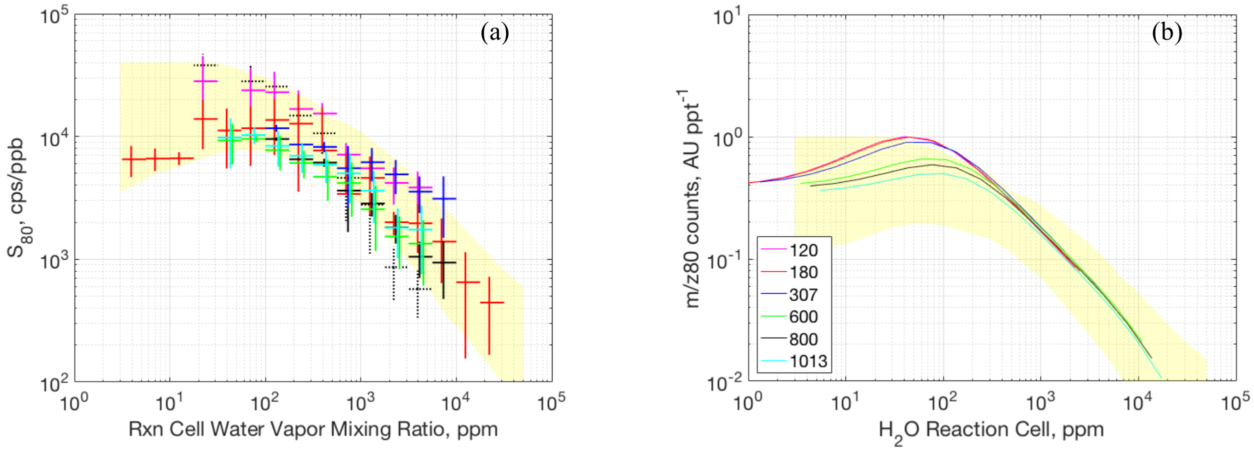

Figure 6: Same as Fig. 5 except for $O_2^-(CH_3OOH)$.

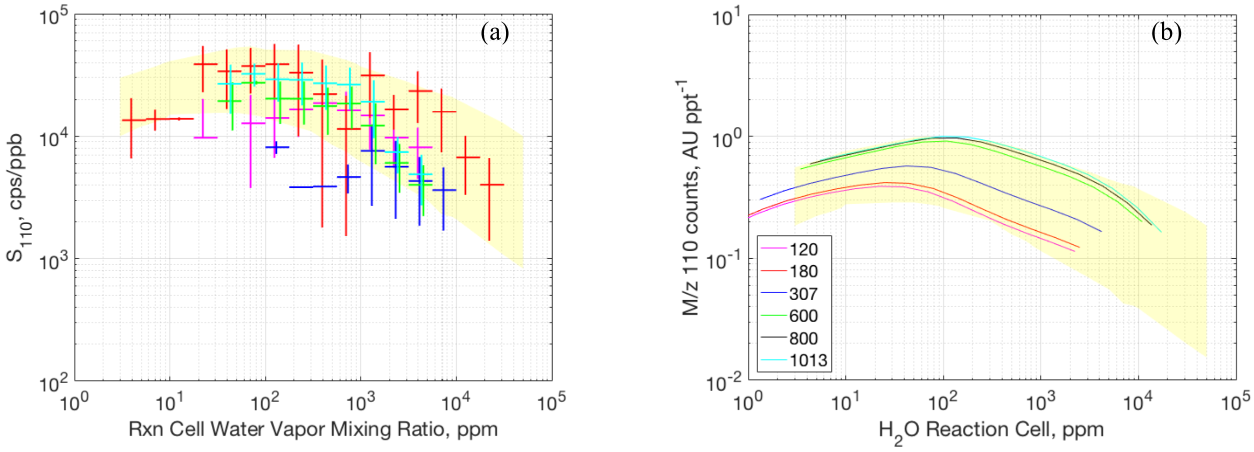

Figure 7: Same as Fig. 5 except for $O_2^-(CO_2)(H_2O_2)$.

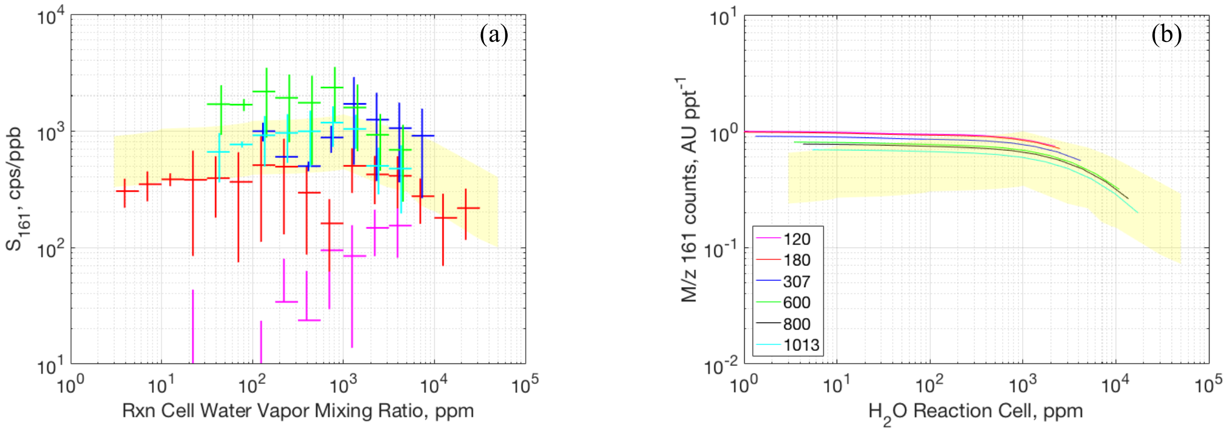

Figure 8: Same as Fig. 5 except for $I^-(H_2O_2)$. Magenta crosses in the left panel correspond to DC3 post mission calibrations without the addition of CH_3I; there had been multiple refillings of the reagent CO_2 in air bottle and the CH_3I reagent gas concentration is presumed to be very small.

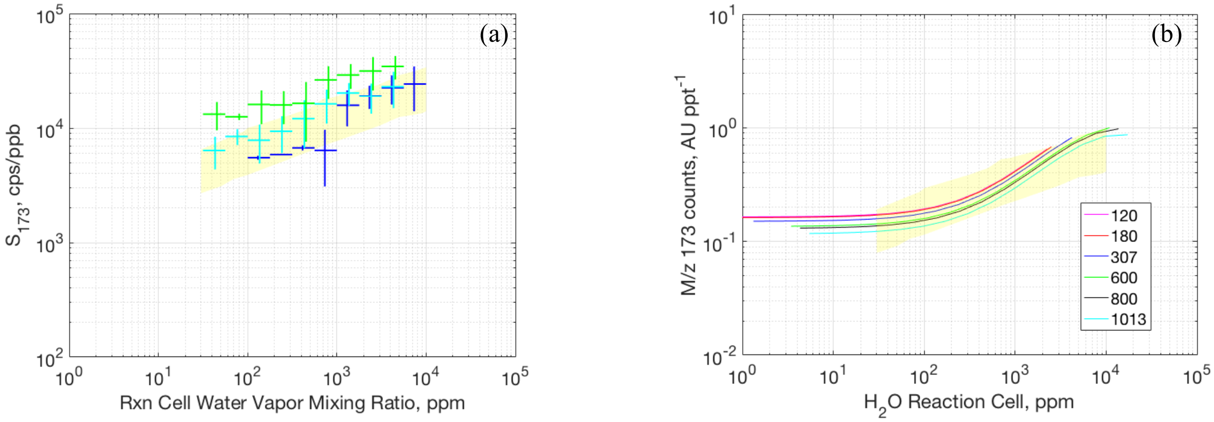

Figure 9: Same as Fig. 5 except for I^-(HFo). Field calibrations for HFo were not performed in DC3.

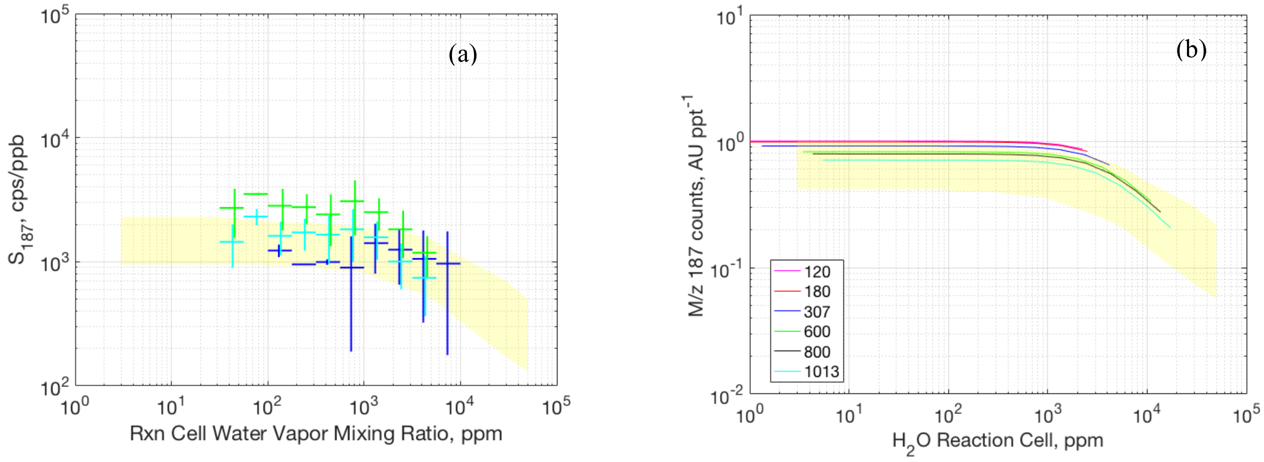

Figure 10: Same as Fig. 9 except for I⁻(HAc). Field calibrations for HAc were not performed in DC3.

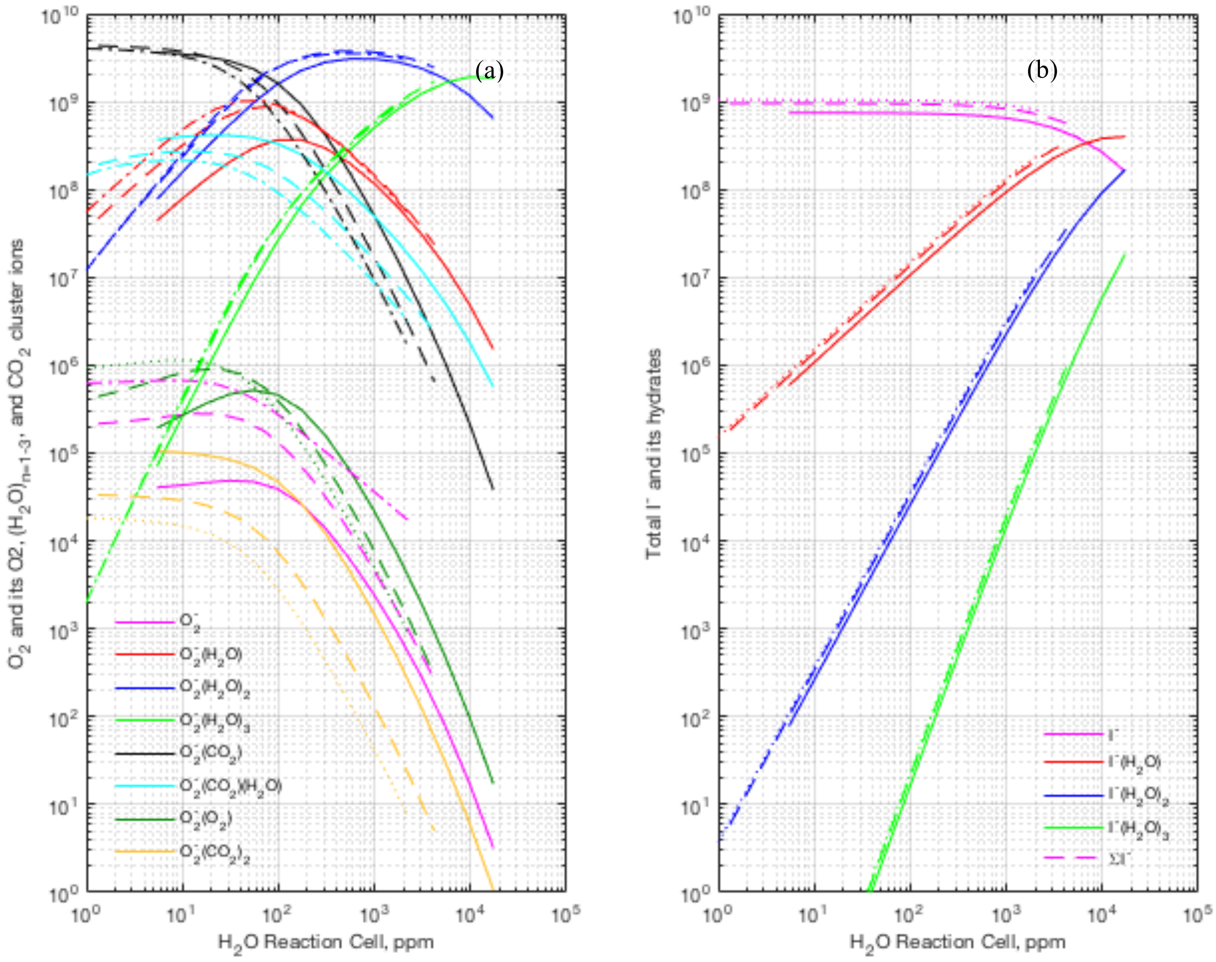

Figure 11: (a) Oxygen anion speciation: O_2^-, $O_2^-(H_2O)_{n=1,3}$, $O_2^-(CO_2)_{n=1,2}$, $O_2^-(CO_2)(H_2O)$ and $O_2^-(O_2)$, as a function of water vapor at sample pressures of 120 (dotted), 300 (dashed) and 1013 (solid) hPa. (b) As in left panel except for iodide speciation: I^-, $I^-(H_2O)$, $I^-(H_2O)_2$ and $I^-(H_2O)_3$.

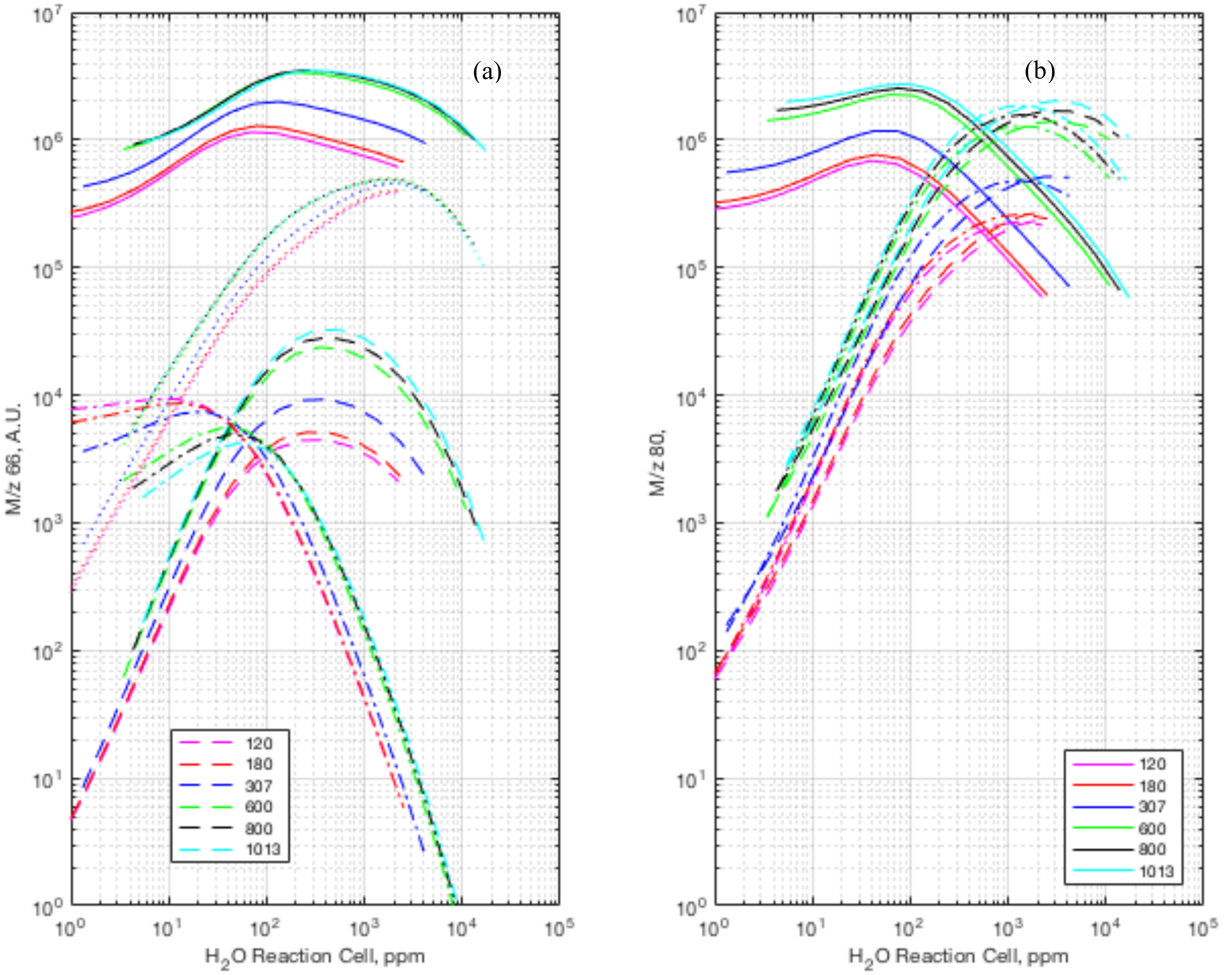

Figure 12: (a) Predicted ion cluster concentrations for species having m/z equal to 66: $O_2^-(H_2O_2)$ solid lines, ^{18}O of $NO_2^-(H_2O)$ dashed lines, $O_3^-(H_2O)$dotted lines, and ^{18}O of $O_2^-(O_2)$ dash-dot lines, for 6 sample pressures (hPa) indicated by color as given in the legend. (b) Predicted ion cluster concentrations for species having m/z equal to 80: $O_2^-(CH_3OOH)$ solid lines, ^{18}O of $CO_3^-(H_2O)$ dashed lines, and $NO_3^-(H_2O)$ dash-dot lines, for 6 sample pressures (hPa) indicated by color as given in the legend. See text for sample air flow rate and composition and reagent gas composition used in the simulation.

Appendix

A1. Instrument Details

The PCIMS instrument is shown schematically in Fig. A1 from the sample inlet to the exhaust. It was manufactured by THS Instruments, LLC (Atlanta, Georgia). The instrument consists of five separate chambers: a sample entrance chamber (labeled *Split*), a reaction drift tube (*RXN cell*), a collision dissociation chamber (*CDC*), main chamber (*Main*), and the quadrupole and detector chamber (*Quad*). The entrance section allows for excess sample flow through the transfer plumbing from a sample's origin to minimize wall surface artifacts. In an aircraft, the sample probe and transfer line were heated to 35 and 70 ^{o}C during DC3 and FRAPPE, respectively. The higher temperature in FRAPPE was used because of a ground contamination problem. The sample stream is split with the fraction entering the PCIMS reaction cell (RXN Cell) determined by a 0.51 mm critical orifice; the high-pressure side was set by the sample inlet pressure and the low-pressure side fixed at 22.4 hPa. The excess flow rate is regulated by an MKS Instruments (Andover, MA) 0-30 slpm mass flow controller (not shown). The reagent gas stream dynamically blends three gas streams: ultra-high purity N_2 (Scott-Marrin, Riverside, CA), 400 ppm CO_2 in ultra-high purity air (Scott-Marrin, Riverside, CA) and 5 ppm CH_3I in ultrahigh purity N_2. These flows are regulated using MKS mass flow controllers (not shown). Representative reagent gas flow rates and mixing ratios for different sample air pressures are listed in Table 2. The total flow through the RXN cell is 4.68 slpm and the sample flow rate can be determined by subtraction of the reagent gas flow rates from the total flow; for example, at a sample pressure of 600 hPa, the sample flow rate was 1.61 slpm. Ions are generated by passing the reagent gas stream through a commercially available Nuclecel Ionizer (Model P2031-1000, NRD LLC., Grand Island, NY), containing an α-emitter, ^{210}Po, with an initial activity of 20 milli-curie. The reagent ion stream is mixed at a right angle to the sample air stream, approximately 12 mm downstream from the sample entrance orifice and 82 mm before the RXN cell to CDC chamber (collision dissociation chamber) and a pumped second port for dumping the bulk of the RXN cell reagent-sample gas stream. The RXN-to-CDC critical orifice diameter is 0.81 mm and with a high-pressure side at 22.4 hPa and a low-pressure side at 0.61 hPa, has a nominal flow rate of 0.11 slpm (http://www.tlv.com/global/TI/calculator/air-flow-rate-through-orifice.html) assuming a discharge coefficient of 1.0. The voltage on the CDC plate is -2.0 V. The PCIMS has two THS Instruments, LLC. octopole ion lenses; one set is in the CDC (DC bias voltage = 20 V, RF voltage = 2 V) and the other is in the main chamber after the CDC (DC bias voltage = 2.49 V, RF voltage = 0.04 V). The CDC plate and first octopole voltages regulated collision energy between molecules and the cluster ions and were used to fragment weakly bound clusters. These voltages were manual adjusted to improve the signal-to-noise ratio at the m/zs of interest. The second octopole acts to focus the ions onto the entrance of the quadrupole mass selector (Extrel 19 mm rod quadrupole, controlled by an Extrel QC-150 oscillator at 2.1 MHz and a THS Instruments control board), and the ions at a selected m/z are counted by a channeltron detector (rear plate at 3.43 kV and front plate at 1.51 kV). The pressures in the CDC and at the main chamber octopole and quadrupole chamber were 0.61, 0.0065, and 0.00011 hPa, respectively. There are two more critical orifices which separate the CDC and the main chambers, 2.08 mm, and the main and quadrupole chambers, 2.57 mm. The nominal flow rates through these orifices are 19 and 1.3 sccm (standard cubic centimeters per second), respectively. From a mechanical perspective, 0.03% of the total flow through the RXN cell enters the quad chamber. The above instrument settings were used throughout the DC3, laboratory, FRAPPE and post FRAPPE laboratory and field work.

The m/z range of the quadrupole filter is 1-500 m/z. The PCIMS controller software provides two modes of mass selection: "hop" and "scan." In scan mode, lower and upper m/z limits, a m/z step size and the dwell time at a m/z step are defined. The smallest step size is 0.3 m/z. A typical dwell time for a scan is 50 ms. In hop mode, a variable number of fixed m/z values can be selected at an increment of 0.05 m/z. The dwell time at each fixed m/z can also be specified. In practice with the Channeltron detector rear plate at 3.43 kV and front plate at 1.51 k, the software-hardware range limits are nominally 0 to $2x10^6$ cps (counts per second) or for a 50 ms dwell time, 0 to 10^5 counts. Random "dark" count noise in 50 ms was <<1 count or <<20 cps. The practical mass resolution of the quadrupole and detector was 1.0 m/z. This was defined as the average of the full-width at half-height of the calibration peaks for $O_2^-(H_2O_2)$, $O_2^-(CH_3OOH)$, $O_2^-(HFo)$, $O_2^-(HAc)$, $O_2^-(CO_2)(H_2O_2)$, $I^-(H_2O)$, $I^-(H_2O_2)$, $I^-(HFo)$, and $I^-(HAc)$ at 66, 78, 80, 92, 110, 145, 161, 173, and 187 m/z, respectively, and determined using a scan step size of 0.3 m/z (mode = 0.9; range 0.9-1.2; n=9) during a HP, MHP, HFo and HAc calibration. Treadaway et al. (2017) showed the full scan from 40 to 190 m/z.

Three schemes were employed to develop calibration mixing ratios. In the laboratory and in flight, a syringe based systems inject $<10^{-9}$ m^3 per min. of an aqueous solution containing the species of choice in to a N_2 carrier stream. This flow is constantly on. Just prior to the CIMS inlet the flow is normally diverted to waste by a "drawback" flow. This flow is turned off when calibration gas is added in to the sample stream - "standard addition". In the laboratory, two Henry's Law equilibration coils with concurrent flows of an aqueous solution containing the species of choice and an ultrahigh purity air stream as carrier. The coils are immersed in a temperature controlled water bath. These systems are show as block diagrams in Fig. A2.

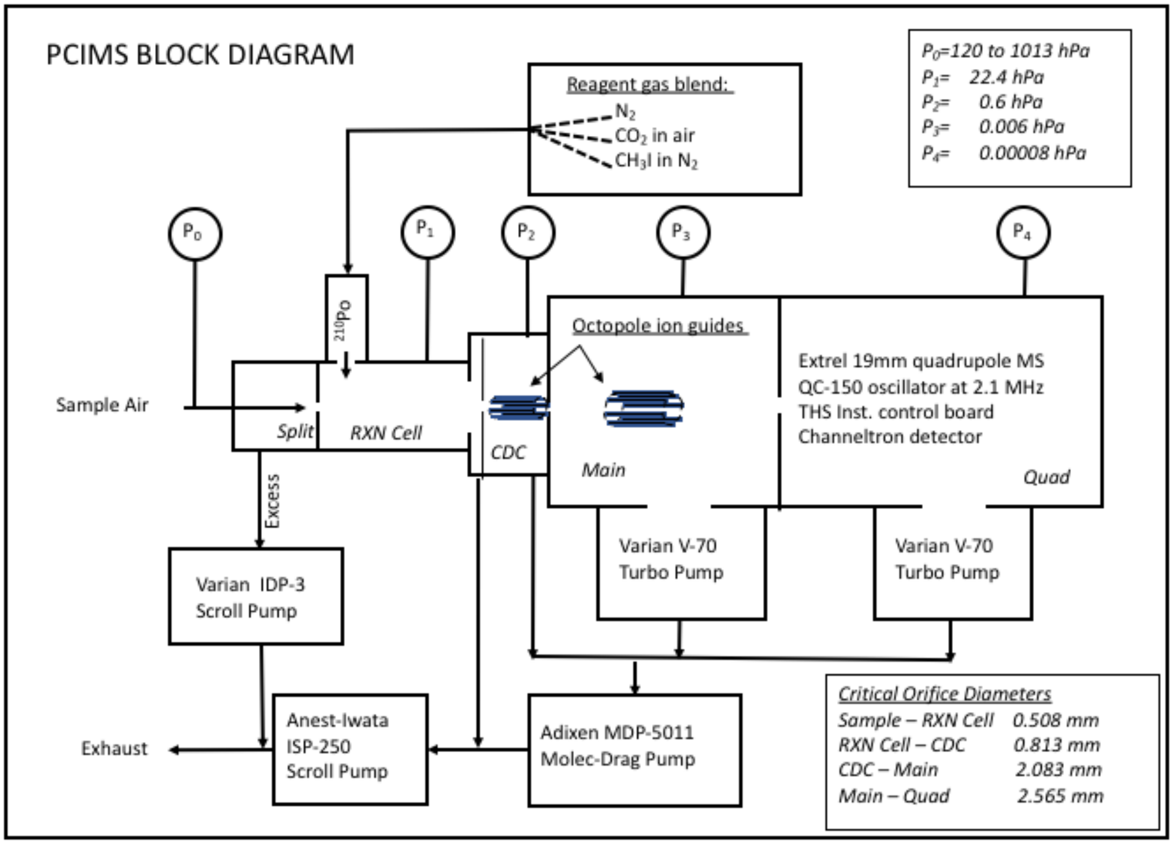

Figure A1: **Block schematic of the PCIMS instrument as used on the aircraft and in the laboratory, mass flow controllers are not shown. After Slusher et al. (2004), Le Breton et al. (2012), O'Sullivan et al. (2017) and Treadaway et al. (2017).**

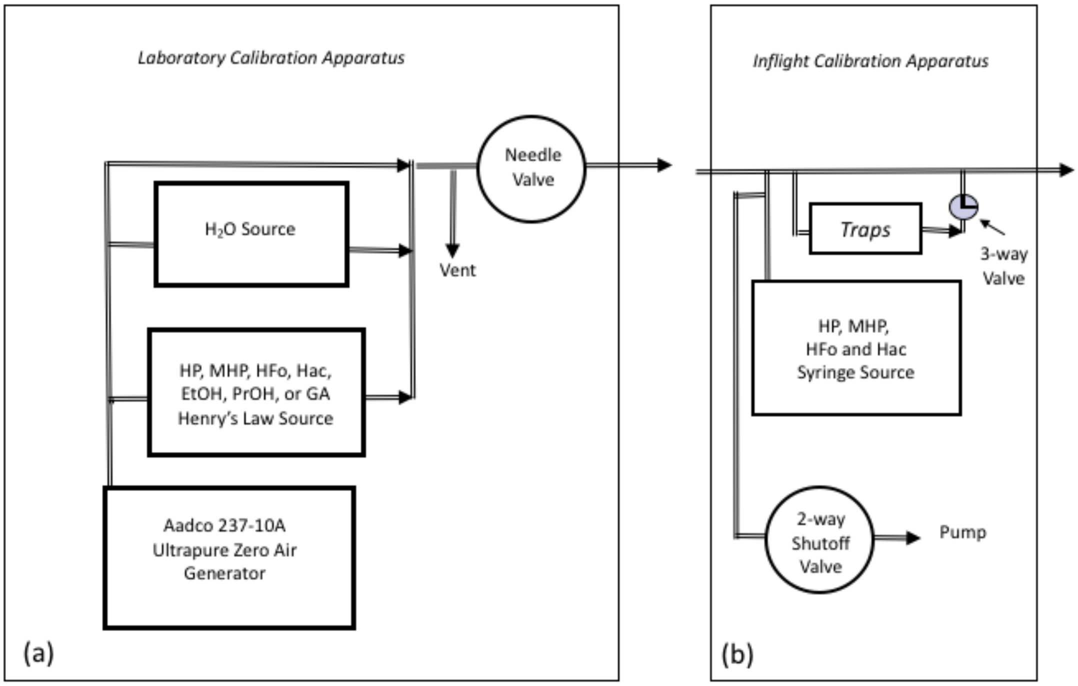

Figure A2: **Block schematic of laboratory (a) and in-flight (b) calibration systems, mass flow controllers are not shown. After Treadaway et al. (2017).**

5

Table A1. Ion and neutral species alphabetically sorted by species/cluster.

Index	Species	Index	Species	Index	Species
Neutral species					
4	CH_3I	20	CH_3OOH	3	CO_2
21	HFo (formic acid)	22	HAc (acetic acid)	55	HNO_3
16	H_2O	19	H_2O_2	1	N_2
41	NO	42	NO_2	2	O_2
10	O_3				
Positive species					
5	N_2^+				
Negative Species					
12	CO_3^-	15	$CO_3^-(H_2O$	31	$CO_3^-(H_2O)_2$
38	$CO_3^-(H_2O)_3$	65	$CO_3^-(H_2O_2)$	67	CO_3^-(CH3OOH)
6	e^-	34	HO^-	59	$HO^-(H_2O)$
60	$HO^-(H_2O)_2$	61	$HO^-(H_2O)_3$	7	I^-
17	$I^-(H_2O)$	39	$I^-(H_2O)_2$	40	$I^-(H_2O)_3$
25	$I^-(H_2O_2)$	27	I^-(HFo)	28	I^-(HAc)
64	$I^-(O_3)$	43	NO^-	44	$NO^-(H_2O)$
45	$NO^-(H_2O)_2$	46	$NO^-(H_2O)_3$	47	NO_2^-
48	$NO_2^-(H_2O)$	49	$NO_2^-(H_2O)_2$	50	$NO_2^-(H_2O)_3$
56	$NO_2^-(H_2O_2)$	51	NO_3^-	62	NO_3^{-*} or $ONOO^-$
58	NO_3^-(HFo)	52	$NO_3^-(H_2O)$	53	$NO_3^-(H_2O)_2$
54	$NO_3^-(H_2O)_3$	72	$NO_3^-(H_2O)_4$	57	$NO_3^-(H_2O_2)$
32	O^-	33	$O^-(H_2O)$	8	O_2^-
26	$O_2^-(CH_3OOH)$	9	$O_2^-(CO_2)$	14	$O_2^-(CO_2)(H_2O)$
69	$O_2^-(CO_2)(H_2O)_2$	73	$O_2^-(CO_2)(H_2O)_3$	23	$O_2^-(CO_2)(H_2O_2)$
13	$O_2^-(H_2O)$	30	$O_2^-(H_2O)_2$	35	$O_2^-(H_2O)_3$
70	$O_2^-(H_2O)_4$	71	$O_2^-(H_2O)_5$	24	$O_2^-(H_2O)(H_2O_2)$
63	$O_2^-(H_2O_2)$	29	$O_2^-(O_2)$	11	O_3^-
68	$O_3^-(CH_3OOH)$	18	$O_3^-(H_2O)$	36	$O_3^-(H_2O)_2$
37	$O_3^-(H_2O)_3$	66	$O_3^-(H_2O_2)$		

Table A2: Ion−neutral reactions sorted alphabetically by reagent ion first and then by neutral species (M denotes a third body reactant, N_2 or O_2; An index sorted list is in the supplemental information.

Reaction	Reaction rate coefficient[1] (reference)[2]	Index
$CO_3^- + CH_3OOH + M \rightarrow CO_3^-(CH_3OOH) + M$	1.0e-28	170
$CO_3^- + H_2O + M \rightarrow CO_3^-(H_2O) + M$	1.0e-28 (*FF, NIST*)	15
$CO_3^- + HNO_3 \rightarrow NO_3^- + CO_2 + HO$	3.5e-10(Kaz)	144
$CO_3^- + H_2O_2 + M \rightarrow CO_3^-(H_2O_2) + M$	1.0e-28(est)	162
$CO_3^- + NO \rightarrow NO_2^- + CO_2$	1.1e-11	83
$CO_3^- + NO_2 \rightarrow NO_3^- + CO_2$	2.0e-10	84
$CO_3^- + N_2O \rightarrow O_2^-(CO_2) + N_2$	5.e-13(*Kov*)	69
$CO_3^-(H_2O) + M \rightarrow CO_3^- + H_2O + M$	3.5e-14(*FF*) 3.9e-14(*Kaz*)	16
$CO_3^-(H_2O) + CH_3OOH \rightarrow CO_3^-(CH_3OOH) + H_2O$	1.0e-9	171
$CO_3^-(H_2O) + H_2O + M \rightarrow CO_3^-(H_2O)_2 + M$	2.1e-28	53
$CO_3^-(H_2O) + H_2O_2 \rightarrow CO_3^-(H_2O_2) + H_2O$	1.0e-9	163
$CO_3^-(H_2O) + NO \rightarrow NO_2^- + CO_2 + H_2O$	3.5e-12	85
$CO_3^-(H_2O) + NO \rightarrow NO_2^-(H_2O) + CO_2$	3.5e-12	86
$CO_3^-(H_2O) + NO_2 \rightarrow NO_3^- + CO_2 + H_2O$	4.0e-11(*Kaz*)	87
$CO_3^-(H_2O) + NO_2 \rightarrow NO_3^-(H_2O) + CO_2$	4.0e-11(*Kaz*)	88
$CO_3^-(H_2O)_2 + M \rightarrow CO_3^-(H_2O) + H_2O + M$	3.7e-12(*NIST*)	54
$CO_3^-(H_2O)_2 + CH_3OOH \rightarrow CO_3^-(CH_3OOH) + 2\ H_2O$	1.0e-10	172
$CO_3^-(H_2O)_2 + H_2O + M \rightarrow CO_3^-(H_2O)_3 + M$	1.7e-28	76
$CO_3^-(H_2O)_2 + H_2O_2 \rightarrow\rightarrow CO_3^-(H_2O_2) + 2\ H_2O$	1.0e-10	164
$CO_3^-(H_2O)_3 + M \rightarrow CO_3^-(H_2O)_2 + H_2O + M$	1.3e-11(*NIST*)	77
$CO_3^-(H_2O)_3 + CH_3OOH \rightarrow CO_3^-(CH_3OOH) + 3\ H_2O$	1.0e-11	173
$CO_3^-(H_2O)_3 + H_2O_2 \rightarrow\rightarrow CO_3^-(H_2O_2) + 3\ H_2O$	1.0e-11	165
$e^- + CH_3I \rightarrow I^- + CH_3$	1.0e-7(*est*)	3
$e^- + O_2 + N_2 \rightarrow O_2^- + N_2$	1.0e-31(*H*)	2
$e^- + O_2 + O_2 \rightarrow O_2^- + O_2$	1.9e-30(*H*)	1
$e^- + O_2 + CO_2 \rightarrow O_2^- + + CO_2$	7/5x1.9e-30(*PP1966*)	not used
$e^- + O_2 + H_2O \rightarrow O_2^- + + H_2O$	7x1.9e-30 (*PP1966*)	not used
$e^- + O_3 \rightarrow O^- + O_2$	9e-12(*Kaz*)	58
$e^- + N_2^+ \rightarrow N_2$	3.6e-8(*Kaz*)	7
$HO^- + CH_3I \rightarrow I^- + HO + CH_3$	3.0e-9(Ike)	135
$HO^- + CO_2 + M \rightarrow HCO_3^- + M$	7.6e-28	66
$HO^- + H_2O + M \rightarrow HO^-(H_2O) + M$	2.5e-28	136
$HO^- + NO_2 \rightarrow NO_2^- + HO$	1.1e-9	90
$HO^- + O_3 \rightarrow O_3^- + HO$	9.e-10	67
$HO^-(H_2O) + M \rightarrow HO^- + H_2O + M$	2.5e-28/4.2e-6(NIST)	137
$HO^-(H_2O) + H_2O + M \rightarrow HO^-(H_2O)_2 + M$	3.5e-28	138
$HO^-(H_2O)_2 + M \rightarrow HO^-(H_2O) + H_2O + M$	3.5e-28/6.7e-12(NIST)	139
$HO^-(H_2O)_2 + H_2O + M \rightarrow HO^-(H_2O)_3 + M$	3.0e-28	140
$HO^-(H_2O)_3 + M \rightarrow HO^-(H_2O)_2 + H_2O + M$	1.85e-13(NIST)	141
$I^- + HAc \xrightarrow{M} I^-(HAc)$	7e-10(Iyer)	42
$I^- + HFo \xrightarrow{M} I^-(HFo)$	1.5e-10(est)	38
$I^- + H_2O + M \rightarrow I^-(H_2O) + M$	1.86e-28 (*Iyer, NIST*)	17

Reaction	Reaction rate coefficient[1] (reference)[2]	Index
$I^- + H_2O_2 \xrightarrow{M} I^-(H_2O_2)$	1e-9(Iyer)	30
$I^- + HNO_3 \rightarrow NO_3^- + HI$	5.0e-11	91
$I^- + O_3 + M \rightarrow I^-(O_3) + M$	1.0e-29(Wil)	158
$I^-(HAc) + M \rightarrow I^- + HAc + M$	2e-9(Iyer)/4.9e7(*NIST*)	43
$I^-(HAc) + H_2O \rightarrow I^-(H_2O) + HAc$	2e-9(*est*)/1.6e4(*NIST*)	45
$I^-(HFo) + M \rightarrow I^- + HFo + M$	1.5e-10(est)/2.01e9(*NIST*)	39
$I^-(HFo) + H_2O \rightarrow I^-(H_2O) + HFo$	2e-9(est)/2.21e5(*NIST*)	41
$I^-(H_2O) + M \rightarrow I^- + H_2O + M$	1.86e-28/2.9e-16 (*Iyer, NIST*)	18
$I^-(H_2O) + HAc \rightarrow I^-(HAc) + H_2O$	2e-9(*est*)	44
$I^-(H_2O) + HFo \rightarrow I^-(HFo) + H_2O$	2e-9(est)	40
$I^-(H_2O) + H_2O + M \rightarrow I^-(H_2O)_2 + M$	1.74e-28	78
$I^-(H_2O) + H_2O_2 \rightarrow I^-(H_2O_2) + H_2O$	2e-9(est)	32
$I^-(H_2O)_2 + M \rightarrow I^-(H_2O) + H_2O + M$	3.57e-12(*NIST*)	79
$I^-(H_2O)_2 + HAc \rightarrow I^-(HAc) + 2H_2O$	3e-9(est)	208
$I^-(H_2O)_2 + HFo \rightarrow I^-(HFo) + 2H_2O$	2e-9(est)	206
$I^-(H_2O)_2 + H_2O + M \rightarrow I^-(H_2O)_3 + M$	2.14e-11*1.28e-17(*NIST*)	80
$I^-(H_2O)_2 + H_2O_2 \rightarrow I^-(H_2O_2) + 2H_2O$	2e-9(est)	204
$I^-(H_2O)_3 + M \rightarrow I^-(H_2O)_2 + H_2O + M$	2.14e-11	81
$I^-(H_2O)_3 + HAc \rightarrow I^-(HAc) + 3H_2O$	<3e-9(not used)	209
$I^-(H_2O)_3 + HFo \rightarrow I^-(HFo) + 3H_2O$	<3e-9(not used)	207
$I^-(H_2O)_3 + H_2O_2 \rightarrow I^-(H_2O_2) + 3H_2O$	<3e-9(not used)	205
$I^-(H_2O_2) + M \rightarrow I^- + H_2O_2 + M$	1e-9/6.33e5(est)	31
$I^-(H_2O_2) + H_2O \rightarrow I^-(H_2O) + H_2O_2$	2e-9/4.26e3(est)	33
$I^-(O_3) + M \rightarrow I^- + O_3 + M$	1.0e-13(Wil)	159
$NO^- + CO_2 \rightarrow e^- + NO + CO_2$	8.3e-12	117
$NO^- + H_2O + M \rightarrow NO^-(H_2O) + M$	2.63e-28	121
$NO^- + NO_2 \rightarrow NO_2^- + NO$	7.4e-10	118
$NO^- + O_2 \rightarrow O_2^- + NO$	5.0e-10	119
$NO^-(H_2O) + M \rightarrow NO^- + H_2O + M$	3.05e-18(NIST)	122
$NO^-(H_2O) + H_2O + M \rightarrow NO^-(H_2O)_2 + M$	2.12e-28	123
$NO^-(H_2O)_2 + M \rightarrow NO^-(H_2O) + H_2O + M$	4.62e-15(NIST)	124
$NO^-(H_2O)_2 + H_2O + M \rightarrow NO^-(H_2O)_3 + M$	1.90e-28	125
$NO^-(H_2O)_3 + M \rightarrow NO^-(H_2O)_2 + H_2O + M$	1.95e-13(NIST)	126
$NO_2^- + H_2O + M \rightarrow NO_2^-(H_2O) + M$	1.6e-28	112
$NO_2^- + H_2O_2 + M \rightarrow NO_2^-(H_2O_2) + M$	1.0e-28(est)	129
$NO_2^- + NO_2 \rightarrow NO_3^- + NO$	2.0e-13	92
$NO_2^- + N_2O \rightarrow NO_3^- + N_2$	1.0e-12	120
$NO_2^- + O_3 \rightarrow NO_3^- + O_2$	1.2e-10	98
$NO_2^-(H_2O) + M \rightarrow NO_2^- + H_2O + M$	3.53e-15(*NIST*)	93
$NO_2^-(H_2O) + H_2O + M \rightarrow NO_2^-(H_2O)_2 + M$	8.0e-29	113
$NO_2^-(H_2O)_2 + M \rightarrow NO_2^-(H_2O) + H_2O + M$	8.3e-14(*NIST*)	94
$NO_2^-(H_2O)_2 + H_2O + M \rightarrow NO_2^-(H_2O)_3 + M$	8.0e-29	114
$NO_2^-(H_2O)_3 + M \rightarrow NO_2^-(H_2O)_2 + H_2O + M$	1.4e-12(*NIST*)	95
$NO_2^-(H_2O_2) + M \rightarrow NO_2^- + H_2O_2 + M$	1.0e-28(est)/1.7e-12(NIST)	130
$NO_3^- + HFo + M \rightarrow NO_3^-(HFo) + M$	1.0e-28(est)	133

Reaction	Reaction rate coefficient[1] (reference)[2]	Index
$NO_3^- + H_2O + M \rightarrow NO_3^-(H_2O) + M$	1.6e-28	115
$NO_3^- + H_2O_2 + M \rightarrow NO_3^-(H_2O_2) + M$	1.0e-28(est)	131
$NO_3^- + NO \rightarrow NO_2^- + NO_2$	3.0e-15	96
$NO_3^- + O_3 \rightarrow NO_2^- + 2\ O_2$	1.0e-13	97
$NO_3^-(HFo) + M \rightarrow NO_3^- + HFo + M$	1.0e-28(est)/9.25e12(NIST)	134
$NO_3^-(H_2O) + M \rightarrow NO_3^- + H_2O + M$	3.0e-14(*NIST*)	99
$NO_3^-(H_2O) + H_2O + M \rightarrow NO_3^-(H_2O)_2 + M$	1.6e-28	116
$NO_3^-(H_2O)_2 + M \rightarrow NO_3^-(H_2O) + M$	6.81e-13(*Kaz*, *NIST*)	100
$NO_3^-(H_2O)_2 + H_2O + M \rightarrow NO_3^-(H_2O)_3 + M$	1.6e-28	127
$NO_3^-(H_2O)_3 + M \rightarrow NO_3^-(H_2O)_2 + H_2O + M$	5.56e-12(NIST)	128
$NO_3^-(H_2O)_3 + H_2O + M \rightarrow NO_3^-(H_2O)_4 + M$	2.0e-29(est)	196
$NO_3^-(H_2O)_4 + M \rightarrow NO_3^-(H_2O)_3 + H_2O + M$	1.0e-11(est, NIST)	197
$NO_3^-(H_2O_2) + M \rightarrow NO_3^- + H_2O_2 + M$	1.0e-28(est)/1.0e10(NIST)	132
$NO_3^{-*} + CO_2 \rightarrow CO_3^- + NO_2$	3.0e-9(FF)	142
$NO_3^{-*} + NO \rightarrow NO_2^- + NO_2$	3.0e-9(FF)	143
$N_2^+ + \sum X^- \xrightarrow{k=6x10^{-8}(300/T)+1.25x10^{-25}[M](300/T)} products$	1.2e-8 (Kaz)	157
$O^- + CH_4 \rightarrow HO^- + CH_3$	1.e-10	59
$O^- + CO_2 + M \rightarrow CO_3^- + M$	3.e-28	60
$O^- + H_2 \rightarrow HO^- + H$	6.e-10	62
$O^- + H_2O + M \rightarrow O^-(H_2O) + M$	1.3e-28	61
$O^- + NO_2 \rightarrow NO_2^- + O$	1.25e-9	101
$O^- + N_2O \rightarrow NO^- + NO$	2.0e-10	102
$O^- + O_2 + M \rightarrow O_3^- + M$	1.5e-31	63
$O^- + O_3 \rightarrow O_3^- + O$	8.e-10	64
$O^-(H_2O) + H_2O \rightarrow HO^-(H_2O) + HO$	6.0e-11(Kaz) >1e-11(Alb)	145
$O^-(H_2O) + O_2 \rightarrow O_3^- + H_2O$	6e-11(*Kaz*)	65
$O_2^- + CH_3I \rightarrow I^- + O_2 + CH_3$	2.0e-9(*est*)	4
$O_2^- + CH_3OOH \xrightarrow{M} O_2^-(CH_3OOH)$	3e-9(*est*)	34
$O_2^- + CO_2 + M \rightarrow O_2^-(CO_2) + M$	4.7e-29(*FF*)	5
$O_2^- + H_2O + M \rightarrow O_2^-(H_2O) + M$	2.2e-28(FF)	10
$O_2^- + H_2O_2 \xrightarrow{M} O_2^-(H_2O_2)$	3e-9(est)	26
$O_2^- + NO_2 \rightarrow NO_2^- + O_2$	8.0e-10(P)	103
$O_2^- + O_2 + M \rightarrow O_2^-(O_2) + M$	3.8e-30(Kaz)	55
$O_2^- + O_3 \rightarrow O_3^- + O_2$	7.8e-10(Fah) 3.0e-10 (*FF*) 7.8e-10 (*Fah*) 6.0e-10 (*Do*) 7.8e-10 (*Kaz*) 4.0e-10 (*Pop*)	8
$O_2^-(CH_3OOH) + M \rightarrow O_2^- + CH_3OOH + M$	3e-9/1.1e42(O'Su)	35
$O_2^-(CH_3OOH) + H_2O \rightarrow O_2^-(H_2O) + CH_3OOH$	2e-9/7.7e6(est)	37
$O_2^-(CO_2) + M \rightarrow O_2^- + CO_2 + M$	4.7e-29/2.34e-11*(FF, NIST*)	6

Reaction	Reaction rate coefficient[1] (reference)[2]	Index
$O_2^-(CO_2) + CH_3OOH \rightarrow O_2^-(CH_3OOH) + CO_2$	2.0e-10	161
$O_2^-(CO_2) + CO_2 + M \rightarrow O_2^-(CO_2)_2 + CO_2 + M$	1.0e-28(est)	200
$O_2^-(CO_2) + H_2O \rightarrow O_2^-(H_2O) + CO_2$	5.8e-10/2.3(*Alb*, *FF*) k(T=298)=2.5e-9(*Kaz*)	13
$O_2^-(CO_2) + H_2O + M \rightarrow O_2^-(CO_2)(H_2O) + M$	1e-28 (*est H, P*)	21
$O_2^-(CO_2) + H_2O_2 \xrightarrow{M} O_2^-(CO_2)(H_2O_2)$	2e-11(est)	22
$O_2^-(CO_2) + H_2O_2 \rightarrow O_2^-(H_2O_2) + CO_2$	1.8e-10	160
$O_2^-(CO_2) + NO \rightarrow NO_3^{-*} + CO_2 + H_2O$	4.8e-11	89
$O_2^-(CO_2) + O_3 \rightarrow O_3^- + CO_2 + O_2$	7.0e-11(*Alb*)	46
$O_2^-(CO_2)_2 + M \rightarrow O_2^-(CO_2) + CO_2 + M$	3.8e-10(est, NIST)	201
$O_2^-(CO_2)_2 + H_2O \rightarrow O_2^-(CO_2)(H_2O) + CO_2$	1.0e-9(est)	202
$O_2^-(CO_2)_2 + H_2O_2 \rightarrow O_2^-(CO_2)(H_2O_2) + CO_2$	1.0e-9(est)	203
$O_2^-(CO_2)(H_2O) + M \rightarrow O_2^-(CO_2) + H_2O + M$	1.0e28/1.9e-13(*est H, NIST*)	14
$O_2^-(CO_2)(H_2O) + M \rightarrow O_2^-(H_2O) + CO_2 + M$	2.7e-15(est, NIST)	198
$O_2^-(CO_2)(H_2O) + H_2O \rightarrow O_2^-(H_2O)_2 + CO_2$	1.0e-9(Fah, est)	148
$O_2^-(CO_2)(H_2O) + H_2O + M \rightarrow O_2^-(CO_2)(H_2O)_2 + M$	1.0e-28	180
$O_2^-(CO_2)(H_2O)_2 + M \rightarrow O_2^-(CO_2)(H_2O) + H_2O + M$	1.0e-13	181
$O_2^-(CO_2)(H_2O)_2 + H_2O \rightarrow O_2^-(H_2O)_3 + CO_2$	1.0e-10	182
$O_2^-(CO_2)(H_2O)_2 + O_3 \rightarrow O_3^-(H_2O)_3 + CO_2$	1.0e-10	183
$O_2^-(CO_2)(H_2O_2) + M \rightarrow O_2^-(CO_2) + H_2O_2 + M$	2e-11/2.e12 *(est*)	23
$O_2^-(CO_2)(H_2O_2) + H_2O \rightarrow O_2^-(CO_2)(H_2O) + H_2O_2$	3e-9/7e9(est) 1.0e-14(*est H, M*)	25
$O_2^-(CO_2)(H_2O) + H_2O_2 \rightarrow O_2^-(CO_2)(H_2O_2) + H_2O$	3e-9(est)	24
$O_2^-(H_2O) + M \rightarrow O_2^- + H_2O + M$	2.2e-28/3.04e-11(*FF, NIST*) k(T=298)=4.33e-18(*Kaz*)	11
$O_2^-(H_2O) + CH_3OOH \rightarrow O_2^-(CH_3OOH) + H_2O$	2e-9(est)	36
$O_2^-(H_2O) + CO_2 \rightarrow O_2^-(CO_2) + H_2O$	5.8e-10(*Alb*) k(T=298)=2.5e-9(*Kaz*)	12
$O_2^-(H_2O) + CO_2 + M \rightarrow O_2^-(CO_2)(H_2O) + M$	1.0e-30	178
$O_2^-(H_2O) + H_2O + M \rightarrow O_2^-(H_2O)_2 + M$	5.4e-28(*PK*)	50
$O_2^-(H_2O) + H_2O_2 \rightarrow O_2^-(H_2O_2) + H_2O$	3e-9(est)	28
$O_2^-(H_2O) + H_2O_2 + M \rightarrow O_2^-(H_2O_2)(H_2O) + M$	1.0e-29(est)	153
$O_2^-(H_2O) + NO \rightarrow NO_3^- + H_2O$	3.1e-10	104
$O_2^-(H_2O) + NO_2 \rightarrow NO_2^- + H_2O + O_2$	9.0e-10	105
$O_2^-(H_2O) + O_2 \rightarrow O_2^-(O_2) + H_2O$	2.5e-15	82
$O_2^-(H_2O) + O_3 \rightarrow O_3^- + H_2O + O_2$	8.0e-10(*Fah*)	47
$O_2^-(H_2O)_2 + M \rightarrow O_2^-(H_2O) + H_2O + M$	1.1e-14(*PK*)	51
$O_2^-(H_2O)_2 + CH_3OOH \rightarrow\rightarrow O_2^-(CH_3OOH) + 2\ H_2O$	3.e-11(est)	151
$O_2^-(H_2O)_2 + CO_2 \rightarrow O_2^-(CO_2)(H_2O) + H_2O$	7.0e-11(Fah)	147
$O_2^-(H_2O)_2 + H_2O + M \rightarrow O_2^-(H_2O)_3 + M$	5.e-28	70
$O_2^-(H_2O)_2 + H_2O_2 \rightarrow\rightarrow O_2^-(H_2O_2) + 2\ H_2O$	7.5-10(est)	149
$O_2^-(H_2O)_2 + NO \rightarrow NO_3^- + 2\ H_2O$	3.0e-10	106
$O_2^-(H_2O)_2 + NO_2 \rightarrow NO_2^- + 2\ H_2O + O_2$	9.0e-10	107
$O_2^-(H_2O)_2 + O_3 \rightarrow O_3^-(H_2O) + H_2O + O_2$	7.8e-10(*Fah*)	52
$O_2^-(H_2O)_3 + M \rightarrow O_2^-(H_2O)_2 + H_2O + M$	5.e-28/3.33e-16(*NIST*)	71
$O_2^-(H_2O)_3 + CH_3OOH \rightarrow\rightarrow O_2^-(CH_3OOH) + 3\ H_2O$	5.0e-14(est)	152
$O_2^-(H_2O)_3 + CO_2 \rightarrow O_2^-(CO_2)(H_2O)_2 + H_2O$	1.0e-14	179
$O_2^-(H_2O)_3 + H_2O + M \rightarrow O_2^-(H_2O)_4 + M$	1.0e-28(H)	192

Reaction	Reaction rate coefficient[1] (reference)[2]	Index
$O_2^-(H_2O)_3 + H_2O_2 \rightarrow\rightarrow O_2^-(H_2O_2) + 3\ H_2O$	1.25e-10(est)	150
$O_2^-(H_2O)_3 + O_3 \rightarrow O_3^-(H_2O)_2 + H_2O + O_2$	6.4e-10(Fah)	146
$O_2^-(H_2O)_3 + NO \rightarrow NO_3^-(H_2O)_2 + H_2O$	1.5e-10(P)	187
$O_2^-(H_2O)_4 + M \rightarrow O_2^-(H_2O)_3 + H_2O + M$	1.2e-12(H, NIST)	193
$O_2^-(H_2O)_4 + H_2O + M \rightarrow O_2^-(H_2O)_5 + M$	5.0e-29(H)	194
$O_2^-(H_2O)_4 + NO \rightarrow NO_3^-(H_2O)_3 + H_2O$	1.2e-10(P)	188
$O_2^-(H_2O)_5 + M \rightarrow O_2^-(H_2O)_4 + H_2O + M$	4.5e-12(H, NIST)	195
$O_2^-(H_2O)_5 + NO \rightarrow NO_3^-(H_2O)_4 + H_2O$	1.2e-10(P)	189
$O_2^-(H_2O_2) + M \rightarrow O_2^- + H_2O_2 + M$	3.e-9/2.96e16(est)	27
$O_2^-(H_2O_2) + CO_2 + M \rightarrow O_2^-(CO_2)(H_2O_2) + M$	3.5e-30(est)	199
$O_2^-(H_2O_2) + H_2O \rightarrow O_2^-(H_2O) + H_2O_2$	3.0e-9/3.9e8(est)	29
$O_2^-(H_2O_2)(H_2O) + M \rightarrow O_2^-(H_2O_2) + H_2O + M$	2.0e-21(est)	154
$O_2^-(H_2O_2)(H_2O) + M \rightarrow O_2^-(H_2O) + H_2O_2 + M$	1.0e-22(est)	155
$O_2^-(H_2O_2)(H_2O) + CO_2 \rightarrow O_2^-(CO_2)(H_2O_2) + H_2O$	7.0e-11(est)	156
$O_2^-(O_2) + M \rightarrow O_2^- + O_2 + M$	1e-14(*Kaz*)	68
$O_2^-(O_2) + CO_2 \rightarrow O_2^-(CO_2) + O_2$	4.3-10(*FF*)	56
$O_2^-(O_2) + H_2O \rightarrow O_2^-(H_2O) + O_2$	1.5e-9(*Ike*)	57
$O_2^-(O_2) + NO \rightarrow NO_3^{-*} + O_2$	2.5e-10	108
$O_3^- + CH_3OOH + M \rightarrow O_3^-(CH_3OOH) + M$	1.0e-28	174
$O_3^- + CO_2 \rightarrow CO_3^- + O_2$	4.0e-10(*F67*)	9
$O_3^- + H_2O + M \rightarrow O_3^-(H_2O) + M$	1.92e-28(*FF*)	19
$O_3^- + H_2O_2 + M \rightarrow O_3^-(H_2O_2) + M$	1.0e-28	166
$O_3^- + NO \rightarrow NO_2^- + O_2$	1.1e-12(*50:50*)	109
$O_3^- + NO \rightarrow NO_3^- + O$	1.1e-12(*50:50*)	110
$O_3^- + NO_2 \rightarrow NO_2^- + O_3$	7.0e-10(P)	191
$O_3^- + NO_2 \rightarrow NO_3^- + O_2$	2.8e-10 >1e-11(Alb)	111
$O_3^-(H_2O) + M \rightarrow O_3^- + H_2O + M$	1.92e-28/1.46e-15(*FF, NIST*)	20
$O_3^-(H_2O) + CH_3OOH \rightarrow O_3^-(CH_3OOH) + H_2O$	1.0e-9	175
$O_3^-(H_2O) + CO_2 \rightarrow CO_3^-(H_2O) + O_2$	1.75e10(Do, Wil)	48
$O_3^-(H_2O) + CO_2 \rightarrow CO_3^- + H_2O + O_2$	1.75e10(Do, Wil)	49
$O_3^-(H_2O) + H_2O + M \rightarrow O_3^-(H_2O)_2 + M$	1.92e-28	72
$O_3^-(H_2O) + H_2O_2 \rightarrow O_3^-(H_2O_2) + H_2O$	1.0e-9	167
$O_3^-(H_2O)_2 + M \rightarrow O_3^-(H_2O) + H_2O + M$	1.28e-13(*NIST*)	73
$O_3^-(H_2O)_2 + CH_3OOH \rightarrow O_3^-(CH_3OOH) + 2\ H_2O$	1.0e-10	176
$O_3^-(H_2O)_2 + CO_2 \rightarrow CO_3^-(H_2O) + H_2O + O_2$	1.0e-10(P)	185
$O_3^-(H_2O)_2 + H_2O + M \rightarrow O_3^-(H2O)_3 + M$	1.68e-28	74
$O_3^-(H_2O)_2 + H_2O_2 \rightarrow O_3^-(H_2O_2) + 2\ H_2O$	1.0e-10	168
$O_3^-(H_2O)_3 + M \rightarrow O_3^-(H_2O)_2 + H_2O + M$	2.17e-12(*NIST*)	75
$O_3^-(H_2O)_3 + H_2O_2 \rightarrow O_3^-(H_2O_2) + 3\ H_2O$	1.0e-11	169
$O_3^-(H_2O)_3 + CH_3OOH \rightarrow O_3^-(CH_3OOH) + 3\ H_2O$	1.0e-11	177
$O_3^-(H_2O)_3 + CO_2 \rightarrow CO_3^-(H_2O)_2 + H_2O + O_2$	5.0e-11(P)	186

[1] Reaction rate coefficient units: unimolecular, s^{-1}; bimolecular, $cm^3\ molec^{-1}\ s^{-1}$; termolecular, $cm^6\ molec^2\ s^{-1}$. First listed reaction rate coefficient for a reaction is used in the model mechanism, others are included to show published range of values. A.Ae-n reads as $A.A\times10^{-n}$.

[2] AK1970 (Arshadi and Kebarle, 1970); Alb (Albritton, 1978); Do1977 (Dotan et al., 1977); F67 (Fehsenfeld et al., 1967); FF1974 (Fehsenfeld and Ferguson, 1974); H (Huertas et al., 1978); HY1992 (Hiraoka and Yamabe, 1992); Ike (Ikezoe et al., 1987) Iyer (Iyer et al., 2016); Kaz (Kazil, 2002); KFP1972 (Kebarle et al., 1972); Kov (Kovacs et al., 2016); M (Mohnen, 1974); NIST (Bartmess, 2016); O'Su (O'Sullivan et al., 2017); P (Popov, 2010); PP1966 (Pack and Phelps, 1966); Wil (Williams et al., 2002).

Table A3: Reactions that yield $O_2^-(H_2O_2)$, $O_2^-(CH_3OOH)$, $O_2^-(CO_2)(H_2O_2)$, $I^-(H_2O_2)$, $I^-(HFo)$ and $I^-(HAc)$.

Cluster Ion	Cluster Ion Source Reaction	Rate	Index
$O_2^-(H_2O_2)$			
	$O_2^- + H_2O_2 \xrightarrow{M} O_2^-(H_2O_2)$	3.0e-9	26
	$O_2^-(H_2O) + H_2O_2 \rightarrow O_2^-(H_2O_2) + H_2O$	3.0e-9	28
	$O_2^-(H_2O)_2 + H_2O_2 \rightarrow\rightarrow O_2^-(H_2O_2) + 2\ H_2O$	7.5-10	149
	$O_2^-(H_2O)_3 + H_2O_2 \rightarrow\rightarrow O_2^-(H_2O_2) + 3\ H_2O$	1.25-10	150
	$O_2^-(H_2O) + H_2O_2 + M \rightarrow O_2^-(H_2O_2)(H_2O) + M$	1.0e-29	153
	$O_2^-(H_2O_2)(H_2O) + M \rightarrow O_2^-(H_2O_2) + H_2O + M$	2.0e-21	154
	$O_2^-(CO_2) + H_2O_2 \rightarrow O_2^-(H_2O_2) + CO_2$	1.8e-10	160
$O_2^-(CH_3OOH)$			
	$O_2^- + CH_3OOH \xrightarrow{M} O_2^-(CH_3OOH)$	3.0e-9	34
	$O_2^-(H_2O) + CH_3OOH \rightarrow O_2^-(CH_3OOH) + H_2O$	2.0e-9	36
	$O_2^-(H_2O)_2 + CH_3OOH \rightarrow\rightarrow O_2^-(CH_3OOH) + 2\ H_2O$	3.0e-11	151
	$O_2^-(H_2O)_3 + CH_3OOH \rightarrow\rightarrow O_2^-(CH_3OOH) + 3\ H_2O$	5.0e-14	152
	$O_2^-(CO_2) + CH_3OOH \rightarrow O_2^-(CH_3OOH) + CO_2$	2.0e-10	161
$O_2^-(CO_2)(H_2O_2)$			
	$O_2^-(CO_2) + H_2O_2 \xrightarrow{M} O_2^-(CO_2)(H_2O_2)$	2.e-11	22
	$O_2^-(CO_2)(H_2O) + H_2O_2 \rightarrow O_2^-(CO_2)(H_2O_2) + H_2O$	3.e-9	24
	$O_2^-(H_2O_2)(H_2O) + CO_2 \rightarrow O_2^-(CO_2)(H_2O_2) + H_2O$	7.0e-11	156
	$O_2^-(H_2O_2) + CO_2 + M \rightarrow O_2^-(CO_2)(H_2O_2) + M$	3.5e-30	199
	$O_2^-(CO_2)_2 + H_2O_2 \rightarrow O_2^-(CO_2)(H_2O_2) + CO_2$	1.0e-9	203
$CO_3^-(H_2O_2)$			
	$CO_3^- + H_2O_2 + M \rightarrow CO_3^-(H_2O_2) + M$	1.0e-28	162
	$CO_3^-(H_2O) + H_2O_2 \rightarrow CO_3^-(H_2O_2) + H_2O$	1.0e-9	163
	$CO_3^-(H_2O)_2 + H_2O_2 \rightarrow\rightarrow CO_3^-(H_2O_2) + 2\ H_2O$	1.0e-10	164
	$CO_3^-(H_2O)_3 + H_2O_2 \rightarrow\rightarrow CO_3^-(H_2O_2) + 3\ H_2O$	1.0e-11	165
$CO_3^-(CH_3OOH)$			
	$CO_3^- + CH_3OOH + M \rightarrow CO_3^-(CH_3OOH) + M$	1.0e-28	170
	$CO_3^-(H_2O) + CH_3OOH \rightarrow CO_3^-(CH_3OOH) + H_2O$	1.0e-9	171
	$CO_3^-(H_2O)_2 + CH_3OOH \rightarrow CO_3^-(CH_3OOH) + 2\ H_2O$	1.0e-10	172
	$CO_3^-(H_2O)_3 + CH_3OOH \rightarrow CO_3^-(CH_3OOH) + 3\ H_2O$	1.0e-11	173
$I^-(H_2O_2)$, $I^-(HFo)$ and $I^-(HAc)$.			
	$I^- + H_2O_2 \xrightarrow{M} I^-(H_2O_2)$	1.0e-9	30
	$I^-(H_2O) + H_2O_2 \rightarrow I^-(H_2O_2) + H_2O$	2.0e-9	32
	$I^-(H_2O)_2 + H_2O_2 \rightarrow I^-(H_2O_2) + 2H_2O$	2e-9	204
	$I^-(H_2O)_3 + H_2O_2 \rightarrow I^-(H_2O_2) + 3H_2O$	<3e-9	205
	$I^- + HFo \xrightarrow{M} I^-(HFo)$	1.5e-10	38
	$I^-(H_2O) + HFo \rightarrow I^-(HFo) + H_2O$	2.0e-9	40
	$I^-(H_2O)_2 + HFo \rightarrow I^-(HFo) + 2H_2O$	2e-9	206
	$I^-(H_2O)_3 + HFo \rightarrow I^-(HFo) + 3H_2O$	<3e-9	207
	$I^- + HAc \xrightarrow{M} I^-(HAc)$	7.0e-10	42
	$I^-(H_2O) + HAc \rightarrow I^-(HAc) + H_2O$	2.0e-9	44
	$I^-(H_2O)_2 + HAc \rightarrow I^-(HAc) + 2H_2O$	3e-9	208
	$I^-(H_2O)_2 + HAc \rightarrow I^-(HAc) + 3H_2O$	<3e-9	209

Table A4: Reaction sequences leading to potential interferences at m/z 66 [$^{18}O\ of\ NO_2^-(H_2O)$, $O_3^-(H_2O)$, and $^{18}O\ of\ O_2^-(O_2)$] for $O_2^-(H_2O_2)$ and at m/z 80 [$^{18}O\ of\ CO_3^-(H_2O)$ and $NO_3^-(H_2O)$] for $O_2^-(CH_3OOH)$.

Interference cluster	Source Description	Cluster formation reaction sequence	Index
$^{18}O\ of\ NO_2^-(H_2O)$	from N_2O to NO^- to NO_2^-	$O^- + N_2O \rightarrow NO^- + NO$	102
		$NO^- + NO_2 \rightarrow NO_2^- + NO$	118
	from NO to NO_2^-	$CO_3^- + NO \rightarrow NO_2^- + CO_2$	83
		$CO_3^-(H_2O) + NO \rightarrow NO_2^- + CO_2 + H_2O$	85
		$CO_3^-(H_2O) + NO \rightarrow NO_2^-(H_2O) + CO_2$	86
	from NO_2 to NO_2^-	$HO^- + NO_2 \rightarrow NO_2^- + HO$	90
		$O_2^- + NO_2 \rightarrow NO_2^- + O_2$	190
		$O_3^- + NO_2 \rightarrow NO_2^- + O_3$	191
		$O^- + NO_2 \rightarrow NO_2^- + O$	101
		$O_2^- + NO_2 \rightarrow NO_2^- + O_2$	103
		$O_2^-(H_2O) + NO_2 \rightarrow NO_2^- + H_2O + O_2$	105
		$O_2^-(H_2O)_2 + NO_2 \rightarrow NO_2^- + 2\ H_2O + O_2$	107
		$O_3^- + NO \rightarrow NO_2^- + O_2$	109
	then the NO_2^- hydrate	$NO_2^- + H_2O \xrightarrow{M} NO_2^-(H_2O)$	112
$O_3^-(H_2O)$		$O_2^- + O_3 \rightarrow O_3^- + O_2$	8
		$O_3^- + H_2O \xrightarrow{M} O_3^-(H_2O)$	19
$^{18}O\ of\ O_2^-(O_2)$		$O_2^- + O_2 \xrightarrow{M} O_2^-(O_2)$	55
$^{18}O\ of\ CO_3^-(H_2O)$		$O_2^- + O_3 \rightarrow O_3^- + O_2$	8
		$O_3^- + CO_2 \rightarrow CO_3^- + O_2$	9
		$CO_3^- + H_2O \xrightarrow{M} CO_3^-(H_2O)$	15
$NO_3^-(H_2O)$			
	from NO to NO_3^-	$O_2^-(H_2O) + NO \rightarrow NO_3^- + H_2O$	104
		$O_2^-(H_2O)_2 + NO \rightarrow NO_3^- + 2\ H_2O$	106
		$O_3^- + NO \rightarrow NO_3^- + O$	110
		$O_2^-(H_2O)_3 + NO \rightarrow NO_3^-(H_2O)_2 + H_2O$	187
		$O_2^-(H_2O)_4 + NO \rightarrow NO_3^-(H_2O)_3 + H_2O$	188
		$O_2^-(H_2O)_5 + NO \rightarrow NO_3^-(H_2O)_4 + H_2O$	189
	from NO_2 to NO_3^-	$CO_3^- + NO_2 \rightarrow NO_3^- + CO_2$	84
		$CO_3^-(H_2O) + NO_2 \rightarrow NO_3^- + CO_2 + H_2O$	87
		$CO_3^-(H_2O) + NO_2 \rightarrow NO_3^-(H_2O) + CO_2$	88
		$O_3^- + NO_2 \rightarrow NO_3^- + O_2$	111
	from NO_2^- to NO_3^-	$NO_2^- + NO_2 \rightarrow NO_3^- + NO$	92
		$NO_2^- + O_3 \rightarrow NO_3^- + O_2$	98
		$NO_2^- + N_2O \rightarrow NO_3^- + N_2$	120
	from HNO_3 to NO_3^-	$I^- + HNO_3 \rightarrow NO_3^- + HI$	91
	then the NO_3^- hydrate	$NO_3^- + H_2O_2 \xrightarrow{M} NO_3^-(H_2O_2)$	131

Table A5: Enthalpy of formation, entropy and Gibb's formation energy for neutral, ion and ion-clusters in the $O_2^- - O_2 - CO_2 - H_2O -$ hydroperoxide system.

Species or Cluster	ΔH_f^o kJ mol^{-1}	S^o J ^{o}K^{-1}mol^{-1}	ΔG_f^o kJ mol^{-1}	Reference[1]
Neutral				
$C_{graphite}$	0	6	0	NIST2016
CH_3OOH	-128	281	-71	Gold2012
CO_2	-394	214	-394	NIST2016; Gold2012
H_2	0	131	0	NIST2016; Gold2012
H_2O	-242	189	-229	NIST2016; Gold2012
H_2O_2	-136	233	-105	NIST2016; Gold2012
O_2	0	205	0	NIST2016; Gold2012
Ion or ion-cluster				
e^-	0	23	0	Bartmess [1994]
O_2^-	-43	210	-38	NIST2016; Bartmess [1994]
$O_2^-(CH_3OOH)$			**-340**[2]	OSull2017; this work
$O_2^-(CO_2)$	**-516**	**322**	**-481**	this work
$O_2^-(CO_2)_2$	**-937**	**460**	**-880**	this work
$O_2^-(CO_2)(H_2O)$	**-819**	**430**	**-747**	this work
$O_2^-(CO_2)(H_2O)_2$	**-1105**	**555**	**-1000**	this work
$O_2^-(CO_2)(H_2O_2)$			**-630**	OSull2017; this work
$O_2^-(H_2O)$	**-362**	**314**	**-318**	this work
$O_2^-(H_2O)_2$	**-676**	**398**	**-588**	this work
$O_2^-(H_2O)_3$	**-982**	**469**	**-846**	this work
$O_2^-(H_2O)_4$			**-1092**	this work
$O_2^-(H_2O)_5$			**-1335**	this work
$O_2^-(H_2O_2)$			**-237**	OSull2017; this work
$O_2^-(O_2)$	**-115**	**310**	**-79**	NIST2016; AK1970; this work

[1] AK1970 [Arshadi and Kebarle, 1970]; Gold2012 [Goldsmith et al., 2012]; NIST2016 [Bartmess, 2016]; OSull2017 [O'Sullivan et al., 2017].

[2] Note: **underline bold** indicates value derived in this work using published formation and reaction enthalpy, entropy and Gibb's energy.

Table A6: Reaction enthalpy, entropy and Gibb's energy for neutral, ion and ion-cluster reactions in the $O_2^- - O_2 - CO_2 - H_2O -$ hydroperoxide system.

Reaction	ΔH_r^o kJ mol^{-1}	ΔS_r^o J ^{o}K^{-1}mol^{-1}	ΔG_r^o kJ mol^{-1}	Reference[1]
$O_2^- + CO_2 \rightleftharpoons O_2^-(CO_2)$	-80	-101	-49	NIST2016, HY1992
$O_2^-(CO_2) + CO_2 \rightleftharpoons O_2^-(CO_2)_2$	-28	-76	-5	NIST2016, HY1992
$O_2^-(CO_2) + H_2O \rightleftharpoons O_2^-(H_2O) + CO_2$	**2**[2]	**17**	**-3**	NIST2016, FF1974 ($\Delta G_r^o = -2.1$), this work
$O_2^-(CO_2) + H_2O \rightleftharpoons O_2^-(CO_2)(H_2O)$	-61	**-81**	**-37**	KFP1972, this work
$O_2^-(CO_2)(H_2O) + H_2O \rightleftharpoons O_2^-(H_2O)_2 + CO_2$	**-9**	**-7**	-7	NIST2016, FF1974, KFP1972, this work
$O_2^-(CO_2)(H_2O) + H_2O \rightleftharpoons O_2^-(CO_2)(H_2O)_2$	-44	**-65**	-25	Mohnen [1972], HFG1978, this work
$O_2^- + H_2O \rightleftharpoons O_2^-(H_2O)$	-77	-84	-52	NIST2016, AK1970
$O_2^-(H_2O) + H_2O \rightleftharpoons O_2^-(H_2O)_2$	-72	-105	-41	NIST2016, AK1970
$O_2^-(H_2O) + CO_2 \rightleftharpoons O_2^-(CO_2)(H_2O)$	**-63**	**-98**	-34	NIST2016, FF1974, this work
$O_2^-(H_2O)_2 + CO_2 \rightleftharpoons O_2^-(CO_2)(H_2O) + H_2O$	**9**	**7**	**7**	this work
$O_2^-(H_2O)_2 + H_2O \rightleftharpoons O_2^-(H_2O)_3$	-64	-118	-29	NIST2016, AK1970
$O_2^-(H_2O)_3 + H_2O \rightleftharpoons O_2^-(H_2O)_4$			-18	NIST2016, AK1970
$O_2^-(H_2O)_4 + H_2O \rightleftharpoons O_2^-(H_2O)_5$			-14	NIST2016, AK1970
$O_2^- + O_2 \rightleftharpoons O_2^-(O_2)$	-44	-102	-13	NIST2016
$O_2^- + CH_3OOH \rightleftharpoons O_2^-(CH_3OOH)$			**-231**	OSull2017, this work
$O_2^- + H_2O_2 \rightleftharpoons O_2^-(H_2O_2)$			**-99**	OSull2017, this work (-94)
$O_2^-(CO_2) + H_2O_2 \rightleftharpoons O_2^-(CO_2)(H_2O_2)$			-43	OSull2017
$O_2^-(H_2O) + CH_3OOH \rightleftharpoons O_2^-(CH_3OOH) + H_2O$			**-181**	OSull2017, this work
$O_2^-(H_2O) + H_2O_2 \rightleftharpoons O_2^-(H_2O_2) + H_2O$			**-42**	this work
$O_2^-(H_2O)_2 + H_2O_2 \rightleftharpoons O_2^-(H_2O_2) + 2H_2O$			**-1**	this work
$O_2^-(H_2O)_3 + H_2O_2 \rightleftharpoons O_2^-(H_2O_2) + 3H_2O$			**28**	this work
$O_2^-(H_2O_2) + CO_2 \rightleftharpoons O_2^-(CO_2)(H_2O_2)$			**7**	this work

[1] AK1970 [Arshadi and Kebarle, 1970]; FF1974 [Fehsenfeld and Ferguson, 1974]; HFG1978 [Huertas et al., 1978]; HY1992 [Hiraoka and Yamabe, 1992]; KFP1972 [Kebarle et al., 1972]; NIST2016 [Bartmess, 2016]; OSull [O'Sullivan et al., 2017].

[2] Note: **underline bold** indicates value derived in this work using published formation and reaction enthalpy, entropy and Gibb's energy.

Supplemental Information: An ion-neutral model to investigate chemical ionization mass spectrometry analysis of atmospheric molecules - application to a mixed reagent ion system for hydroperoxides and organic acids.

Brian G. Heikes[1], Victoria Treadaway[1], Ashley S. McNeill[1,2], Indira K. C. Silwal[3,4] and Daniel W. O'Sullivan[3]

[1]Graduate School of Oceanography, University of Rhode Island, Narragansett, RI, 02882, USA
[2]Department of Chemistry, University of Alabama, Tuscaloosa, AL, 35401, USA
[3]Chemistry Department, United States Naval Academy, Annapolis, MD, 21402, USA
[4]Department of Chemistry, University of Maine, Orono, 04469, USA

Correspondence to: Brian Heikes (bheikes@uri.edu)

1. Notes on mechanism development and adjustment of kinetic rates to resolve pressure and humidity trends in $O_2^-(H_2O_2)$, $O_2^-(CH_3OOH)$, $O_2^-(CO_2)(H_2O_2)$, $I^-(HFo)$ and $I^-(HAc)$ sensitivities.

1.1 Base thermodynamic data for the $O_2^- - O_2 - CO_2 - H_2O -$ hydroperoxide system.

Formation enthalpy (ΔH_f^o), entropy (ΔS^o), and Gibb's formation energy (ΔG_f^o), data are published for some of the neutral, ion and ion-cluster species involved in the $O_2^- - O_2 - CO_2 - H_2O -$ hydroperoxide system. Reaction enthalpy(ΔH_r^o), entropy (ΔS_r^o), and Gibb's energy (ΔG_r^o) data are also available for some of the reactions involved in this system. These thermodynamic data are summarized in Table A5 and Table A6. The NIST Chemistry WebBook (Bartmess, 2016) was used extensively in this analysis as it provides summary information from primary sources. In cases for which multiple values are available and without a recommended value, we have indicated which primary data set we adopted. Additional formation and reaction energies were taken from *ab initio* calculations by Messer et al. (2000), Cappa and Elrod (2001), Goldsmith et al. (2012) and O'Sullivan et al. (2017). For ions and ion-cluster species and reactions, care must be exercised as to the notation used for the energy terms. Often, but not always, the ion and ion-neutral cluster species and reaction literature follows a negative sign convention with respect to the neutral species and neutral reaction literature. Here we have adopted a sign convention such that exothermic reactions have a negative reaction enthalpy and spontaneous reactions have a negative Gibb's reaction energy.

The following thermodynamic relationship is used to calculate energy terms which were not previously available from the primary literature or the NIST Chemistry WebBook,

$$\Delta H_r^o - T_o \times \Delta S_r^o = \Delta G_r^o$$

where $T_o = 298.15$ K, ΔH_r^o is the stoichiometric sum of the formation enthalpies, ΔH_f^o, of the products (j index) minus the stoichiometric sum of the formation enthalpies of the reactants (i index),

$$\Delta H_r^o = \sum_j^J \nu_j\, H_{f,j}^o - \sum_i^I \nu_i\, H_{f,i}^o,$$

ΔS_r^o is the stoichiometric sum of the standard entropies, S^o, of the products minus the stoichiometric sum of the standard entropies of the reactants,

$$\Delta S_r^o = \sum_j^J \nu_j\, S_j^o - \sum_i^I \nu_i\, S_i^o,$$

and ΔG_r^o is the stoichiometric sum of the Gibb's formation energies, ΔG_f^o , of the products minus the stoichiometric sum of the Gibb's formation energies of the reactants,

$$\Delta G_r^o = \sum_j^J \nu_j\, G_{f,j}^o - \sum_i^I \nu_i\, G_{f,i}^o,$$

where, ν represents the stoichiometric coefficient for a species in a reaction. Formation energies for a reactant or product species are calculated using published ΔH_f^o and ΔG_f^o for that species as the sole product and the reactants are taken to be in their standard state and form with $\Delta G_f^o \equiv 0$ and $\Delta H_f^o \equiv 0$. In the case of the *ab initio* calculations, the Gibb's energy at 298.15 K and 1013.25 hPa, G^o, is calculated for each reactant and product and ΔG_r^o is calculated by stoichiometrically summing the *ab initio* Gibb's energies (Ochterski, 2000) of the products and then subtracting the stoichiometric sum of the reactants:

$$\Delta G_r^o = \sum_j^J \nu_j\, G_j^o - \sum_i^I \nu_i\, G_i^o = \sum_j^J \nu_j\, G_{f,j}^o - \sum_i^I \nu_i\, G_{f,i}^o.$$

The formation and reaction energies so calculated in this work are underlined and bold-faced in the Tables A5 and A6.

Goldsmith et al. (2012) estimated formation enthalpies, entropies and Gibb's formation energies for CH_3OOH and many other low molecular weight combustion related compounds. O'Sullivan et al. (2017) estimated Gibb's reaction energies at 298.15 K and 1013.25 hPa for:

$$O_2^- + CH_3OOH \rightleftharpoons O_2^-(CH_3OOH) \qquad \Delta G_r^o = -231\ kJ\ mol^{-1} \qquad \text{(s1)}$$

$$O_2^-(H_2O) + CH_3OOH \rightleftharpoons O_2^-(CH_3OOH) + H_2O \qquad \Delta G_r^o = -181\ kJ\ mol^{-1} \qquad \text{(s2)}$$

and

$$O_2^- + H_2O_2 \rightleftharpoons O_2^-(H_2O_2) \qquad \Delta G_r^o = -99\ kJ\ mol^{-1} \qquad \text{(s3)}$$

The Gibb's reaction energy given for (s2) has been modified from O'Sullivan's original value as outlined below. The ΔG_r^o value for (s3) compares favorably to that estimated using the linear correlation between ion-protonation energy and the Gibb's reaction energies for ion-H_2O_2 cluster formation (see main paper, $\Delta G_r^o = -94\ kJ\ mol^{-1}$). The O'Sullivan et al. calculated ΔG_r^os for ion-hydrates also agreed well (nominally within 7 kJ mol^{-1}; sixth significant figure in the calculated Gibb's energy) with the NIST Chemistry WebBook tabulations. However, there was a large inconsistency between the

Gibb's reaction energies for (s1) and (s2) and the ΔG_f^o for $O_2^-(CH_3OOH)$ derived from their calculations using NIST or NIST derived reactant and product ΔG_f^os from Table A6. The ΔG_f^o of $O_2^-(CH_3OOH)$ calculated from either (s1) or (s2) was expected to be within 7 kJ mol^{-1} but was found to be -340 or -521 kJ mol^{-1}, respectively, using O'Sullivan's original species specific Gibb's energies. The discrepancy was traced to a potential calculation issue for $O_2^-(H_2O)$. The Gibb's energy for $O_2^-(H_2O)$ was recalculated using the NIST Gibb's reaction energy for $O_2^- + H_2O \rightleftharpoons O_2^-(H_2O)$ (Table A6) and the O'Sullivan calculated Gibb's energies for O_2^- and H_2O. Applying this hybrid Gibb's energy for $O_2^-(H_2O)$ in (s2) rectified the ΔG_f^o of $O_2^-(CH_3OOH)$ between (s1) and (s2). The resultant ΔG_f^o of $O_2^-(CH_3OOH)$ was -340 kJ mol^{-1} and the modified ΔG_r^o for reaction (s2) was -181 kJ mol^{-1}. These values are listed in Table A5 and Table A6, respectively.

A second issue exists between the derived NIST Gibb's formation energies and the O'Sullivan et al. (2017) Gibb's reaction energies for the formation of $O_2^-(CO_2)(H_2O_2)$. One pathway to $O_2^-(CO_2)(H_2O_2)$ formation is:

$$O_2^-(CO_2) + H_2O_2 \rightleftharpoons O_2^-(CO_2)(H_2O_2) \qquad \Delta G_r^o = -43\ kJ\ mol^{-1} \qquad \text{(s4)}$$

where the Gibb's reaction energy for (s4) is from O'Sullivan et al. A second pathway to $O_2^-(CO_2)(H_2O_2)$ is:

$$O_2^-(H_2O_2) + CO_2 \rightleftharpoons O_2^-(CO_2)(H_2O_2) \qquad \Delta G_r^o = -85\ kJ\ mol^{-1} \qquad \text{(s5)}$$

and was proposed by us to reconcile the sensitivity trends observed in $O_2^-(CO_2)(H_2O_2)$ as a function of sample flow rate (sample pressure) and humidity. The O'Sullivan et al. calculated Gibb's reaction energy for (s5) is shown. The Gibb's reaction energies suggest both reactions would be spontaneous and the equilibrium constants would strongly favor the products. The Gibb's formation energy of $O_2^-(CO_2)(H_2O_2)$ was determined to be -630 kJ mol^{-1} using the Gibb's formation energies for $O_2^-(CO_2)$ and H_2O_2 derived from NIST data and the O'Sullivan et al. Gibb's reaction energy for (s4). Alternatively using the Gibb's formation energies for $O_2^-(H_2O_2)$ and CO_2 derived from NIST data and the Gibb's reaction energy for (s5), the Gibb's formation energy for $O_2^-(CO_2)(H_2O_2)$ would be -721 kJ/mol^{-1}, a -91 kJ mol^{-1} difference from that determined from (s4). At this point the reaction energies for (s4) and (s5) favored the production of $O_2^-(CO_2)(H_2O_2)$ by both reactions.

The Gibb's formation energies and Gibb's reaction energies for (s4) and (s5) were rectified similarly to the reconciliation of (s1) and (s2) thermodynamics above, but in so doing it reduces the argument for $O_2^-(CO_2)(H_2O_2)$ production by (s5). A key step in this reconciliation was a reanalysis of the energetics of $O_2^-(CO_2)$ production through reaction (s6)

$$O_2^- + CO_2 \rightleftharpoons O_2^-(CO_2) \qquad \Delta G_r^o = -49\ kJ\ mol^{-1} \qquad \text{(s6)}$$

where, the reaction energy is derived from NIST data alone. The O'Sullivan et al. *ab initio* calculated reaction energy for (s6) was -141 kJ mol^{-1} or 92 kJ mol^{-1} lower than the NIST derived value. Ascribing the difference fully to the calculated Gibb's energy of $O_2^-(CO_2)$ in O'Sullivan's calculation, reducing this quantity by 91 kJ mol^{-1} while keeping the Gibb's reaction energies (s4) the same, necessitated reducing the calculated Gibb's energy for $O_2^-(CO_2)(H_2O_2)$ by the same amount. Propagating this change into the calculation of the Gibb's reaction energy for (s5), lead to ΔG_r^o = +7 kJ mol^{-1} for this reaction. Both (s4) and (s5) now yield the same Gibb's formation energy for $O_2^-(CO_2)(H_2O_2)$, which is equal to -630 kJ/mol^{-1}. The species Gibb's formation energies and the Gibb's reaction energies for (s4), (s5), and (s6) are thereby self-consistent but at the expense of the calculated reaction energy for (s5) which is now positive and suggestive of a non-spontaneous reaction with an equilibrium constant slightly favoring the reactants. This only partially weakened the case for reaction (s5) in the formation of $O_2^-(CO_2)(H_2O_2)$ because, while (s5) as revised is weakly endergonic, the reaction remains exothermic with an enthalpy of ~-20 kJ mol^{-1} as its expected reduction in entropy is of order 10^2 J mol^{-1} K^{-1} based upon analogy with other hydroperoxide clustering reaction data (i.e., Böhringer et al., 1984; Messer et al. 2000; Cappa and Elrod, 2001).

1.2 Modified kinetics data for the $O_2^- - O_2 - CO_2 - H_2O -$ hydroperoxide system with $I^- - H_2O - H_2O_2 - HFo - HAc$ chemistry.

After the ion-source tube, the reagent ion stream was assumed to instantaneously mix with ambient air. This air contains myriad other compounds most notably in terms of our reagent ion system: H_2O, O_2, CO_2 and O_3. The model mechanism with respect to O_2^- and its cluster ions with H_2O and additional CO_2 and O_2 follows Mohnen (1971), Kebarle et al. (1972), Fehsenfeld and Ferguson (1974) and Fahey et al. (1982). The full set of species considered and their reactions are listed in Tables A1 and A2, respectively. The species and reactions were developed in stages and the species and reaction indices (the number preceding the reaction) reflect that development. The main paper contains a list of reactions organized by the reacting ion.

Reagent ion hydration was critical. For the first hydrate, hydration can occur directly

$O_2^- + H_2O + M \rightarrow O_2^-(H_2O) + M$ k_f=2.2x10^{-28} (M=O_2) (10)

or indirectly through $O_2^-(O_2)$ and possibly $O_2^-(CO_2)$

$O_2^- + O_2 + M \rightarrow O_2^-(O_2) + M$ k_f=3 - 5x10^{-31} (Ike; M=O_2) (55)

$O_2^-(O_2) + H_2O \rightarrow O_2^-(H_2O) + O_2$ k_f=1.5x10^{-9} (Ike) (57)

$O_2^- + CO_2 + M \rightarrow O_2^-(CO_2) + M$ k_f=4.7x10^{-29} (M=O_2) (5)

$O_2^-(O_2) + CO_2 \rightarrow O_2^-(CO_2) + O_2$ k_f=4.3x10^{-10} (FFB) (56)

$O_2^-(CO_2) + H_2O \rightarrow O_2^-(H_2O) + (CO_2)$ k_f<10^{-15} (see discussion) (13)

In these and subsequent reaction statements, M denotes a third molecule and the references by: Ada = Adams et al. (1970); Alb = Albritton (1978); Ike = Ikezoe et al. (1986); Fah = Fahey et al. (1982); FF = Fehsenfeld and Ferguson (1974); FFB = Fehsenfeld et al. (1969); Hue = Huertas et al. (1978); PK = Payzant and Kebarle (1972); PP = Pack and Phelps (1966). The reaction rate coefficient for (13), k_{13}, was set equal to 2.5x10^{-10}. This value of k_{13} was calculated assuming the switching reaction pair, (12) and (13),

a. $O_2^-(H_2O) + CO_2 \rightleftharpoons O_2^-(CO_2) + H_2O$ k_{12}=5.8x10^{-10} (Ada) (12)

$K_{eq}= k_{12}/k_{13}=2.3$ (FF)

could be combined to form a simple forward/reverse reaction sequence with the equilibrium constant equal to 2.3 (Fehsenfeld and Ferguson,1974).

1.3 Mono-carbonate and poly-hydrates.

Payzant and Kebarle (1972) and Huertas et al. (1978) treated the formation of the second hydrate of O_2^- as a termolecular reaction,

$O_2^-(H_2O) + H_2O + M \rightarrow O_2^-(H_2O)_2 + M$ $k_f=5.4\text{x}10^{-28}$ ($M=O_2$) (50)

whereas, Kazil (2002) treated this as a bimolecular reaction at pressures above some high-pressure threshold (unstated), $k_f=1.0\text{x}10^{-9}$.

$O_2^-(H_2O)_2 + M \rightarrow O_2^-(H_2O) + H_2O + M$ $k_f=1.1\text{x}10^{-14}$ (PK, FF) (51)

Kebarle et al. (1972) and Fehsenfeld and Ferguson (1974) further suggest a sequence involving $O_2^-(CO_2)$ as a hydration path to $O_2^-(H_2O)_2$ formation:

$O_2^-(CO_2) + H_2O + M \rightarrow O_2^-(CO_2)(H_2O) + M$ $k_f(est)=10^{-28}$ (Hue) (21)

followed by:

$O_2^-(CO_2)(H_2O) + H_2O \rightarrow O_2^-(H_2O)_2 + CO_2$ $k_{148}(est)=1\text{x}10^{-9}$ (Fah) (148)

$k_{148}(est)=1\text{x}10^{-10}$ (Hue)

especially, when $P(CO_2) > P(H_2O)$ such as in the upper troposphere and above. Note, k_{148} presumed by Huertas et al. (1978) is an order of magnitude smaller than the assumed value used by Fahey et al. (1982) and is inconsistent with the reaction rate coefficient for reaction (147) measured by Fahey et al. and the equilibrium constants reported by Kebarle et al. (1972) and Fehsenfeld and Ferguson (1974). Kebarle et al. (1972) and Fehsenfeld and Ferguson (1974) gave equilibrium constants of 7 and 15, respectively, for the switching reaction pair (148) and (147),

$O_2^-(H_2O)_2 + CO_2 \rightarrow O_2^-(CO_2)(H_2O) + H_2O$ $k_{147}=7\text{x}10^{-11}$ (Fah) (147)

Further, the reaction products of (147) were not explicitly stated in Fahey et al. (1982) and those shown here were inferred from their discussion and the discussion of Mohnen (1972). The $O_2^-(CO_2)(H_2O)$ cluster generated in reaction (147) provides an alternative $O_2^-(CO_2)$ generating mechanism, (147) followed by (14):

$O_2^-(CO_2)(H_2O) + M \rightarrow O_2^-(CO_2) + H_2O + M$ $k_{14}(est)=10^{-14}$ (Hue) (14)

Huertas et al. (1978) attributed his presumed reaction rate coefficient for (14) to Mohnen (1974). Reaction (14) combined with reaction (21) yields a simple equilibrium constant of $9\text{x}10^4$ (atm^{-1}; $K_{eq}=k_{21}/k_{14}$). The equilibrium constant for the combined equilibrium reactions $K_{eq}(12,13)$ and $K_{eq}(21,14)$ of $2.1\text{x}10^5$ was within a factor of 5 of the NIST (2016) value for reaction (178)

$O_2^-(H_2O) + CO_2 + M \rightarrow O_2^-(CO_2)(H_2O) + M$ $K_{eq}=9.1\text{x}10^5$ (atm^{-1}) (NIST) (178)

$k_f(est)=1\text{x}10^{-28}$(Hue)

$k_r(est)=2.7x10^{-15}=k_f/K_{eq}$

Kebarle et al. (1972) proposed reactions of the form:

$$O_2^-(H_2O)_{n>2} + CO_2 \rightarrow O_2^-(CO_2)(H_2O)_{n-1} + H_2O$$

in their preliminary mechanism. Mohnen (1972) indicated these reactions were unlikely for n>3 and Fahey et al. (1982) indicated these reactions are endothermic and slow for n>1. There is some evidence for $O_2^-(CO_2)$ hydrates up to *n=2* in Mohnen (1972) and reactions:

$$O_2^-(CO_2)(H_2O) + H_2O + M \rightarrow O_2^-(CO_2)(H_2O)_2 + M \qquad (180)$$

and

$$O_2^-(CO_2)(H_2O)_2 + M \rightarrow O_2^-(CO_2)(H_2O) + H_2O + M \qquad (181)$$

were included in our mechanism. Mohnen (1971) and Kebarle et al. (1972) included these reactions in their O_2^-, CO_2, and H_2O mechanisms and Kebarle et al. gave a measured reaction enthalpy. In one of the O_2^-, CO_2, and H_2O drift-tube experiments of Mohnen (1972), Mohnen called out strong signals attributed to $O_2^-(CO_2)$ and $O_2^-(CO_2)(H_2O)$ and weaker signals attributed to $O_2^-(H_2O)_{n=4-7}$. While not specifically mentioned, weaker signals were also present in his data figure at masses of 50, 68, 86 and 112, which correspond to $O_2^-(H_2O)_{n=1-3}$ and $O_2^-(CO_2)(H_2O)_2$, respectively. Huertas et al. (1976) included the reaction pair, (180) and (181), in their mechanism following Kebarle et al. and assumed the reaction rate coefficients were $1x10^{-28}$ and $1x10^{-13}$, respectively. The latter value for k_{181} was stated to be from Mohnen (1974), which in turn refers to Mohnen (1971; 1972) but was not explicitly found within these three references. Here, we have included only the first and second order hydrates of $O_2^-(CO_2)$ in our model scheme. Higher order O_2^- hydrates (up to n=5) are included (see reactions 70, 71, 192, 193, 194, and 195) as they comprise a significant fraction of O_2^-at higher ambient and laboratory humidities.

The sensitivity trends in ion-hydroperoxide chemistry were difficult to reproduce and additional reaction schemes were employed. First it was thought the problem lay within reaction rate coefficients for reactions (12), (13), (14), (21), (24), (147), and (148) describing the $O_2^- - (H_2O) - (CO_2)$ switching system as outlined below. Next, ozone, O_3, present in the sample air could alter PCIMS hydroperoxide sensitivity as O_3 reacts with O_2^- reducing the O_2^- concentration and producing O_3^- and CO_3^- ions. Reactions capturing this chemistry were included. Also, a slower rate of reaction for (13) was required. Through systematic adjustment, we found k_{13} needed to be at or below 10^{-12} to leave sufficient O_2^-, $O_2^-(H_2O)$ and $O_2^-(CO_2)$ to fit our sensitivity data. This was approximately two orders of magnitude lower than predicted by the reaction (12)-(13) equilibrium. The following supported a potentially lower reaction rate coefficient for (13):

1) Banic and Iribarne (1985) argue $O_2^-(CO_2)$ is a "very stable" ion cluster in the troposphere and assumed it to be covalently bonded based upon Fehsenfeld and Ferguson (1974). In Fehsenfeld and Ferguson (1974) a covalently bonded $O_2^-(CO_2)$ cluster is not explicitly discussed although covalent bonding is discussed by them with respect to $HO^- + SO_2$ and $Cl^- + SO_2$ cluster reactions. They did, however, discuss reaction (13) indirectly, implying it

was “slow”. We infer this “slowness” is what lead to Banic and Iribarne’s suggestion of covalent bonding in the $O_2^-(CO_2)$ cluster ion, as stronger covalent bonding would be expected in a slowly reacting cluster ion such as (13).

2) Hiraoka and Yamabe (1992) discuss evidence of covalent bonding in the $O_2^-(CO_2)$ ion because of a noted jump in cluster reaction enthalpy for the addition of additional CO_2 to $O_2^-(CO_2)$ as compared to the reaction enthalpy changes noted with the addition of CO_2 to CO_3^- and NO_2^- ions. This was interpreted as an indication of covalent bonding in $O_2^-(CO_2)$.

3) Hayhurst et al. (1992) show $O_2^-(CO_2)$ to increase in dry or wet air “rich” in CO_2 (>100 ppm, and in keeping with our system) with a maximum in dry CO_2 rich air but to virtually disappear in wet air “deficient” in CO_2 (<2 ppm).

4) Fehsenfeld and Ferguson further stated hydrated $O_2^-(CO_2)$ [i.e., $O_2^-(CO_2)(H_2O)$] reacts with H_2O eliminating CO_2 thereby making $O_2^-(H_2O)_2$. In turn $O_2^-(H_2O)_2$ can undergo dehydration to $O_2^-(H_2O)$. Thus, the reaction sequence:

$O_2^-(CO_2) + H_2O + M \rightarrow O_2^-(CO_2)(H_2O) + M$ $k_{21}<1\text{x}10^{-30}$ (est) (21)

$O_2^-(CO_2)(H_2O) + H_2O \rightarrow O_2^-(H_2O)_2 + CO_2$ $k_{148}(\text{est})=1\text{x}10^{-9}$ (Fah) (148)

$k_{148}(\text{est})=1\text{x}10^{-10}$ (Hue)

$O_2^-(H_2O)_2 + M \rightarrow O_2^-(H_2O) + H_2O + M$ $k_{51}=1.1\text{x}10^{-14}$ (PK, FF) (51)

results in a reaction sequence with products identical to those in (13).

5) O’Sullivan et al. (2017) simulated the bonding in $O_2^-(CO_2)$ using an *ab initio* method and suggested it is an adduct with weak covalent bonding.

6) Last, the value shown for k_{21} fits our $O_2^-(CO_2)(H_2O_2)$ sensitivity trend with water vapor much better than the reaction rate coefficient of $1\text{x}10^{-28}$ estimated by Huertas et al. (1978) and subsequently cited by others (e.g., Popov, 2010). Mohnen (1971) also estimated a value of $1\text{x}10^{-29}$ and which was smaller than that in Huertas.

We hypothesize a reaction sequence like (21), (148) and (51) together with (12) could give rise to a steady-state system in which a reaction like (13) appears in the net but occurs slowly if at all directly.

Reactions or reaction sequences represented by (149)-(152)

$O_2^-(H_2O)_2 + H_2O_2 \rightarrow O_2^-(H_2O_2) + 2\ H_2O$ $k_{149}=5.0\text{x}10^{-10}$(est) (149)

$O_2^-(H_2O)_3 + H_2O_2 \rightarrow O_2^-(H_2O_2) + 3\ H_2O$ $k_{150}=2.5\text{x}10^{-10}$(est) (150)

$O_2^-(H_2O)_2 + CH_3OOH \rightarrow O_2^-(CH_3OOH) + 2\ H_2O$ $k_{151}=1.0\text{x}10^{-10}$(est) (151)

$O_2^-(H_2O)_3 + CH_3OOH \rightarrow O_2^-(CH_3OOH) + 3\ H_2O$ $k_{152}=5.0\text{x}10^{-12}$(est) (152)

followed by (160) and (161):

$O_2^-(CO_2) + H_2O_2 \rightarrow O_2^-(H_2O_2) + CO_2$ $k_{160}=6.0\text{x}10^{-10}$(est) (160)

$O_2^-(CO_2) + CH_3OOH \rightarrow O_2^-(CH_3OOH) + CO_2$ $k_{161}=4.0\text{x}10^{-10}$(est) (161) were added to the mechanism. Their inclusion improved the pressure dependent sensitivity and water vapor trends for the O_2^- hydroperoxide clusters but did not significantly improve the pressure and water vapor sensitivity trends in $O_2^-(CO_2)(H_2O_2)$.

Next ozone effects on the chemistry were included. O_3 present in the sample air could alter the peroxide chemical ionization mass spectrometer (PCIMS) hydroperoxide sensitivity as O_3 reacts with O_2^- reducing the O_2^- concentration and producing O_3^- and CO_3^- ions:

$$O_2^- + O_3 \rightarrow O_3^- + O_2 \quad (8)$$

$$O_3^- + CO_2 \rightarrow CO_3^- + O_2 \quad (9)$$

Additionally, O_3 reacts with $O_2^-(CO_2)$ and O_2^- hydrate clusters:

$$O_2^-(CO_2) + O_3 \rightarrow O_3^- + CO_2 + O_2 \quad (46)$$

$$O_2^-(H_2O) + O_3 \rightarrow O_3^- + H_2O + O_2 \quad (47)$$

$$O_2^-(H_2O)_2 + O_3 \rightarrow O_3^-(H_2O) + H_2O + O_2 \quad (52)$$

$$O_2^-(H_2O)_3 + O_3 \rightarrow O_3^-(H_2O)_2 + H_2O + O_2 \quad (146)$$

to produce additional O_3^-, CO_3^- and their hydrates. The O_3 reaction rate coefficients were assigned the same value regardless of the extent of O_2^- hydration and carbonation in keeping with Fahey et al. (1982) who pointed out the addition of CO_2 or H_2O did not significantly reduce the reaction rate coefficient between O_2^- or its cluster ions with O_3. O_3 has the potential to shift the ion population from O_2^-, $O_2^-(H_2O)_n$ and $O_2^-(CO_2)_m$ to O_3^- and CO_3^-.

1.4 Iodide

Iyer et al. (2016) using *ab initio* methods estimated reaction rate coefficients and binding energies for I^- with HFo and HAc. They also calculated binding energies for I^- reactions with H_2O_2 and CH_3OOH using the same methodology (Iyer, Pers. Comm., 2016). The respective binding energies for $I^-(HFo)$, $I^-(HAc)$, $I^-(H_2O_2)$, and $I^-(CH_3OOH)$ are 100, 73, 70, and 60 kJ mol^{-1}. Iyer et al. predicted sensitivities for many organic compounds based on the correlation of their calculated binding energies and the experimental sensitivities for organic acids published in Lee et al. (2014) for a CIMS TOF I^- instrument. We have normalized their predicted sensitivities to $I^-(HFo)$ and the relative sensitivities are 1.000, 0.034, 0.007, and 0.001for $I^-(HFo)$, $I^-(HAc)$, $I^-(H_2O_2)$, and $I^-(CH_3OOH)$, respectively. This ranking is consistent with the observations of O'Sullivan et al. (2017) in which they noted observing $I^-(H_2O_2)$ but not $I^-(CH_3OOH)$ clusters with the PCIMS instrument and with Treadaway et al. (2017) in which they observed a weak standard addition calibration signal for $I^-(CH_3OOH)$ in the laboratory and during FRAPPE (Treadaway et al., 2017; Fig. 3). Fig. 8-10 (main paper) showed the sensitivity for $I^-(H_2O_2)$, $I^-(HFo)$, and $I^-(HAc)$ as a function of water vapor. The sensitivity of $I^-(CH_3OOH)$ appeared to be independent of water vapor from the laboratory work, although the FRAPPE field calibrations suggested (Treadaway et al. 2017; Fig. 4) the sensitivity may increase with water like $I^-(HFo)$ whereas, $I^-(H_2O_2)$ and $I^-(HAc)$ decrease over the limited range in humidity encountered in FRAPPE.

2. References

Adams, N. G., Bohme, D. K. , Dunkin, D. B. , Fehsenfeld, F. C. , and Ferguson, E. E. :Flowing afterglow studies of formation and reactions of cluster ions of O_2^+, O_2^- , and O^-, J. Chem. Phys., 52, 3133-3140, doi: 10.1063/1.1673449, 1970.

Albritton, D. L., : Ion-neutral reaction-rate constants measured in flow reactors through 1977, Atom. Data Nucl. Data Tables, 22, 1-101, 1978.

Banic, C. M. and Iribarne, J. V. ,: Equilibrium constants for clustering of neutral molecules about gaseous ions, J. Chem. Phys., 83, 6432-6448, doi: 10.1063/1.449543, 1985.

Bartmess, J. E.: "Negative Ion Energetics Data" in NIST Chemistry WebBook, NIST Standard Reference Database Number 69, Eds. P. J. Linstrom and W. G. Mallard, National Institute of Standards and Technology, Gaithersburg MD, 20899, http://webbook.nist.gov, retrieved August 19, 2016.

Böhringer, H., Fahey, D. W., Fehsenfeld, F. C., and Ferguson, E. E.: Bond energies of the molecules H_2O, SO_2, H_2O_2, and HCl to various atmospheric negative ions, J. Chem. Phys., 81, 2805-2810, doi: 10.1063/1.447953, 1984.

Cappa, C. D. and Elrod, M. J.;A computational investigation of the electron affinity of CO_3 and thethermodynamic feasibility of $CO_3^-(H_2O) + ROOH$ reactions, Phys. Chem. Chem. Phys., 3, 2986-2994, doi: 10.1039/b102981a, 2001.

Fahey, D.W., Böhringer, H., Fehsenfeld, F.C., and Ferguson, E.E.: Reaction rate constants for $O_2^-(H_2O)_n$ ions n = 0 to 4, with O_3, NO, SO_2, and CO_2, J. Phys. Chem., 76, 1799-1805, doi: 10.1063/1.443220, 1982.

Fehsenfeld, F. C., Ferguson, E. E., and Bohme, D. K.: Additional flowing afterglow measurements of negative ion reactions of D-region interest, Planet. Space Sci., 17, 1759-1762, 1969.

Fehsenfeld, F. C. and Ferguson, E. E.: Laboratory studies of negative ion reactions with atmospheric trace constituents, 3181-3193, doi: 10.1063/1.1682474, 1974.

Goldsmith, C.F., Magoon, G. R., and Green, W. H.: Database of small molecule thermochemistry for combustion, J. Phys. Chem. A, 116, 9033-9057, 2012.

Hayhurst, C. J., Watts, P., and Wilders, A.: Studies on gas-phase negative ion/molecule reactions of relevance to ion mobility spectrometry: mass analysis and ion identification of the negative reactant ion peak in "clean" air, Intl. J. Mass Spect. Ion Proc., 121, 127-139, 1992.

Hiraoka, K. and Yamabe, S.: Formation of the chelate bonds in the cluster $O_2^-(CO_2)_n$, $CO_3^-(CO_2)_n$, and $NO_2^-(CO_2)_n$, J. Chem. Phys., 97, 643-650, doi:10.1063/1.463560, 1992.

Huertas, M. L., Fontan, J., Gonzalez, J.: Evolution times of tropospheric negative ions, Atmos. Environ., 12, 2351-2362, 1978.

Ikezoe, Y., Matsuoka, S., Takebe, M., and Viggiano, A.A.: Gas phase ion-molecule reaction rate constants through 1986, Ion Reaction Research Group of The Mass Spectroscopy Society of Japan, Tokyo, 1987.

Iyer, S., Lopez-Hilfiker, F., Lee, B. H., Thornton, J. A., and Kurtén, T.: Modeling the detection of organic and inorganic compounds using iodide-based chemical ionization, J. Phys. Chem. A, 120, 576−587, doi: 10.1021/acs.jpca.5b09837, 2016.

Kazil, J.: The University of Bern atmospheric ion model: time-dependent ion modeling in the stratosphere, mesosphere and lower thermosphere, Ph.D. Thesis, University of Bern, Bern, Switzerland, 2002.

Kebarle, P., French, M., and Payzant, J. D.: Reaction mechanisms and bonding energies for ion-hydrates (ion-water clusters) of ionospheric interest, in: Aeronomy Report No. 48, COSPAR Symposium on D- and E-Region Ion Chemistry - An Informal Record, Eds. C. F. Sechrist, Jr., and M.A. Geller, University of Illinois at Urbana-Champaign, Urbana, IL, 1972.

Lee, B. H., Lopez-Hilfiker, F. D., Mohr, C., Kurtén, T., Worsnop, D. R., andThornton, J. A.: An iodide-adduct high-resolution time-of-flight chemical-ionization mass spectrometer: application to atmospheric inorganic and organic compounds, Environ. Sci. Tech., 48, 6309-6317, doi: 10.1021/es500362a, 2014.

Messer, B. M., Stielstra, D. E., Cappa, C. D., Scholtens, K. W., and Elrod, M. J.: Computational and experimental studies of chemical ionization mass spectrometric detection techniques for atmospherically relevant peroxides, Intl. J. Mass Spect., 197, 219-235, 2000.

Mohnen, V.A.: Discussion of the formation of major positive and negative ions up to the 50 km level, P. Appl. Geophys., 84, 141-151, 1971.

Mohnen, V. A.: Negative ions in air-like gas mixtures, P. Appl. Geophys., 100, 123-132, 1972.

Mohnen, V. A.: Formation, nature, and mobility of ions of atmospheric importance, 5th Intl. Conf. on Atmos. Elect., Garmisch Partenkirchen, Germany, 2-7 September, 1974.

Ochterski, J. W.: Thermochemistry in Gaussian, help@gaussian.com, http://gaussian.com/thermo/, pdf file downloaded: 5 December 2012.

O'Sullivan, D. W., Silwal, I. K. C., McNeill, A. S., Treadaway, V., and Heikes, B. G.: Quantification of gas phase hydrogen peroxide and methyl hydroperoxide in ambient air: Using atmospheric pressure chemical ionization mass spectrometry with O_2^-, $O_2^-(CO_2)$ reagent ions, submitted to: Int'l. J. Mass Spectrom., 2017.

Pack, J. L. and Phelps, A. V.: Electron attachment and detachment II. Mixtures of O_2 and CO_2 and O_2 and H_2O, J. Chem. Phys., 45, 4316-4329, 1966.

Payzant, J. D. and Kebarle, P.: Kinetics of reactions leading to $O_2^-(H_2O)_n$ in moist oxygen, J. Chem. Phys., 56, 3482,doi: 10.1063/1.1677723, 1972.

Popov, N. A.: Evolution of the negative ion composition in the afterglow of a streamer discharge in air, Plasma Physics Reports, 36, 812–818, 2010, translated from Fizika Plazmy, 36, 867–873, 2010.

Treadaway, V., Heikes, B.G., McNeill, A. S., Silwal, I. K. C., and O'Sullivan, D. W.: Measurement of formic acid, acetic acid, hydrogen peroxide, and methyl peroxide in air by chemical ionization mass spectroscopy: airborne method development, in prep. Atmos. Meas. Tech., 2017.